Dimensionless learning based on information

Yuan Yuan[1*] & Adrián Lozano-Durán[1,2]

[1]Department of Aeronautics and Astronautics, Massachusetts Institute of Technology, Cambridge, MA

[2]Graduate Aerospace Laboratories, California Institute of Technology, Pasadena, CA.

[*]Corresponding author. Email: yuany999@mit.edu

Dimensional analysis is one of the most fundamental tools for understanding physical systems. However, the construction of dimensionless variables, as guided by the Buckingham-π theorem, is not uniquely determined. Here, we introduce IT-π, a model-free method that combines dimensionless learning with the principles of information theory. Grounded in the irreducible error theorem, IT-π identifies dimensionless variables with the highest predictive power by measuring their shared information content. The approach is able to rank variables by predictability, identify distinct physical regimes, uncover self-similar variables, determine the characteristic scales of the problem, and extract its dimensionless parameters. IT-π also provides a bound of the minimum predictive error achievable across all possible models, from simple linear regression to advanced deep learning techniques, naturally enabling a definition of model efficiency. We benchmark IT-π across different cases and demonstrate that it offers superior performance and capabilities compared to existing tools. The method is also applied to conduct dimensionless learning for supersonic turbulence, aerodynamic drag on both smooth and irregular surfaces, magnetohydrodynamic power generation, and laser-metal interaction.

Introduction

Physical laws and models must adhere to the principle of dimensional homogeneity (*1,2*), i.e., they must be independent of the units used to express their variables. A similar idea was first introduced by Newton in his *Principia*, under the term "dynamically similar systems" (*3*), although Galileo had already employed the notion of similar systems when discussing pendulum motions. Over the following centuries, the concept of similar systems was loosely applied in a variety of fields, including engineering (Froude, Bertrand, Reech), theoretical physics (van der Waals, Onnes, Lorentz, Maxwell, Boltzmann), and theoretical and experimental hydrodynamics (Stokes, Helmholtz, Reynolds, Prandtl, Rayleigh) (*3*). The approach was formally articulated in the early 20th century, laying the foundation for what is known today as dimensional analysis (*1, 4, 5*).

The applications of dimensional analysis extend beyond the construction of dimensionally consistent physical laws. It provides the conditions under which two systems share identical behavior (dynamic similarity), allowing predictions from laboratory experiments to be

extended to real-world applications (*3, 6*). Dimensional analysis also facilitates dimensionality reduction, i.e., simplifying physical problems to their most fundamental forms, thus decreasing the amount of data required for analysis (*7, 8*). Another application is the discovery of self-similar variables, for which systems exhibit invariant solutions under appropriate scaling (*9*). Finally, dimensional analysis can reveal the physical regimes in which different phenomena dominate (e.g., incompressible versus compressible flow), enabling researchers to identify the most influential physical mechanisms in a given context (*10*).

A key landmark of dimensional analysis is the Buckingham-π theorem (*1*), which offers a systematic framework for deriving dimensionless variables. However, the solution is not unique, as there are infinitely many possible ways to construct these variables. To address this limitation, recent studies have developed data-driven tools to identify unique dimensionless variables that minimize the error for a given model structure, particularly in the data-rich context enabled by modern simulations and experiments. These methods combine dimensional analysis with machine learning techniques to identify dimensionless variables using multivariate linear regression (*11*), polynomial regression (*12–14*), ridge regression (*15*), hypothesis testing (*16*), Gaussian process regression (*17*), neural networks (*13, 15, 18, 19*), sparse identification of nonlinear dynamics (*12, 15*), clustering (*20*), symbolic regression (*13, 21, 22*) and entropic principles (*23, 24*). Table 1 offers a non-exhaustive comparative overview of data-driven methods for discovering dimensionless variables, highlighting their respective capabilities. These include applicability to ordinary and partial differential equations (ODEs/PDEs), the ability to rank dimensionless variables by predictability (and thus relative importance), identification of distinct physical regimes, detection of self-similar behavior, and extraction of characteristic scales (e.g., length and time scales of the system). Another key capability is whether the method can determine a bound on the minimum possible error across all models–which in turn enables the definition of a model efficiency. The comparison in Table 1 indicates that, although many approaches incorporate several of these properties, no single method currently supports all of these capabilities simultaneously. One notable shortcoming of previous data-driven methods is that they are not model-free; i.e., the discovery of dimensionless variables relies on a predefined model structure (e.g., linear regressions, neural networks,...). This can lead to potentially biased results, as the dimensionless variables identified may not be optimal for other models. A detailed account of the challenges in dimensionless learning can be found in the Supplementary Materials.

In this work, we present IT-π, an information-theoretic, model-free method for dimensionless learning. An overview of the method is shown in Fig. 2. Our approach is motivated by a fundamental question: Which dimensionless variables are best suited for predicting a quantity of interest, *independent of the modeling approach?* IT-π addresses this question by unifying the Buckingham-π theorem with the irreducible error theorem. The central idea is that the predictive capability of a model is bounded by the amount of information shared between the input (dimensionless variables) and the output (dimensionless quantity of interest) (*25, 26*).

This manuscript is organized as follows. We begin by introducing the information-theoretic irreducible error theorem, which establishes the minimum achievable error across all possible models. This theorem serves as the foundation for a generalized formulation of the Buckingham-π theorem, while enabling all capabilities outlined in Table 1. We then apply IT-π to a broad set of validation and application cases. The validation cases, which have

Method	ODE/PDE	Model-Free	Input Ranking	Regime Detection	Self-Similar	Characteristic Scales	Irreducible Error	Model Efficiency
Scaling LAWs (*11*)	×	×	✓	×	–	–	×	×
Active Subspaces (*17*)	✓	×	✓	×	–	–	×	×
AI Feynman (*13*)	×	×	×	×	–	–	×	×
Clustering (*20*)	✓	×	✓	✓	–	–	×	×
PyDimension (*12*)	✓	×	×	×	✓	✓	×	×
BuckiNet (*15*)	✓	×	✓	×	✓	✓	×	×
BSM (*21*)	✓	×	×	×	✓	✓	×	×
IT-π (Current)	✓	✓	✓	✓	✓	✓	✓	✓

Table 1: **Overview of some data-driven dimensionless learning methods and their capabilities.** These capabilities include whether each method is applicable to ODEs/PDEs, operates in a model-free manner, ranks inputs by predictability, identifies distinct physical regimes, uncovers self-similarity, determines characteristic scales and dimensionless parameters, provides a bound on the irreducible error, and evaluates model efficiency. Entries marked with "–" indicate that although the method could potentially be extended to infer the corresponding physical property after deriving the dimensionless variables, the authors did not explicitly perform this step.

known analytical solutions, are used to benchmark the performance of IT-π. In contrast, the application cases—where no optimal solution is known—are used to discover new dimensionless variables governing the underlying physics. Finally, we compare the performance of IT-π with other dimensionless learning methods across all studied cases.

Results

Dimensionless learning based on information

A physical model (or law) aims to predict a dimensional quantity q_o using a set of n dimensional input variables, $\mathbf{q} = [q_1, q_2, \ldots, q_n]$, through the relation $\hat{q}_o = \mathcal{F}(\mathbf{q})$, where $\hat{q}_o$ is an estimate of q_o. As an example, consider the prediction of the gravitational force between two objects, $q_o = F_g$, which depends on $\mathbf{q} = [m_1, m_2, r, G]$, where m_1 and m_2 are the masses of the objects, r is the distance between their centers of mass, and G is the gravitational constant. According to the Buckingham-π theorem (*1*), physical models can be reformulated in a dimensionless form as $\hat{\Pi}_o = f(\mathbf{\Pi})$, where $\hat{\Pi}_o$ denotes the predicted dimensionless output, and $\mathbf{\Pi} = [\Pi_1, \Pi_2, \ldots, \Pi_l]$ is the set of dimensionless input variables. Each dimensionless variable has the form $\Pi_i = q_1^{a_{i1}} q_2^{a_{i2}} \cdots q_n^{a_{in}}$ and the number of required dimensionless inputs is upper bounded by $l = n - n_u$, where n_u is the number of fundamental units involved in the problem (e.g., length, time, mass, electric current, temperature, amount of substance, and luminous intensity). For a given L_p-norm, the success of the model is measured by the error $\epsilon_f = \|\Pi_o - \hat{\Pi}_o\|_p$.

Irreducible error as lack of information. Our approach is grounded in the information-theoretic irreducible error theorem [see proof in the Supplementary Materials] (*27, 28*). The key insight is that prediction accuracy of any model is fundamentally limited by the amount of information the input contains about the output, where information here is defined within the framework of information theory (*29*). More precisely, the error across all possible models

f is lower-bounded by

$$\epsilon_f \geq e^{-I_\alpha(\Pi_o;\mathbf{\Pi})} \cdot c(\alpha, p, h_{\alpha,o}) \equiv \epsilon_{LB}, \tag{1}$$

where $I_\alpha(\Pi_o; \mathbf{\Pi})$ is the Rényi mutual information of order α (*30*), which measures the shared information between Π_o and $\mathbf{\Pi}$. The value of $c(\alpha, p, h_{\alpha,o})$ depends on the L_p-norm, α and the information content of Π_o, denoted by $h_{\alpha,o}$ [see Methods]. The irreducible (lower bound) error is denoted as ϵ_{LB}. The inequality in Eq. (1) represents a fundamental mathematical constraint that holds regardless of the complexity of the statistical relationship between input and output, and must therefore be satisfied by any predictive model, irrespective of its form. When an exact functional relationship exists between the input and the output, the information measure $I_\alpha(\Pi_o; \mathbf{\Pi})$ converges to infinity, indicating that an exact model is possible ($\epsilon_{LB} = 0$). In contrast, if some of the variables influencing Π_o are inaccessible or unmeasurable, $I_\alpha(\Pi_o; \mathbf{\Pi})$ remains finite, leading to an irreducible error ($\epsilon_{LB} > 0$) that cannot be eliminated. It is interesting to note that the inequality in Eq. (1) holds for a range of values of α. However, the most useful case occurs when ϵ_{LB} is maximized, yielding the tightest bound. A detailed analysis of the role of α in Eq. (1) is provided in the Supplementary Material.

The irreducible error ϵ_{LB} has several useful properties. First, it is independent of any particular model f. Second, it is invariant under bijective transformations of inputs when the output is fixed, reflecting the principle that such transformations produce alternative yet equivalent model formulations. Third, it is sensitive to the choice of the L_p-norm for the error. For example, predicting extreme events (captured by high L_p-norms) may be more challenging and require different variables than predicting weaker, common events (captured by low L_p-norms) [see example in the Supplementary Materials]. Finally, Eq. (1) naturally leads to the definition of the normalized irreducible error $\tilde{\epsilon}_{LB} = e^{-I_\alpha(\Pi_o;\mathbf{\Pi})}$, which ranges from 0—when exact predictions are possible—to 1—when predictions are essentially random guesses. Occasionally, we will refer to the percentage form of $\tilde{\epsilon}_{LB}$, defined as $\%\tilde{\epsilon}_{LB} = \tilde{\epsilon}_{LB} \times 100$.

Information-theoretic Buckingham-π theorem (IT-π). Following Eq. (1), we define the optimal dimensionless inputs $\mathbf{\Pi}^* = [\Pi_1^*, \Pi_2^*, \ldots, \Pi_{l^*}^*]$ and dimensionless output Π_o^* for a given L_p-norm as those satisfying

$$\mathbf{\Pi}^*, \ \Pi_o^* = \arg\min_{\mathbf{\Pi},\Pi_o} \max_\alpha [\epsilon_{LB}]. \tag{2}$$

Figure 1 illustrates the optimization process from Eq. (2). This model-free formulation ensures that the identified dimensionless variables yield the highest predictive capabilities irrespective of the modeling approach. If desired, the output can be fixed in dimensionless form, requiring only $\mathbf{\Pi}^*$ to be discovered. The irreducible error using the optimal dimensionless inputs $\mathbf{\Pi}^*$ is denoted by $\epsilon_{LB}^* = \epsilon_{LB}(\mathbf{\Pi}^*)$. It is satisfied that $\epsilon_f \geq \epsilon_{LB} \geq \epsilon_{LB}^*$. The optimization problem from Eq. (2) can be efficiently solved by employing the covariance matrix adaptation evolution strategy (CMA-ES) (*31*) constrained to the dimensionless candidates for $\mathbf{\Pi}$ and Π_o from the (classical) Buckingham-π theorem [see Methods]. Next, we discuss the different capabilities enabled by IT-π, with illustrative examples provided in Figure 2.

Ranking of dimensionless variables by predictability. The variables in $\mathbf{\Pi}^*$ can be ranked by predictability according to $\epsilon_{LB}(\Pi_1^*) \geq \epsilon_{LB}(\Pi_2^*) \geq \cdots \geq \epsilon_{LB}(\Pi_{l^*}^*)$. This ranking
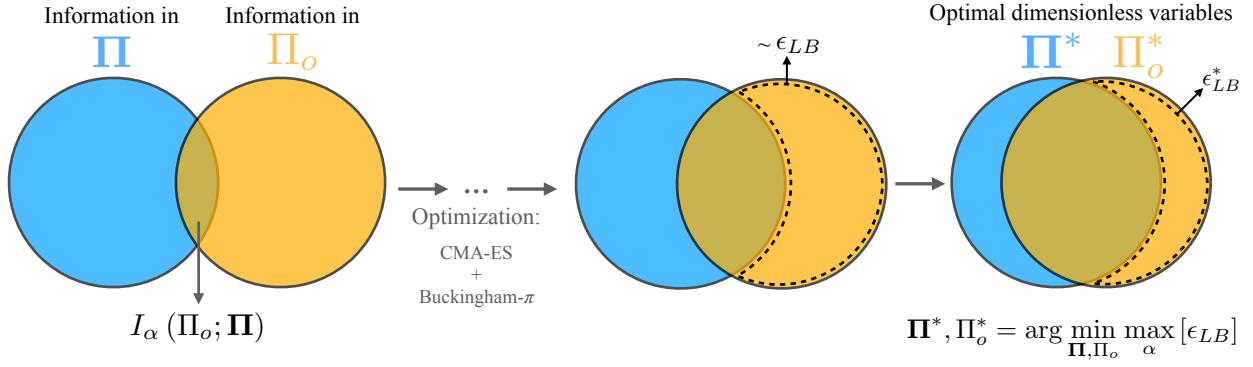
Figure 1: Schematic of the optimization process in IT-π. Circles represent the information content of the dimensionless input ($\mathbf{\Pi}$) and output (Π_o). The overlapping region denotes their mutual information of order α, $I_\alpha(\Pi_o; \mathbf{\Pi})$. The area enclosed by the dashed line corresponds to the amount of information in Π_o that cannot be inferred from $\mathbf{\Pi}$, which is related to the irreducible error ϵ_{LB}. The optimization is conducted with CMA-ES and proceeds from left to right, evaluating candidate pairs of $\mathbf{\Pi}$ and Π_o to minimize ϵ_{LB} until the optimal value ϵ_{LB}^* is reached. The candidates are constrained to be dimensionless by the Buckingham-π theorem. The value of α determines the sensitivity of IT-π to different L_p-norms and is learned as part of the optimization process.
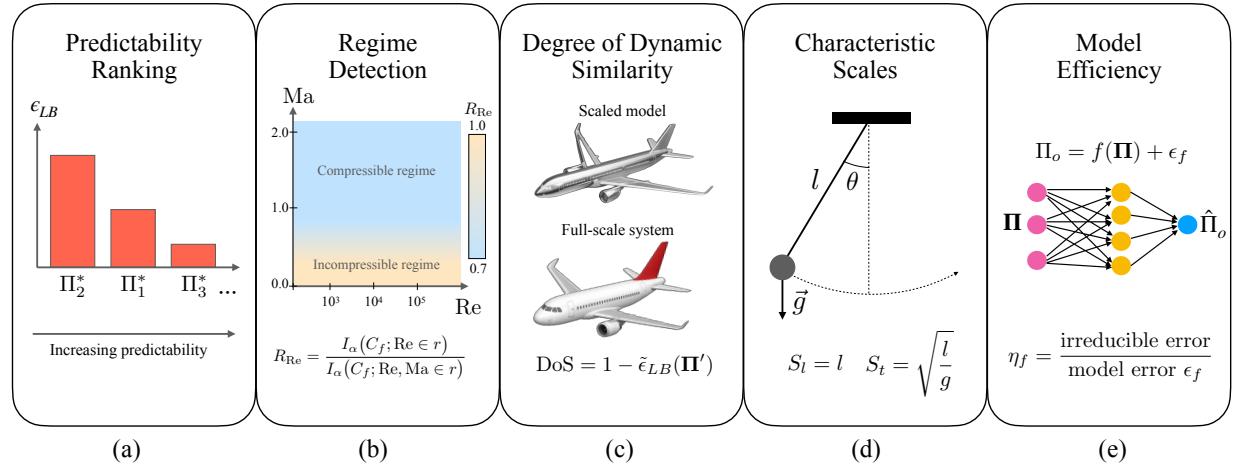

Figure 2: Illustration of the dimensionless learning capabilities enabled by IT-π. (a) Ranking of candidate dimensionless variables based on their predictability. (b) Example of regime detection for the skin friction coefficient C_f in a wall-bounded turbulent flow, with Reynolds number (Re) and Mach number (Ma) as dimensionless inputs. The score R_{Re} quantifies the relative importance of Re in predicting C_f. (c) Degree of dynamic similarity (DoS) between the lift coefficient of a wind tunnel–scaled aircraft model and that of the corresponding full-scale vehicle. (d) Characteristic length scale (S_l) and time scale (S_t) identified for a simple pendulum. (e) Model efficiency in predicting a target quantity Π_o using a neural network with inputs $\mathbf{\Pi}$ and prediction error ϵ_f. Additional details and discussion of the examples are provided in the text.

applies not only to individual variables but also to pairs of variables, such as $\epsilon_{LB}([\Pi_1^*, \Pi_2^*]) \geq \epsilon_{LB}([\Pi_1^*, \Pi_3^*])$, triplets, and so on. If considering additional variables no longer provides new information about the output, then the error does not decrease further, i.e., $\epsilon_{LB}([\Pi_1^*, \Pi_2^*, \ldots, \Pi_{l^*}^*]) = \epsilon_{LB}([\Pi_1^*, \Pi_2^*, \ldots, \Pi_{l^*+1}^*]) = \epsilon_{LB}^*$, where l^* is the minimum number of dimensionless variables to maximize predictability of the output. Note that the number of dimensionless variables provided by the original Buckingham-π theorem, $l = n - n_u$ (*1*), represents an upper bound—i.e., the actual number of dimensionless variables required for a predictive model may be smaller. In contrast, the value of l^* is tight, improving upon both Buckingham's original bound, $l \geq l^*$, and the subsequent refinement proposed by Sonin (*7*). Identifying the exact number of required inputs has several advantages. For instance, it provides a clear guideline for selecting the optimal set of inputs to balance model complexity with prediction accuracy. In the Applications section, we present a case in which Buckingham-π yields $l = 7$ dimensionless variables, whereas IT-π identifies a significantly smaller set with $l^* = 2$.

Detection of physical regimes. Physical regimes are distinct operating conditions of a system, each governed by a particular set of dimensionless variables. As these variables vary and fall within specific intervals, the system transitions to a different regime, where new effects become dominant. For instance, in fluid mechanics, incompressible and compressible flow represent two distinct physical regimes, each governed by unique flow characteristics. In the incompressible regime, the flow physics are governed solely by the dimensionless Reynolds number. In contrast, compressible flows require both the Reynolds and Mach numbers to accurately characterize the dynamics.

IT-π identifies physical regimes by evaluating the predictive significance of each dimensionless input, Π_i^*, within specific regions of the dimensionless space. First, $\mathbf{\Pi}^*$ is divided into M regions, labeled as $r_1, r_2, \ldots, r_M$. In each region r_k, a prediction score for Π_i^* is computed as $R_i(r_k) = I_\alpha(\Pi_o^*; \Pi_i^* \in r_k) / I_\alpha(\Pi_o^*; \mathbf{\Pi}^* \in r_k) \in [0, 1]$. The score $R_i(r_k)$ represents the relative importance of Π_i^* in predicting the output Π_o^* within the region r_k. By comparing these scores across regions, one can categorize dimensionless inputs into distinct physical regimes. Consider the example of predicting the skin friction of a turbulent flow in a pipe, the Reynolds number (Re) dominates in the incompressible flow regime without the influence of additional physical effects (e.g., buoyancy, magnetic forces, etc), as it would be indicated by a prediction score $R_{\text{Re}}(r_{\text{incompressible}}) \approx 1$. However, in the compressible flow regime, $R_{\text{Re}}(r_{\text{compressible}}) < 1$, indicating the need for an additional dimensionless number to fully determined the skin friction—in this case, the Mach number.

Degree of dynamic similarity. According to classical dimensional analysis, dynamic similarity is achieved when all dimensionless inputs governing a physical system are exactly matched between the scaled model and full-scale system. IT-π generalizes this concept by requiring similarity only for the optimal subset of l^* dimensionless variables, relaxing the conservative requirement of matching all l variables prescribed by classical theory. Furthermore, the quantity $\text{DoS} = 1 - \tilde{\epsilon}_{LB} \in [0, 1]$ measures the *degree of dynamic similarity* that can be achieved. Consider, for example, a wind tunnel experiment of a scaled model of an aircraft where technical limitations restrict the control to only a few dimensionless variables $\mathbf{\Pi}'$. In this scenario, the value of $\text{DoS} = 1 - \tilde{\epsilon}_{LB}(\mathbf{\Pi}')$ quantifies the degree of dynamic similarity attainable matching only those variables. This contrasts with traditional theory, which

merely indicates whether dynamic similarity is or is not attained without offering insight into the extent of similarity when it is not perfectly achieved.

Characteristic scales. The characteristic scales of a physical problem refer to the length, time, mass, and other fundamental quantities that can be constructed from the parameters involved in the system under study. These are essential not only for non-dimensionalization, but also for understanding the order of magnitude of the variables controlling the system. To define these scales, we can divide the dimensional inputs into two sets $\mathbf{q} = [\mathbf{q}_v, \mathbf{q}_p]$, where $\mathbf{q}_v$ consists of variables that vary in each simulation/experiment (i.e., dependent and independent variables), and $\mathbf{q}_p$ consists of variables that remain fixed for a given simulation/experiment but change across problem configurations (i.e., parameters). The characteristic scales are constructed from $\mathbf{q}_p$. For example, for a pendulum with the governing equation $\mathrm{d}/\mathrm{d}t[\theta, \dot{\theta}] = \left[\dot{\theta}, -g/l\sin\theta\right]$, the variables are time (t), angular displacement (θ), and angular velocity ($\dot{\theta}$), yielding $\mathbf{q}_v = [t, \theta, \dot{\theta}]$, whereas the parameters include the pendulum length (l) and gravitational acceleration (g), giving $\mathbf{q}_p = [l, g]$. As such, the characteristic length and time scales of the pendulum are obtained from $\mathbf{q}_p$ as $[S_l, S_t] = [l, \sqrt{l/g}]$.

IT-π extracts the characteristic scales, $\mathbf{S} = [S_1, S_2, \ldots, S_{n_u}]$, from $\mathbf{\Pi}^*$ by identifying the combination of quantities in $\mathbf{q}_p$ required to non-dimensionalize the variables in $\mathbf{q}_v$ [see the Supplementary Materials for the theory and algorithm]. In the previous example of the pendulum, IT-π will identify the optimal variable $\Pi^* = \dot{\theta} S_t$ with characteristic time scale $S_t = \sqrt{l/g}$. If the dimensional group Π_i depends solely on quantities from $\mathbf{q}_p$, then it represents a *dimensionless parameter* (rather than a dimensionless variable), as it encapsulates a relationship only between characteristic scales. One example of dimensionless parameter is the Reynolds number, that can be expressed as a ratio of two length scales and does not change for a given flow setup.

Self-similarity. Another capability of IT-π is the detection of self-similar variables—those that cannot be made dimensionless using only the parameters in $\mathbf{q}_p$. In such instances, IT-π identifies the need to incorporate additional variables from $\mathbf{q}_v$ to non-dimensionalize Π^*. The latter variable is then classified as self-similar, as it reveals an invariance between the ratios of the dependent and/or independent variables that govern the system.

Model efficiency. A foundational property of IT-π is its model-free formulation. This naturally leads to a definition of model performance relative to the theoretical optimum. Specifically, we introduce the model efficiency $\eta(f) = \epsilon^*_{LB}/\epsilon_f \in [0, 1]$, which quantifies how closely the predictions of the model, $\hat{\Pi}_o = f(\mathbf{\Pi})$, approach the theoretical limit. A low value of η indicates that the model underperforms relative to the optimal model. This underperformance may stem from inadequate inputs or insufficient model complexity (e.g., too few layers or neurons in an artificial neural network). Conversely, a value of η close to 1 implies that the model is extracting all the useful information from the inputs, and further improvements are not possible. An interesting interpretation of this efficiency is its analogy to the Carnot cycle in thermodynamics (*32*); in this context, it serves as the *Carnot cycle of physical laws*, setting a theoretical benchmark for the limits of predictive model performance. A diagnostic tool for assessing whether a model is suboptimal, optimal, or overfitting under finite-sample

conditions is provided in the Supplementary Materials.

Validation

We validate IT-π on physical systems with known optimal dimensionless inputs and physical properties. Our test cases include the Rayleigh problem, the Colebrook equation, and the Malkus-Howard-Lorenz water wheel. Figure 3 summarizes these cases by presenting the system equations alongside the physical properties identified by IT-π, such as the optimal dimensionless inputs and outputs, self-similarity, physical regimes, characteristic scales, input ranking, and the information-theoretic irreducible error. Although IT-π infers a complete set of properties for each case, the figure highlights only the most relevant ones for clarity. Additional validation cases—including turbulent Rayleigh-Bénard convection and the Blasius laminar boundary layer—are discussed in the Methods.

The Rayleigh Problem (*33*) (see Figure 3, Column 2) involves an infinitely long wall that suddenly starts moving with a constant velocity U in the wall-parallel direction within an initially still, infinite fluid. In the absence of a pressure gradient, the analytical solution for the flow velocity is $u = U \operatorname{erfc}(\xi/2)$, where $\xi = y/\sqrt{\mu t/\rho}$ is a self-similar variable that combines the distance from the wall (y), viscosity (μ), density (ρ), and time (t) such that the flow profile remains constant when scaled by U.

We generated samples of the velocity over time, $q_o = u$, with input variables $\mathbf{q} = [\mathbf{q}_v, \mathbf{q}_p]$, where $\mathbf{q}_v = [y, t]$ and $\mathbf{q}_p = [U, \mu, \rho]$, and performed dimensionless learning using IT-π. The optimal dimensionless input and output discovered are $\Pi^* = y\rho^{0.5}/(t^{0.5}\mu^{0.5})$ and $\Pi_o^* = u/U$, respectively. These dimensionless variables coincide with the analytical solution and successfully collapse the velocity profiles across different times, as shown in Figure 3(d). IT-π further identifies Π^* as a self-similar variable because the characteristic length and time scales cannot be constructed using only U, μ and ρ. Finally, the near-zero irreducible error reported in Figure 3(f) indicates that there exists a model capable of exactly predicting the output. Consequently, no additional dimensionless inputs are required. Note that IT-π identifies the need of only one dimensionless input ($l^* = 1$), which is less than the number of two inputs ($l = 2$) inferred from the Buckingham-π theorem.

The Colebrook Equation (*34*) (see Figure 3, Column 3) is a widely used formula in fluid mechanics for calculating the friction coefficient, C_f, which measures the resistance encountered by turbulent flow inside a pipe. Accurately determining C_f is crucial for designing efficient piping systems and predicting energy losses due to friction in various engineering applications (*35*). This coefficient depends on several factors, including the average roughness in the interior surface of the pipe (k), its diameter (D), the flow velocity (U), density (ρ), and viscosity (μ).

After generating samples for $q_o = C_f$ and $\mathbf{q} = [U, \rho, D, k, \mu]$, IT-$\pi$ discovered the optimal dimensionless inputs $\Pi_1^* = k/D$, and $\Pi_2^* = \mu/(U\rho D)$, both of which are consistent with the equation. The former represents the relative roughness height, whereas the latter is related to the Reynolds number $Re_D \equiv 1/\Pi_2^*$. The ranking in Figure 3(g) shows that Π_1^* and Π_2^* individually yield normalized irreducible errors ($\tilde{\epsilon}_{LB}$) in the output prediction of 40% and 20%, respectively. When both inputs are considered, they reduce the normalized irreducible
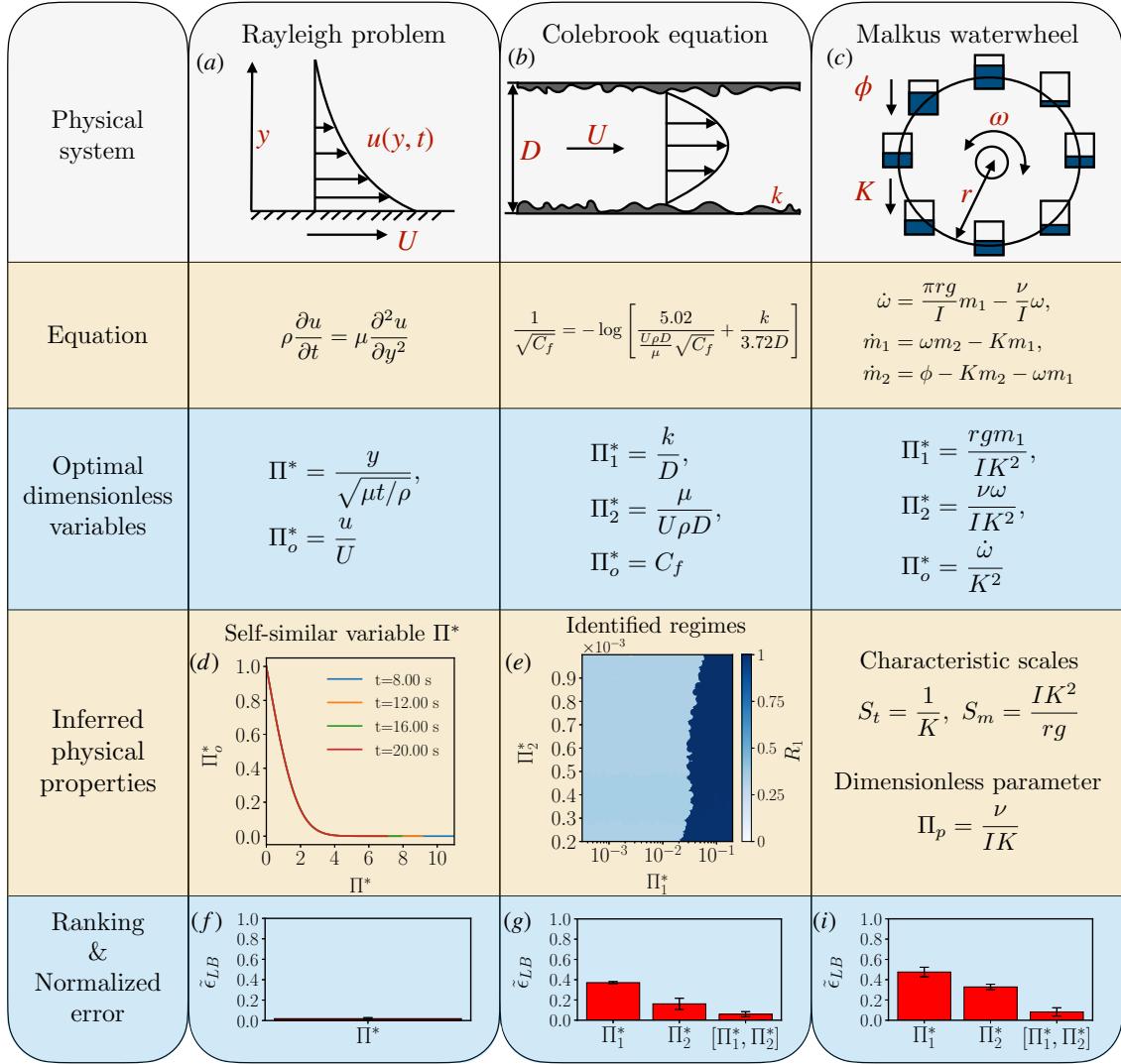
Figure 3: **Summary of validation cases.** Schematic representations of the physical systems (a, b, c), the corresponding systems of equations, and the optimal dimensionless inputs and outputs discovered by IT-π, are shown alongside the inferred physical properties, including self-similarity, distinct physical regimes, characteristic scales, relevant dimensionless parameters (where applicable), and the irreducible model error. (d) Rayleigh problem: Optimal dimensionless velocity profiles (Π_o^*) as a function of Π^*, with colors indicating different times t. (e) Colebrook equation: Contour plot of the prediction score R_1 (i.e., the relative importance of Π_1^*) as a function of the dimensionless inputs. The result is obtained by dividing the dimensionless inputs $\mathbf{\Pi}^*$ into 10 clusters using the KNN method. (f, g, i) Normalized irreducible error ($\tilde{\epsilon}_{LB}$) for individual components of $\mathbf{\Pi}^*$ and for all components combined, for (f) the Rayleigh problem, (g) the Colebrook equation, and (i) the Malkus waterwheel. Error bars indicate the uncertainty in the normalized irreducible error, computed as the difference between the error bound estimated using the full dataset and that estimated using half the data. Additional details regarding the symbols and definitions of all variables are provided in the main text.

error to nearly 0%. The physical regimes identified by IT-π are illustrated in panel (e) of Figure 3. The figure depicts the prediction score R_1 for Π_1^* across the dimensionless input space, that quantifies the importance of the roughness height in predicting the friction coefficient C_f. The results reveal two flow regimes: one where the relative roughness height, Π_1^*, predominantly determines the friction factor ($R_1 \approx 1$), and a second regime where both the relative roughness height, Π_1^*, and the Reynolds number, Π_2^*, are needed to explain C_f. A similar conclusion can be drawn from R_2, which is omitted here for brevity. The regimes identified by IT-π are consistent with those from classical rough-wall turbulence analysis: the fully rough regime, where pressure drag dominates over viscous drag, and the transitionally rough regime, where both pressure and viscous drag influence the total drag (*36, 37*).

The Malkus-Howard-Lorenz Water Wheel (*38*) (see Figure 3, Column 4) is a mechanical system that exhibits chaotic dynamics. Water flows into compartments on a rotating wheel, creating complex, unpredictable motion similar to that observed in the Lorenz system (*39*). The dynamics of the system depend on the angular velocity (ω) and mass distributions (m_1 and m_2). The key system parameters include the wheel's radius (r), gravitational acceleration (g), moment of inertia (I), rotational damping (ν), leakage rate (K), and the water influx (ϕ).

Without loss of generality, we focus on the output $\dot{\omega}$, although the same approach extends to the other outputs, $\dot{m}_1$ and $\dot{m}_2$. The optimal dimensionless inputs discovered by IT-π are $\Pi_1^* = rgm_1/(IK^2)$ and $\Pi_2^* = \nu\omega/(IK^2)$ with the dimensionless output $\Pi_o^* = \dot{\omega}/K^2$, which recover the analytically derived dimensionless variables. The ranking in Figure 3(i) reports the predictive capabilities of the discovered $\mathbf{\Pi}^*$ groups. Using Π_1^* or Π_2^* alone as inputs results in $\%\tilde{\epsilon}_{LB}$ of 50% and 30%, respectively, while considering both of them reduces considerably the normalized irreducible error. Finally, IT-π uncovers the characteristic time and mass scales as $S_t = 1/K$ and $S_m = IK^2/(rg)$, along with the dimensionless parameter $\Pi_p = \nu/(IK)$. Hence, the dimensionless input and output can be rewritten as $\Pi_o^* = \dot{\omega}S_t^2$, $\Pi_1^* = m_1/S_m$, and $\Pi_2^* = \omega S_t \Pi_p$.

Applications

We have applied IT-π to dimensionless learning across several challenging problems, including supersonic turbulence, aerodynamic drag on both smooth and irregular surfaces, magnetohydrodynamic power generation, and laser-metal interaction. Here, we focus on the discovery of previously unknown scaling laws for supersonic flows over smooth and rough surfaces. The other applications can be found in the Methods section.

Accurate prediction of high-speed turbulence near solid boundaries is essential for advancing both commercial aviation and space exploration (*40*). However, significant challenges arise due to the complex interplay of the variables within these systems. The challenges are twofold. From a fundamental physics perspective, it is necessary to determine the scaling laws that govern key quantities of interest, such as mean velocity and wall fluxes. From a computational modeling standpoint, developing parsimonious models is needed for achieving accurate predictions. We leverage IT-π to tackle both challenges. We also demonstrate the use of the model efficiency in guiding the complexity of artificial neural network (ANN) to
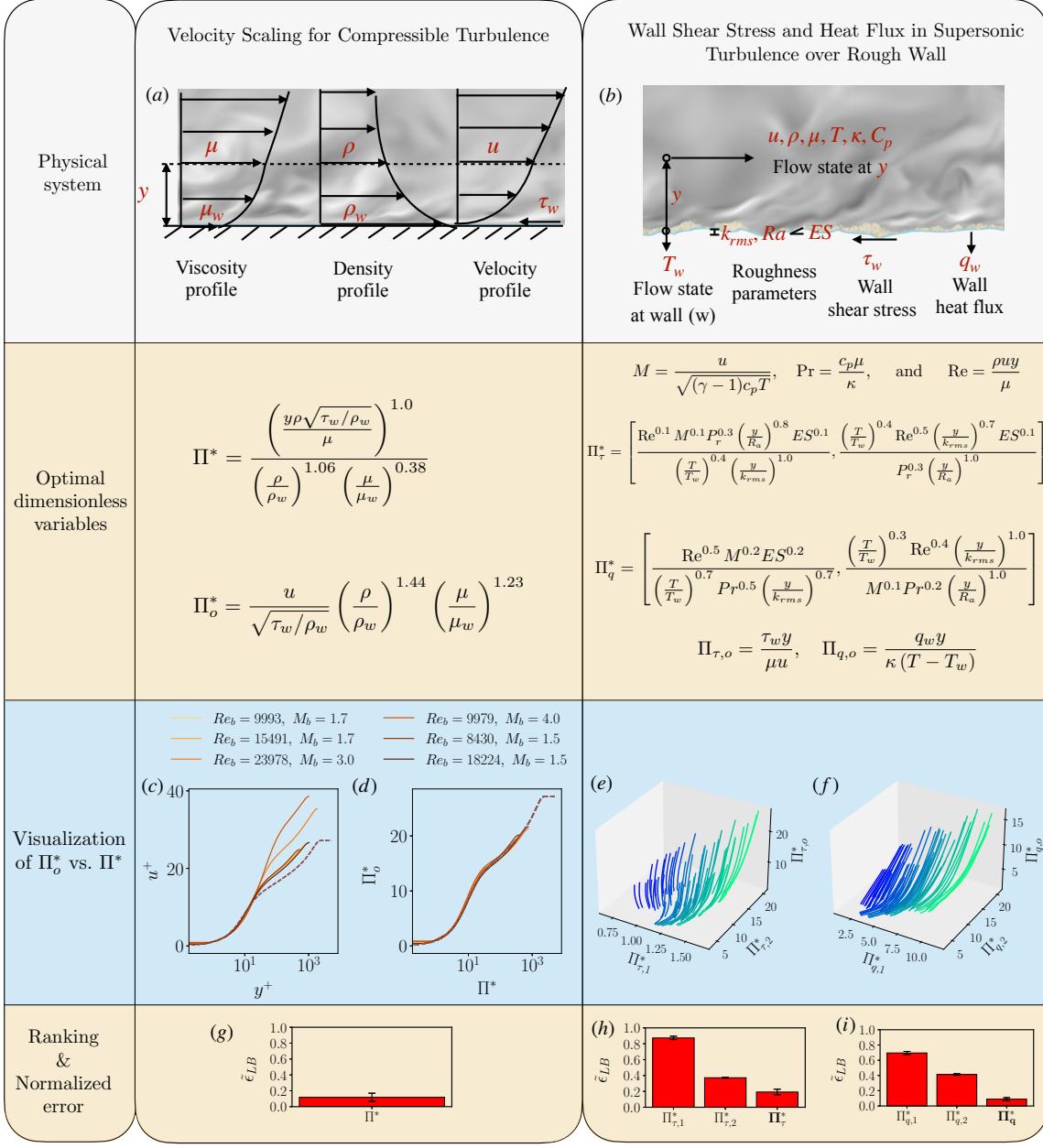
10

Velocity Scaling for Compressible Turbulence

Wall Shear Stress and Heat Flux in Supersonic Turbulence over Rough Wall

Physical system

(a)

μ ρ u

y

μ_w ρ_w τ_w

Viscosity profile · Density profile · Velocity profile

(b)

$u, \rho, \mu, T, \kappa, C_p$
Flow state at y

y

$k_{rms}, Ra < ES$

T_w Roughness parameters τ_w q_w
Flow state at wall (w) · Wall shear stress · Wall heat flux

Optimal dimensionless variables

$$\Pi^* = \frac{\left(\frac{y\rho\sqrt{\tau_w/\rho_w}}{\mu}\right)^{1.0}}{\left(\frac{\rho}{\rho_w}\right)^{1.06}\left(\frac{\mu}{\mu_w}\right)^{0.38}}$$

$$\Pi_o^* = \frac{u}{\sqrt{\tau_w/\rho_w}}\left(\frac{\rho}{\rho_w}\right)^{1.44}\left(\frac{\mu}{\mu_w}\right)^{1.23}$$

$$M = \frac{u}{\sqrt{(\gamma-1)c_pT}}, \quad Pr = \frac{c_p\mu}{\kappa}, \quad \text{and} \quad Re = \frac{\rho u y}{\mu}$$

$$\Pi_\tau^* = \left[\frac{Re^{0.1}M^{0.1}P_r^{0.3}\left(\frac{y}{R_a}\right)^{0.8}ES^{0.1}}{\left(\frac{T}{T_w}\right)^{0.4}\left(\frac{y}{k_{rms}}\right)^{1.0}}, \frac{\left(\frac{T}{T_w}\right)^{0.4}Re^{0.5}\left(\frac{y}{k_{rms}}\right)^{0.7}ES^{0.1}}{P_r^{0.3}\left(\frac{y}{R_a}\right)^{1.0}}\right]$$

$$\Pi_q^* = \left[\frac{Re^{0.5}M^{0.2}ES^{0.2}}{\left(\frac{T}{T_w}\right)^{0.7}Pr^{0.5}\left(\frac{y}{k_{rms}}\right)^{0.7}}, \frac{\left(\frac{T}{T_w}\right)^{0.3}Re^{0.4}\left(\frac{y}{k_{rms}}\right)^{1.0}}{M^{0.1}Pr^{0.2}\left(\frac{y}{R_a}\right)^{1.0}}\right]$$

$$\Pi_{\tau,o} = \frac{\tau_w y}{\mu u}, \quad \Pi_{q,o} = \frac{q_w y}{\kappa(T-T_w)}$$

Visualization of Π_o^* vs. Π^*

$Re_b = 9993, \ M_b = 1.7$ — $Re_b = 9979, \ M_b = 4.0$
$Re_b = 15491, \ M_b = 1.7$ — $Re_b = 8430, \ M_b = 1.5$
$Re_b = 23978, \ M_b = 3.0$ — $Re_b = 18224, \ M_b = 1.5$

(c) u^+ vs y^+

(d) Π_o^* vs Π^*

(e) $\Pi_{\tau,o}^*$ vs $\Pi_{\tau,1}^*$, $\Pi_{\tau,2}^*$

(f) $\Pi_{q,o}^*$ vs $\Pi_{q,1}^*$, $\Pi_{q,2}^*$

Ranking & Normalized error

(g) $\tilde{\epsilon}_{LB}$ — Π^*

(h) $\tilde{\epsilon}_{LB}$ — $\Pi_{\tau,1}^*$, $\Pi_{\tau,2}^*$, Π_τ^*

(i) $\tilde{\epsilon}_{LB}$ — $\Pi_{q,1}^*$, $\Pi_{q,2}^*$, Π_q^*

Figure 4: **Summary of compressible wall-bounded turbulence applications.** Left column: Velocity scaling for compressible turbulence. Right column: Wall shear stress and heat flux in supersonic turbulence over rough walls. (a, b) Schematic representations of the physical systems. (c, d): Solid lines of different colors represent velocity profiles at various Mach and Reynolds numbers; the dashed line corresponds to the incompressible turbulence velocity profile. (c) Viscous velocity profile u^+ versus y^+, where $u^+ = u/\sqrt{\tau_w/\rho_w}$ and $y^+ = y\rho\sqrt{\tau_w/\rho_w}/\mu$. (d) Dimensionless velocity profile obtained using IT-π scaling. (e, f): Dimensionless (e) wall shear stress and (f) wall heat flux plotted against the optimal dimensionless inputs. For compactness, the optimal dimensionless variables are expressed in terms of the Mach number (M), Prandtl number (Pr), and Reynolds number (Re), with definitions provided in the figure panels. The continuous lines represent data from the same simulation, colored by their mean Π_1^* to aid visualization. (g, h, i): Normalized irreducible error, with uncertainty shown as error bars reported in Figure 3, for (g) dimensionless velocity profile, (h) wall shear stress, and (i) wall heat flux. Additional details regarding the symbols and definitions of all variables are provided in the main text.

11

predict wall heat flux.

Dimensionless learning for mean velocity. Firstly, we discover a local scaling for the mean velocity profile in compressible turbulent channels using high-fidelity simulation data from existing literature (*41, 42*). The dataset, which spans different Reynolds and Mach numbers, includes the mean velocity $q_o = u$ and the flow state $\mathbf{q} = [y, \rho, \mu, \rho_w, \mu_w, \tau_w]$, where y is the wall-normal distance, ρ and μ are the local density and viscosity, ρ_w and μ_w are the density and viscosity at the wall, and τ_w is the wall shear stress. By limiting the number of inputs to one, IT-π identifies the optimal dimensionless variable with the highest predictive capabilities. The dimensionless inputs and outputs discovered by IT-π are summarized in Figure 4 (Column 2, Row 2). Panels (c) and (d) demonstrate that the scaling identified by IT-π improves the collapse of the compressible velocity profiles across the range of Mach and Reynolds numbers considered compared to the classic viscous scaling (*43*). A closer inspection of the dimensionless input and output variables reveals that this improvement is accomplished by accounting for local variations in density and viscosity.

Dimensionless learning for wall fluxes. Next, we identify the optimal dimensionless variables for predicting wall fluxes in compressible turbulence over rough walls (*23*). The output variables are the wall stress and heat flux, $q_o = [\tau_w, q_w]$, while the input variables are $\mathbf{q} = [y, u, \rho, T, T_w, \mu, \kappa, c_p, k_{rms}, R_a, ES]$. Here, y is the wall-normal distance; u, ρ, T, and μ represent the velocity, density, temperature, and viscosity, respectively; T_w is the wall temperature; κ is the thermal conductivity; and c_p is the specific heat capacity. The last three inputs (k_{rms}, R_a, ES) characterize the geometric properties of the surface roughness. These include the root-mean-square roughness height (k_{rms}), the first-order roughness height fluctuations (R_a), and the effective slope (ES) (*23*).

Figure 4 (Column 3, Row 2) summarizes the dimensionless forms of the optimal inputs and outputs discovered by IT-π. These forms combine the local Reynolds, Mach, Prandtl, and roughness numbers. The dimensionless wall shear stress and heat flux are presented in Figure 4(e,f) as functions of the identified dimensionless inputs. For both wall shear stress and heat flux, two dimensionless inputs were sufficient to achieve $\tilde{\epsilon}_{LB}^* \approx 0.1$, while the addition of further variables resulted in only marginal improvements in the irreducible error. Note that this number of variables is considerably smaller than the seven dimensionless variables anticipated by the Buckingham-π theorem.

Artificial neural network model for wall heat flux. To illustrate the application of the model efficiency η in guiding model complexity, we train three separate ANNs to predict the wall heat flux using the optimal dimensionless inputs from IT-π. The models are denoted by ANN_1, ANN_2 and ANN_3. Each model exhibits a different degree of complexity: ANN_1 has 9 tunable parameters (i.e., weights and biases), ANN_2 has 120, while ANN_2 has 781. The simplest model, ANN_1, achieves an efficiency of $\eta_1 = 30\%$, indicating the need for additional layers and neurons to better capture the underlying input-output relationships. The second model, ANN_2, improves upon this with an efficiency of $\eta_2 = 65\%$. The third model, ANN_3, attains an efficiency of $\eta_3 = 98\%$, essentially matching the information-theoretic limit in predictability. As a result, we can conclude that no additional model complexity is needed beyond ANN_3. We show in the Supplementary Materials that training an ANN of similar

complexity to ANN$_3$ using four suboptimal inputs from the Buckingham-π theorem results in a reduced efficiency of 82% despite using four inputs instead of two.

Comparison of IT-π with previous dimensionless learning methods

We compare IT-π against four dimensionless learning methods: Active Subspaces (*17*), PyDimension (*12*), BuckiNet (*15*), and BSM (*21*). BuckiNet specifically refers to the constrained optimization approach via kernel ridge regression, which is one of the three approaches proposed by Bakarji *et al.* (2022). The comparison spans all validation and application cases discussed above. A summary of each method's capabilities was provided in Table 1, and further details on their formulations are available in the Supplementary Materials.

The results are summarized in Table 2. The specific dimensionless variables identified by each method, along with implementation details and model parameters, are provided in the Methods section. Here, we offer an overview of the performance. In the validation cases, success is measured by the ability to recover the analytical optimal dimensionless variables. For the application cases—where ground-truth solutions are unknown—performance is quantified by the normalized irreducible error $\tilde{\epsilon}_{LB}$ associated with the input and output variables identified by each method, with lower values indicating better performance. The results clearly demonstrate that IT-π consistently outperforms or matches the other methods across both validation and application cases, particularly in the latter. It is worth noting that even in scenarios where existing methods successfully identify the optimal dimensionless variables, only IT-π is capable of simultaneously inferring key physical properties such as self-similar variables, distinct physical regimes, characteristic scales, and governing dimensionless parameters. Moreover, none of the other methods can provide a lower error bound that is independent of specific modeling assumptions.

In terms of computational cost, all methods generate solutions within seconds to minutes for the cases considered [see Table 3 in Methods]. Therefore, the predictability of the discovered dimensionless inputs and outputs is more important than the sheer computational cost of the method. This situation may change when dealing with a large number of samples. In such scenarios, IT-π offers efficient linear scaling with respect to the number of samples, performing similarly to or better than other methods. Beyond scaling, computational efficiency also depends on the structural design of the algorithm itself. Some of the previous approaches rely on a two-level optimization process, involving an outer loop that searches over candidate input combinations (e.g., powers of dimensionless groups), and an inner loop that fits model parameters (e.g., regression coefficients) to evaluate the performance of each candidate. In contrast, IT-π eliminates this overhead by directly evaluating the irreducible model error, bypassing the need to fit any model.

Discussion

The concept of dimensional homogeneity—i.e., the invariance of physical laws under transformation of units—is arguably one of the most fundamental principles in physics. This simple yet powerful idea gave rise to the field of dimensional analysis, which is widely used across multiple disciplines. In this work, we have introduced IT-π, a formulation of dimensional anal-

Method	Active Subspaces	PyDim-ension	Bucki-Net	BSM	IT-π (Current)
Rayleigh problem	✓	✓	✓	✓	✓
Colebrook equation	✓	×	✓	×	✓
Malkus waterwheel	×	×	×	×	✓
Rayleight-Bénard convection	×	✓	×	×	✓
Blasius boundary layer	✓	✓	✓	✓	✓
Velocity scaling	72%	21%	50%	N/A	12%
Wall shear stress	78%	54%	74%	N/A	19%
Wall heat flux	62%	44%	37%	N/A	9%
Skin friction	19%	27%	75%	N/A	17%
MHD generator	7%	7%	98%	N/A	5%
Laser–metal interaction	94%	25%	100%	N/A	23%

Table 2: Comparison of Active Subspaces, PyDimension, BuckiNet, and BSM across validation and application cases: Rayleigh problem, Colebrook equation, Malkus waterwheel, Rayleight-Bénard convection, Blasius boundary layer, Velocity scaling, Wall flux, Skin friction, MHD generator, Laser-metal interaction. For the validation cases, the table presents whether the methods could identify the correct dimensionless variables for validations cases (✓ or ×). For the application cases, the table shows the normalized irreducible error $\tilde{\epsilon}_{LB}$ associated to the dimensionless input and output variables identified by each method with lower values indicating better performance.

ysis based on information. Our approach is rooted in the information-theoretic irreducible error, which allows us to identify the most predictive dimensionless numbers with respect to a quantity of interest. The idea goes beyond merely identifying a unique set of variables; it is the realization that the information content in the variables of a system is fundamental to understanding the governing physical laws and their inherent limitations (*25, 44, 45*). One can view IT-π as the *Carnot cycle of physical laws*: just as the thermodynamic Carnot cycle sets an upper limit on the work extractable from two thermal reservoirs—irrespective of the engine's technology—IT-π extends this principle to predictive models irrespective of the modeling approach. In this interpretation, the predictive power of a set of variables is fundamentally constrained by the amount of information they share with the quantity to be predicted, regardless of whether the relationships are modeled through linear regression, sophisticated neural networks, or analytical equations.

We have shown that IT-π offers a complete set of dimensionless learning tools, including ranking inputs by predictability, identifying distinct physical regimes, uncovering self-similar variables, and extracting characteristic scales and dimensionless parameters. IT-π is also sensitive to the norm used to quantify errors and the optimal set of dimensionless variables may vary depending on the error metric of interest (e.g., prediction of ordinary versus rare events). Although some of these features are available through other methods, none encompass them all. Even in cases where alternative methods apply, IT-π distinguishes itself by being grounded in a theorem rather than relying on heuristic reasoning. This makes IT-π independent of specific modeling assumptions.

In additional to its model-free nature, IT-π offers unique capabilities that other methods

do not, such as establishing bounds on the irreducible error and evaluating model efficiency. The former allows us to precisely determine the actual number of relevant dimensionless variables, l^*, which is typically overestimated by the Buckingham-π theorem. Moreover, IT-π quantifies the degree of dynamic similarity achievable with the optimal variables, rather than providing merely a binary yes-or-no answer as classical dimensional analysis does. This feature can be decisive in designing laboratory experiments for extrapolation to real-world applications. For example, consider predicting the heat flux over a rough surface as discussed in the application above. According to Buckingham-π, seven dimensionless variables would be required. If three different values must be measured to capture the scaling behaviour of each variable, that would entail approximately $3^7 = 2,187$ experiments. In contrast, IT-π determined that only two dimensionless variables are necessary to achieve a dynamic similarity of 92% (i.e., an 8% normalized irreducible error). This entails a significantly reduced effort of only $3^2 = 9$ experiments. The same reasoning applies to the construction of predictive modeling: models with fewer inputs require orders of magnitude less training data compared to those with high-dimensional inputs. In the previous example, this factor would be of the order of 1,000.

Model efficiency is another distinctive feature of IT-π that can guide the structural complexity in model design. For instance, machine-learning models are typically built with various architectures and tunable parameters (e.g., weights and biases). In this context, the model efficiency can determine whether a model operates near its theoretical optimum— eliminating the need to explore alternative architectures—or if there is potential for further improvement. We have applied this concept to determine the optimal number of tunable parameters for developing an ANN model for wall heat prediction. Our results have shown that ANNs with only a few tens of parameters fail to fully leverage the available input information, whereas nearly 1,000 parameters are necessary to extract that information efficiently.

We have successfully validated IT-π using cases with established optimal dimensionless variables. These include classic problems in fluid dynamics and dynamical systems, such as the Rayleigh problem, the Colebrook equation, the Malkus-Howard-Lorenz water wheel, the Rayleigh-Bénard convection, and the Blasius laminar boundary layer. Moreover, IT-π was applied to conduct dimensionless learning for supersonic turbulence, aerodynamic drag on both smooth and irregular surfaces, MHD power generation, and high-energy material processing. In all cases, IT-π has been shown to outperform or match existing methods for dimensionless learning.

It is also important to acknowledge some shortcomings of the approach. The first relates to its model-free nature. As mentioned above, one of the key strengths of IT-π is that its results do not depend on any underlying model. However, some may view this as a weakness, as it leaves the task of identifying the optimal model to the practitioner. A more evident challenge is the amount of data required. When many variables are involved, IT-π necessitates the estimation of mutual information in high dimensions. Although advanced tools exist for high-dimensional estimation (*46–50*), the curse of dimensionality can render results inconclusive in certain scenarios. Therefore, estimating the uncertainty in the normalized irreducible error is crucial to determine whether the conclusions drawn from IT-π are statistically significant or merely reflect insufficient data. In all the results presented above, we have quantified the statistical uncertainty in the irreducible error, $\Delta\epsilon_{LB}$, which is represented by the error bars in the plots. The methodology used to estimate uncertainty in IT-π under a finite sample

regime is detailed in the Supplementary Materials, along with a further evaluation of the sensitivity of IT-π to the amount of available data.

In conclusion, IT-π offers a new perspective to dimensional analysis rooted in information. Its broad applicability makes it a useful tool across diverse disciplines—from fluid dynamics and thermodynamics to electromagnetism, astrophysics, materials science, and plasma physics. By effectively addressing challenges in scaling laws, similarity solutions, and the identification of governing dimensionless parameters, IT-π provides a powerful tool for dimensionless learning of complex physical systems.

Methods

Constructing dimensionless variables using the Buckingham-π theorem

The Buckingham-π theorem is used to construct dimensionless candidates $\mathbf{\Pi}$ and Π_o. The i-th dimensionless variable has the form

$$\Pi_i = q_1^{a_{i1}} \cdot q_2^{a_{i2}} \cdots q_n^{a_{in}} \equiv \mathbf{q}^{\mathbf{a}_i},$$

where $\mathbf{a}_i = [a_{i1}, a_{i2}, \ldots, a_{in}]^T$ is the vector of exponents for Π_i. The input candidate $\mathbf{\Pi}$ is then obtained from the solution to $\mathbf{D}\mathbf{a}_i = 0$, where $\boldsymbol{D}$ is the dimension matrix containing the powers of the fundamental units for $\mathbf{q}$, $\mathbf{D} = [\mathbf{d}_1, \mathbf{d}_2, \ldots, \mathbf{d}_n]$, and $\mathbf{d}_i$ is the dimensional vector for the physical quantity q_i. For example, the velocity $q_1 = u = [\text{length}]^1[\text{time}]^{-1}$ has $\mathbf{d}_1 = [1, -1, 0, 0, 0, 0, 0]^T$ and so on. The solution $\mathbf{a}_i$ can be expressed as $\mathbf{a}_i = \sum_{j=1}^{n-n_u} c_{ij}\mathbf{w}_j = \mathbf{W}\mathbf{c}_i$, where $\mathbf{W} = [\mathbf{w}_1, \mathbf{w}_2, \ldots, \mathbf{w}_{n-n_u}]$ is the matrix of basis vectors of the null space of $\mathbf{D}$, and $\mathbf{c}_i = \left[c_{i1}, c_{i2}, \ldots, c_{i(n-n_u)}\right]^T$ is the coefficient vector corresponding to $\mathbf{a}_i$. In conclusion, non-dimensional variables are obtained by $\mathbf{\Pi} = \mathbf{q}^{\mathbf{WC}} = \left[\mathbf{q}^{\mathbf{Wc}_1}, \mathbf{q}^{\mathbf{Wc}_2}, \ldots, \mathbf{q}^{\mathbf{Wc}_l}\right]$, where $\mathbf{C} = [\mathbf{c}_1, \mathbf{c}_2, \ldots, \mathbf{c}_l]$. The dimensionless output Π_o is constructed similarly with the matrix of basis vectors $\mathbf{W}_o$ and coefficients $\mathbf{c}_o$. An important consideration when some variables q_i may be negative is to generalize the formulation to avoid imaginary numbers. Specifically, we define $\Pi_i = \text{sgn}(q_1)\,|q_1|^{a_{i1}}\,\text{sgn}(q_2)\,|q_2|^{a_{i2}} \cdots \text{sgn}(q_n)\,|q_n|^{a_{in}}$, where $|\cdot|$ denotes the absolute value and $\text{sgn}(\cdot)$ is the sign function. This approach preserves the sign information of each q_i while ensuring that the resulting dimensionless variables remain real-valued.

Information content of variables

Consider the random variables Π_o and $\mathbf{\Pi}$, whose realizations are denoted by π_o and π, respectively. They are characterized by the joint probability distribution $\rho_{\Pi_o, \mathbf{\Pi}}(\pi_o, \pi)$ with corresponding marginal distributions $\rho_{\Pi_o}(\pi_o)$ and $\rho_{\mathbf{\Pi}}(\pi)$. The Rényi mutual information of order $\alpha > 0$ (*30*) between Π_o and $\mathbf{\Pi}$ is

$$I_\alpha(\Pi_o; \mathbf{\Pi}) = h_\alpha(\Pi_o) - h_\alpha(\Pi_o \mid \mathbf{\Pi}),$$

where $h_\alpha(\Pi_o)$ and $h_\alpha(\Pi_o|\mathbf{\Pi})$ are the Rényi entropy and conditional Rényi entropy, respectively, which are given by

$$h_{\alpha,o} \equiv h_\alpha(\Pi_o) = \lim_{\alpha' \to \alpha} \frac{1}{1-\alpha'} \log\left(\int \rho_{\Pi_o}^{\alpha'}(\pi_o)\, \mathrm{d}\pi_o\right),$$

$$h_\alpha(\Pi_o|\mathbf{\Pi}) = \lim_{\alpha' \to \alpha} \frac{1}{1-\alpha'} \int \rho_{\mathbf{\Pi}}(\pi) \log\left(\int \rho_{\Pi_o|\mathbf{\Pi}}^{\alpha'}(\pi_o \mid \pi)\, d\pi_o\right) d\pi.$$

The Rényi mutual information between Π_o and $\mathbf{\Pi}$ quantifies the amount of information about Π_o that can be extracted from $\mathbf{\Pi}$. It generalizes the Shannon mutual information (*29*) by introducing the order parameter α, which is particularly valuable in situations where emphasis on tail distributions is critical. IT-π leverages the parameter α to adjust sensitivity with respect to the L_p-norm, balancing the influence of high-probability events against that of low-probability events. When the value of α is equal to one, the Rényi entropy corresponds to the Shannon entropy (*29*).

Optimization with CMA-ES

The optimal dimensionless input and output variables are identified by solving Eq. (2), where the candidate sets $\mathbf{\Pi}$ and Π_o are constructed using the previously defined coefficient matrix $\mathbf{C}$. The optimization is carried out over the entries of $\mathbf{C}$. Specifically, the problem $\arg\min_{\mathbf{\Pi},\Pi_o} \max_\alpha[\epsilon_{LB}]$ is solved using the Covariance Matrix Adaptation Evolution Strategy (CMA-ES) (*31*), a stochastic, derivative-free algorithm designed for non-linear and non-convex continuous optimization problems. CMA-ES generates candidate solutions by sampling from a multivariate Gaussian distribution and iteratively updates its mean and covariance matrix to efficiently explore the search space and converge toward an optimal solution that maximizes the mutual information. To determine the value of α that yields the tightest possible bound, $\max_\alpha[\epsilon_{LB}]$, we perform a golden-section search over the interval $\alpha \in (1/(1+p), 10]$ (*51*). A schematic overview of the IT-π workflow for discovering optimal dimensionless variables is shown in Fig. 5, and the corresponding pseudocode is provided in the Supplementary Materials.

In the main text, the error norm is set to $p = 2$, which is the standard choice for measuring prediction errors. An illustrative example demonstrating the use of alternative L_p norms is provided in the Supplementary Materials. The CMA-ES algorithm is executed with a population size of 300, coefficient bounds $c_{ij} \in [-2, 2]$, a maximum of 50,000 iterations, and an initial standard deviation of 0.5. For all cases presented above, the exponents c_{ij} are rounded to a finite number of significant digits without compromising the value of ϵ_{LB}. When Π_o^*, p, and α are fixed, the function $c(\alpha, p, h_{\alpha,o})$ becomes identical, and the task of identifying the most predictive non-dimensional input simplifies to maximizing mutual information: $\mathbf{\Pi}^* = \arg\max_{\mathbf{\Pi}} I_\alpha(\Pi_o^*; \mathbf{\Pi})$.

Details about validations cases

The Rayleigh problem dataset consists of samples uniformly generated over $y \in [0, 1]$m, $t \in [0.01, 5]$s, $U \in [0.5, 1.0]$m/s, $\mu \in [10^{-3}, 10^{-2}]\,\mathrm{kg/m/s}$ and $\rho = 1\mathrm{kg/m}^3$. For the Colebrook
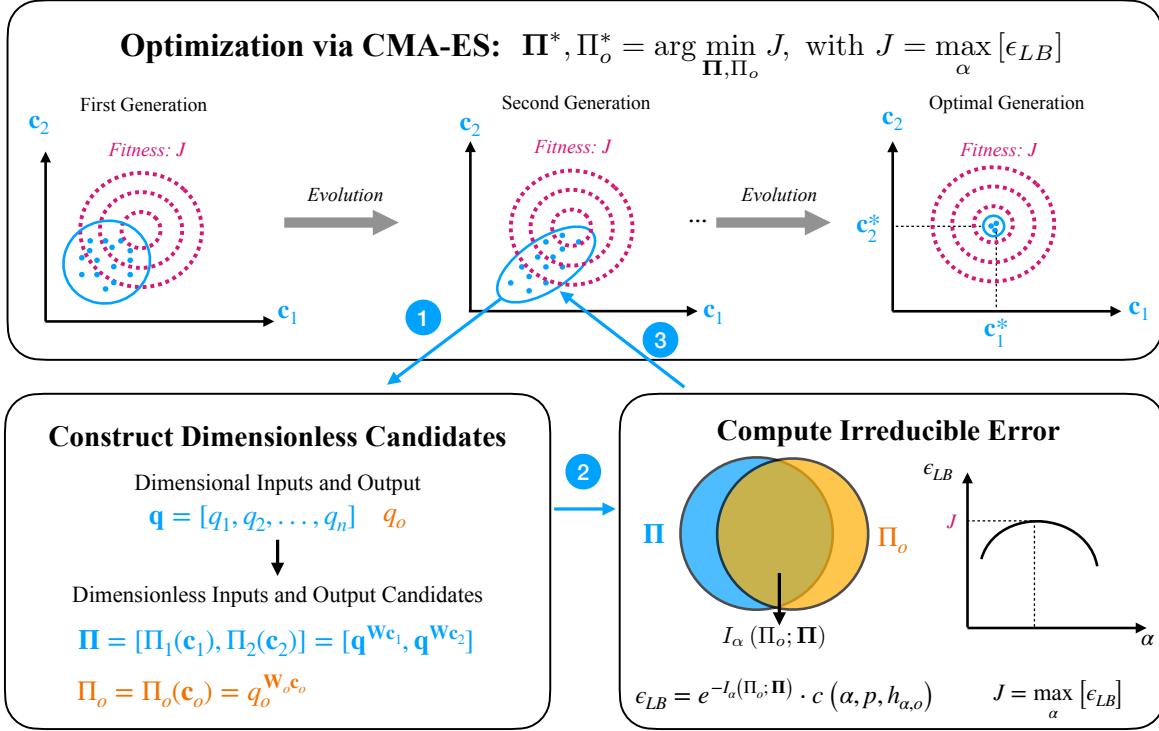
Figure 5: Workflow of IT-π for discovering optimal dimensionless variables. This schematic illustrates a specific example in which the input dimensionless variables $\mathbf{\Pi} = [\Pi_1, \Pi_2]$ are optimized. Each generation of the CMA-ES algorithm maintains a population of candidate solutions (represented by blue dots), where each individual encodes a set of exponents $(\mathbf{c}_1, \mathbf{c}_2)$ that define the candidate dimensionless variables. For each individual, the variables are constructed as $\Pi_1 = \mathbf{q}^{\mathbf{Wc}_1}$ and $\Pi_2 = \mathbf{q}^{\mathbf{Wc}_2}$, where $\mathbf{q}$ represents the set of dimensional quantities and $\mathbf{W}$ is the matrix of basis vectors. The fitness of each candidate is evaluated using the irreducible error across Rényi orders, $J = \max_\alpha[\epsilon_{LB}] = \max_\alpha \left[e^{-I_\alpha(\Pi_o; \mathbf{\Pi})} \cdot c(\alpha, p, h_{\alpha, o}) \right]$, where I_α denotes the Rényi mutual information. The optimal α is found through golden-section search in the range $(1/(1 + p), 10]$. The algorithm evolves the population across generations by updating the mean and covariance of the sampling distribution, navigating the fitness landscape (whose constant-value contours are shown as dark purple dashed lines) to minimize the irreducible error. The final generation yields the maximally predictive dimensionless variables $\mathbf{\Pi}^* = [\Pi_1^*, \Pi_2^*] = [\mathbf{q}^{\mathbf{Wc}_1^*}, \mathbf{q}^{\mathbf{Wc}_2^*}]$. The dimensionless output Π_o can either be included in the optimization or treated as fixed. For clarity, this schematic illustrates only the optimization of $\mathbf{c}_1$ and $\mathbf{c}_2$ associated with the input variables.

dataset, $\log_{10} Re_D$ is uniformly sampled in $[3,5]$, yielding Reynolds numbers in $[10^3, 10^5]$, and $\log_{10}(k/D)$ is uniformly sampled in $[-5, -0.7]$. The discovered dimensionless inputs $[\Pi_1^*, \Pi_2^*]$ are divided into 10 clusters using the K-Nearest Neighbors (KNN) clustering algorithm (*52*). For the Malkus waterwheel dataset, the physical variables are uniformly sampled within the following ranges: radius $r \in [0.3, 0.7]$m, water influx rate $q \in [0.0001, 0.0005]$kg/s, moment of inertia $I \in [0.05, 0.2]$kg$\cdot$m^2, rotational damping $\nu \in [0.01, 0.1]$kg$\cdot$m^2/s, and water leakage

rate $K \in [0.01, 0.1]\mathrm{s}^{-1}$, gravitational acceleration $g = 9.8\mathrm{m/s}^2$. The system is simulated over a time span of $t \in [0, 50]\mathrm{s}$ with 500 evaluation points.

Details about application cases

Data for compressible wall-bounded turbulence application
The dataset for mean-velocty transformation comprises mean flow profiles from direct numerical simulation (DNS) of four compressible channel flows and two compressible pipe flows (*41,42*), characterized by bulk Mach numbers $\left(M_b = U_b/\sqrt{\gamma RT_w}\right)$ between 1.5 and 4.0, and bulk Reynolds numbers $(Re_b = \rho_b U_b \delta/\mu_w)$ from 8430.2 to 23977.6, where $\rho_b = 1/\delta \int_0^\delta \rho dy$ and $U_b = 1/\delta \int_0^\delta u dy$ are the bulk density and velocity, respectively; T_w and μ_w are the mean temperature and dynamic viscosity at the wall; and δ is the channel half-height. The dataset for wall shear stress and heat flux in supersonic turbulence over rough wall includes DNS of turbulent channel flows over and rough surfaces (*23*). Ten irregular, multiscale rough surfaces were generated using Gaussian probability density functions. Simulations were driven with uniform momentum and energy sources to achieve $M_c = U_c/\sqrt{\gamma RT_w} = 0.5, 1, 2, 4$ and $Re_c = \rho_c U_c \delta/\mu_w = 4000, 8000, 16000$, where ρ_c and U_c are the mean density and velocity at the channel centerline, respectively; T_w and μ_w are the mean temperature and dynamic viscosity at the wall; and δ is the channel half-height.

Neural networks for predicting the wall flux
The data is split into training (70%), validation (15%), and testing (15%) sets, with L_2 regularization (factor 0.9) used to control overfitting. Each network follows a feedforward architecture. The simplest network ANN_1 consists of 1 hidden layers with 2 neurons, ANN_2 have 2 hidden layers with 10 neurons per layer, while ANN_3 have 4 hidden layers with 15 neurons per layer. All are trained using gradient descent with momentum and an adaptive learning rate. The training process employs a learning rate of 10^{-5}, with a maximum of 50000 iterations and a validation tolerance of 40,000 epochs without improvement before stopping.

Additional validation cases

We validate IT-π using datasets from previous studies (*12,15,21*) with known optimal dimensionless inputs: the turbulent Rayleigh–Bénard convection and the Blasius laminar boundary layer. Figure 6 summarizes each case, detailing the system equations, optimal dimensionless inputs and outputs discovered from IT-π. The figure also shows a visualization of Π_o^* as a function of $\mathbf{\Pi}^*$.

The Rayleigh–Bénard convection system (Figure 6, Column 2) describes convection occurring in a planar horizontal layer of fluid heated from below in a container with height h. The system is governed by the equations in Figure 6 (Column 2, Row 2), with parameters include viscosity (μ), density (ρ), temperature differences between the top and the bottom plane (ΔT), thermal expansion coefficient (α), and thermal diffusivity (κ). The dimensionless output is set to the Nusselt number $\Pi_o^* = q_w h/(\lambda \Delta T)$, where q_w is the heat flux, λ is the thermal conductivity. The data (*12*) include samples of the output

$q_o = q_w$, inputs $\mathbf{q} = [h, \Delta T, \lambda, g, \alpha, \mu, \rho, \kappa]$. IT-$\pi$ discovered the optimal dimensionless input $\Pi^* = \rho h^3 \Delta T g \alpha / (\mu \kappa)$, which is consistent with the Rayleigh number (*53*).

The Blasius laminar boundary layer (Figure 6, Column 3) describes the two-dimensional laminar boundary layer that forms on a semi-infinite plate which is held parallel to a constant unidirectional flow. The system is governed by the equations in Figure 6 (Column 3, Row 2), with variables including the streamwise velocity (u), wall-normal velocity (v), free-stream velocity (U), pressure (p), viscosity (μ), density (ρ), streamwise distance (x) and wall normal distance (y). We focus on the output u. The data (*15*) include samples of the output $q_o = u$, and inputs $\mathbf{q} = [U, \mu, \rho, x, y]$. IT-$\pi$ discovers the optimal, self-similar, dimensionless input $\Pi^* = U^{0.5} y^{1.0} \rho^{0.5} / (\mu^{0.5} x^{0.5})$, which is equivalent to the analytical Blasius similarity variable (*54*).

Additional application cases

Skin friction under pressure gradient effects
We apply IT-π to identify the most predictive model for wall friction in turbulent flow over smooth surfaces under different mean pressure gradients. Friction scaling and predictive modeling in smooth-wall turbulence have been extensively studied for over a century, owing to their crucial role in reducing operational costs in engineering applications such as pipeline transport and aviation. We use the data compiled by Dixit et al. (*55*), which includes experimental measurements and simulation results for various flow conditions: mean zero-pressure-gradient (ZPG) flows in channels, pipes, and turbulent boundary layers; mean adverse-pressure-gradient (APG) turbulent boundary layers; mean favorable-pressure-gradient (FPG) turbulent boundary layers; and turbulent boundary layers on the pressure side of an airfoil. For a detailed description of the data, please refer to Dixit et al. (*55*) and the references therein.

The dimensional input variables include $q = [U_\infty, \mu, \rho, M, \delta, \delta^*, \theta_m]$, where U_∞ is the free-stream velocity, μ is the viscosity, ρ is the density, $M = \int_0^\delta u^2 dy$ is the total mean-flow kinetic energy, δ is the boundary layer thickness at 99% of the free-stream, $\delta^* = \int_0^\delta (1 - u/U_\infty) \, dy$ is the boundary layer displacement thickness, and $\theta_m = \int_0^\delta u/U_\infty (1 - u/U_\infty) \, dy$ is the boundary layer momentum thickness, where y is the wall-normal distance. The output variable $q_o = u_\tau = \sqrt{\tau_w / \rho_w}$ is the friction velocity, with τ_w the wall shear stress and ρ_w the flow density at the wall. We define the dimensionless output as $\Pi_o^* = u_\tau / U_\infty$, where u_τ is the friction velocity, as this is a common form for modeling skin friction. For simplicity, we restrict the number of input variables to one. Under these conditions, IT-π identifies the most predictive single variable as

$$\Pi^* = \left(\frac{\rho U_\infty \delta}{\mu} \right)^{\frac{4}{7}} \left(\frac{\delta^*}{\theta_m} \right)^{\frac{9}{10}} \left(\frac{U_\infty \mu}{\rho M} \right)^{\frac{4}{9}},$$

with the exponents constrained to be rational numbers. Figure 7(g),(h) demonstrates that the scaling identified by IT-π significantly improves the collapse of the friction velocity data compared to the classic approach (*43*). Π^* is the product of three dimensionless groups: the first two correspond to the classic free-stream Reynolds number and the shape factor. The
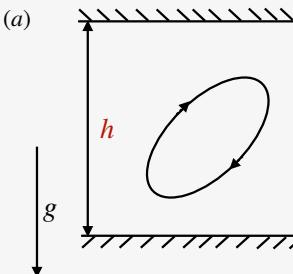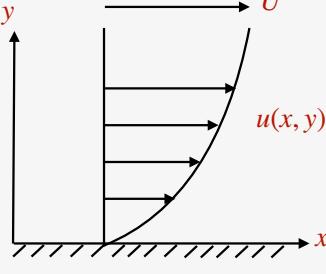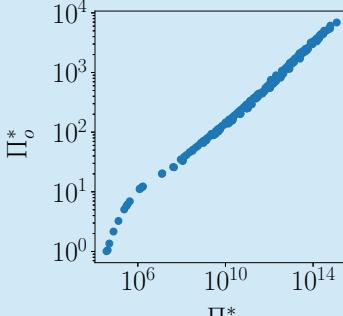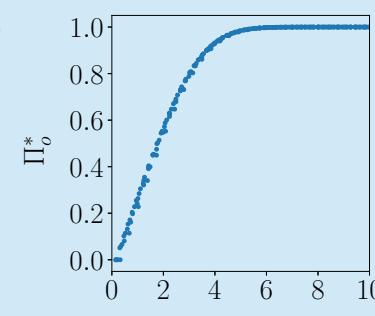
	Turbulent Rayleigh-Bénard convection	Blasius laminar boundary layer
Physical system	(a) T, h, g, Heat flux: q_w, Fluid properties: $\lambda, \alpha, \mu, \rho, \kappa$, $T + \Delta T$	(b) y, U, $u(x,y)$, x
Equation	(c) $\dfrac{\partial \mathbf{u}}{\partial t} + \mathbf{u} \cdot \nabla \mathbf{u} = -\dfrac{\nabla p}{\rho} + \dfrac{\mu}{\rho}\nabla^2 \mathbf{u} + g\alpha\Delta T$ $\nabla \cdot \mathbf{u} = 0$ $\dfrac{\partial T}{\partial t} + \mathbf{u} \cdot \nabla T = \kappa \nabla^2 T$ $q_w = -\lambda \dfrac{\partial T}{\partial y}$	(d) $\dfrac{\partial u}{\partial x} + \dfrac{\partial v}{\partial y} = 0$ $u\dfrac{\partial u}{\partial x} + v\dfrac{\partial u}{\partial y} = -\dfrac{1}{\rho}\dfrac{\partial p}{\partial x} + \dfrac{\mu}{\rho}\dfrac{\partial^2 u}{\partial y^2}$ $\dfrac{\partial p}{\partial y} = 0$
Optimal dimensionless variables	(e) $\Pi^* = \dfrac{\rho h^3 \Delta T g \alpha}{\mu \kappa}$ $\Pi_o^* = \dfrac{q_w h}{\lambda \Delta T}$	(f) $\Pi^* = \dfrac{U^{0.5} y^{1.0} \rho^{0.5}}{\mu^{0.5} x^{0.5}}$ $\Pi_o^* = \dfrac{u}{U}$
Visualization of Π_o^* vs. Π^*	(g)	(h)

Figure 6: **Summary of additional validation cases**. System equations, optimal dimensionless inputs and outputs discovered from IT-π, visualization of Π_o^* as a function of Π^*. Additional details regarding the symbols and definitions are provided in the main text.

third term is more interesting: it represents the transfer of kinetic energy from mean flow to large eddies of turbulence, which is derived from the momentum integral equation by Dixit et *al.* (*56*) .

Magnetohydrodynamics power generator

Magnetohydrodynamic (MHD) generators represent an innovative solution for sustainable and clean energy production (*57, 58*). Unlike conventional generators that rely on moving mechanical components—such as turbines—MHD generators convert thermal energy directly into electrical power. This direct conversion not only minimizes mechanical losses but also allows these systems to operate efficiently at extremely high temperatures (*58*). Moreover, owing to their unique operational characteristics, MHD generators offer the highest theoretical thermodynamic efficiency among all established methods of electricity generation. In this section, we employ IT-π to identify the critical dimensionless input variables governing the flow velocity within the generator.

The dataset used is obtained from numerical simulations of steady-state MHD duct flow reported by Glaws *et al.* (*59*). In this MHD generator configuration, an electric current is induced by propelling a conducting fluid through a square cross-sectional duct at a specified flow rate while subjecting it to an externally applied vertical magnetic field. The interaction between the moving fluid and the magnetic field causes the field lines to bend, thereby producing a horizontal electric current. The set of dimensional input variables is defined as $\mathbf{q} = \left[h, \mu, \rho, \frac{dp}{dx}, \eta, B_0\right]$, where h denotes the side length of the square duct, μ and ρ represent the viscosity and density of the conducting fluid, respectively, $\frac{dp}{dx}$ is the applied pressure gradient, η is the magnetic resistivity of the fluid, and B_0 is the magnitude of the applied magnetic field.

The quantity to predict is the average flow velocity, u, and we are interested in identifying the single dimensionless input with the highest predictive capability. Using the dimensionless output $\Pi_o^* = u\,\rho\,h/\mu$, IT-π identifies the most predictive dimensionless input as $\Pi^* = h^3\,\rho\,\frac{dp}{dx}/\mu^2$. This result is consistent with physical intuition: the average flow velocity is fundamentally governed by the balance between the driving force (represented by the pressure gradient) and the resisting force (arising from viscosity). Hence, the dimensionless group Π^* encapsulates the interplay between these competing effects.

Laser-metal interaction

Quantifying laser–metal interactions is critical for improving precision in advanced manufacturing processes such as additive manufacturing, laser cutting, and welding in aerospace applications (*60*). We employ IT-π to identify the single most predictive dimensionless input governing the formation of a keyhole in a puddle of liquid metal melted by the laser.

The dataset used comes from high-speed X-ray imaging experiments of keyhole dynamics reported by Xie *et al.* (*12*). The set of dimensional input variables is defined as

$$\mathbf{q} = \left[\eta P, V_s, r_0, \alpha, \rho, C_p, T_1 - T_0\right],$$

where ηP denotes the effective laser power, V_s represents the laser scan speed, r_0 is the laser beam radius, and α, ρ, and C_p are the thermal diffusivity, density, and heat capacity of the material, respectively. $T_1 - T_0$ is the temperature difference between melting and ambient
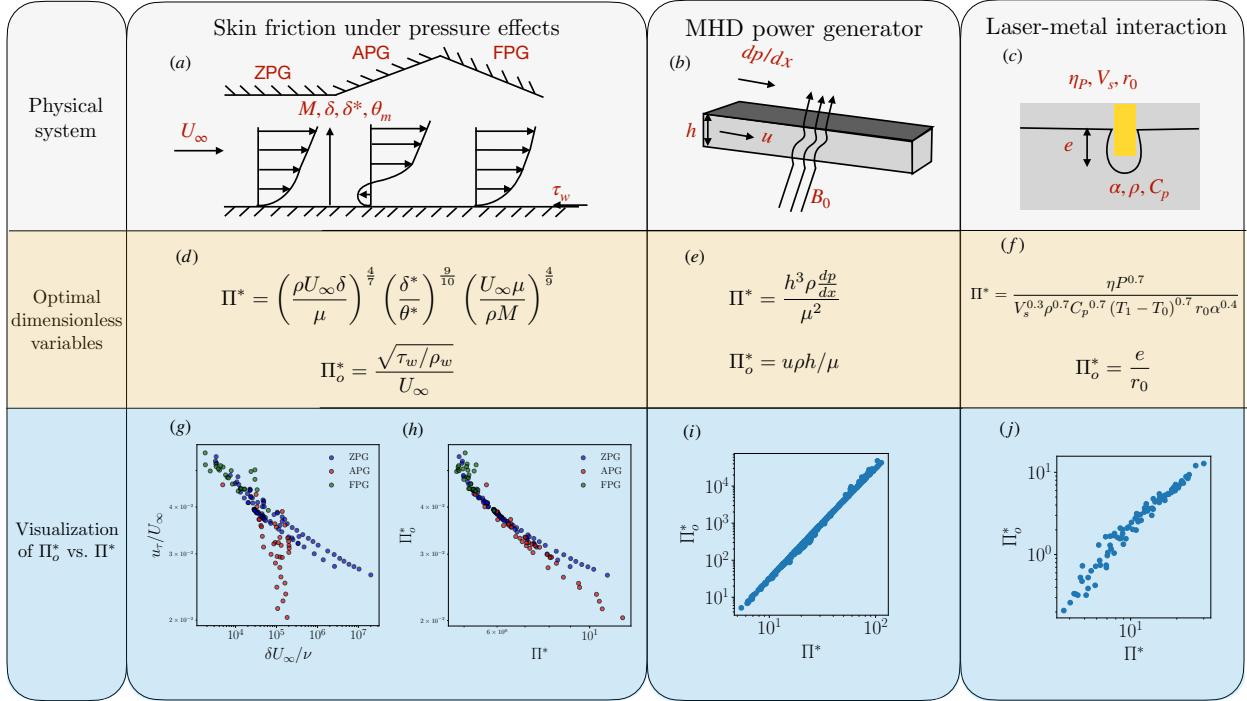
Figure 7: **Summary of additional application cases**. System schematic, optimal dimensionless inputs and outputs discovered from IT-π, visualization of Π_o^* as a function of Π^*. Additional details regarding the symbols and definitions are provided in the main text.

conditions. The quantity of interest is the normalized keyhole depth, defined as $\Pi_o^* = e/r_0$. IT-π identifies the most predictive dimensionless input as $\Pi^* = \frac{\eta P^{0.7}}{V_s^{0.3}\rho^{0.7}C_p^{0.7}(T_1-T_0)^{0.7}r_0\alpha^{0.4}}$.

Details about comparison with other dimensionless learning methods

The dimensionless input discovered by other methods using the same output Π_o^*, is summarized in the Supplementary Material. Active Subspaces employs Gaussian Process Regression with a radial basis function (RBF) kernel, which is initialized with a width of 1 and optimized using 5 restarts. The gradients of the response surface are estimated using finite differences. PyDimension uses a 10th-order polynomial regression model, optimizing the basis coefficients with a pattern search method that is initialized on a grid ranging from -1 to 1 in intervals of 0.1. BuckiNet utilizes Kernel Ridge Regression with an RBF kernel (width $= 1$) and a regularization parameter of 1×10^{-4}. Its optimization includes an L_1 regularization term of 1×10^{-3}. For BSM, the optimization minimizes a distance-based loss over 40 iterations, balancing prediction accuracy and dimensional consistency with a weight of 1×10^{-3}. It is also worth noting that the results were found to be sensitive to the model parameters for each method. For all validation cases where the optimal solution is known, we tune the hyperparameters of all baseline methods to best match the known results. In application cases (where the true solution is not known), we evaluate the performance of existing methods using the standard or recommended hyperparameter settings provided by their original

implementations. This approach reflects practical usage scenarios, where domain users often rely on default or minimally tuned settings. A discussion on the influence of hyperparameters and the sensitivity of each method is provided in the Supplementary Material.

Method	Active Subspaces	PyDimension	Bucki-Net	BSM	IT-π (Current)
Rayleigh problem	10.1	0.2	7.1	1.4	8.8
Colebrook equation	8.6	0.1	14.3	N/A	2.5
Malkus waterwheel	36.5	1.2	269	N/A	214
Rayleight-Bénard convection	2.6	2.7	1.8	N/A	7.0
Blasius boundary layer	0.6	0.4	1.7	1.6	1.2
Velocity scaling	23.9	4.8	9.5	N/A	10.6
Wall shear stress	522	109	236	N/A	29.4
Wall heat flux	688	288	894	N/A	28.6
Skin friction	0.2	3.5	0.5	N/A	1.5
MHD generator	1.5	1.4	6.3	N/A	3.0
Laser–metal interaction	1.6	0.9	0.2	N/A	0.8

Table 3: Comparison of running times (in seconds) to compute the dimensionless variables for Active Subspaces, PyDimension, BuckiNet, BSM, and IT-π across different validation and application cases.

The corresponding running times for methods across various cases are summarized in Table 3. Assuming identical optimization methods and candidate solutions across all approaches, the primary cost differences arise from the function evaluation of a single solution. Active Subspaces and BuckiNet require kernel matrix inversions with a computational cost of $O(N_{\mathrm{samples}}^3)$, where N_{samples} is the number of data samples. For PyDimension, fitting an m-th order polynomial model incurs a cost of $O(N_{\mathrm{samples}}^2 m^2)$. In the case of BSM, the cost is $O\left(N_{\mathrm{samples}} \cdot n_t^2\right)$, where n_t is the number of independent variables. For IT-π, when using the histogram method with N_{bins} bins to estimate the probability distribution, the computational cost is $O\left(N_{\mathrm{samples}} + N_{\mathrm{bins}}^{l+1}\right)$.

Data availability

The data generated in this study as well as the analysis code have been deposited in a Zenodo database (*61*) under identifier `https://doi.org/10.5281/zenodo.17080657`.

Code availability

The code for this work is available at `https://github.com/ALD-Lab/IT_PI`.

References

1. E. Buckingham, On physically similar systems; illustrations of the use of dimensional equations. *Phys. Rev.* **4** (4), 345 (1914).

2. T. Szirtes, *Applied Dimensional Analysis and Modeling* (Butterworth-Heinemann) (2007).

3. S. G. Sterrett, Physically similar systems-a history of the concept. *Springer handbook of model-based science* pp. 377–411 (2017).

4. A. C. Palmer, *Dimensional analysis and intelligent experimentation* (World Scientific) (2008).

5. B. Lysik, M. Rybaczuk, *Dimensional Analysis in the Identification of Mathematical Models* (World Scientific Publishing) (1990).

6. O. Reynolds, An experimental investigation of the circumstances which determine whether the motion of water shall be direct or sinuous, and of the law of resistance in parallel channels. *Philos. Trans. R. Soc. Lond.* **174**, 935–982 (1883).

7. A. A. Sonin, A generalization of the Π-theorem and dimensional analysis. *Proc. Natl. Acad. Sci. U.S.A.* **101** (23), 8525–8526 (2004).

8. L. A. Segel, Simplification and Scaling. *SIAM Rev.* **14** (4), 547–571 (1972).

9. G. I. Barenblatt, *Scaling, Self-similarity, and Intermediate Asymptotics*, no. 14 in Cambridge Texts Appl. Math. (Cambridge Univ. Press) (1996).

10. J. L. Callaham, J. V. Koch, B. W. Brunton, J. N. Kutz, S. L. Brunton, Learning dominant physical processes with data-driven balance models. *Nat. Commun.* **12** (1), 1016 (2021).

11. P. F. Mendez, F. Ordonez, Scaling laws from statistical data and dimensional analysis. *J. Appl. Mech.* **72** (5), 648–657 (2005).

12. X. Xie, A. Samaei, J. Guo, W. K. Liu, Z. Gan, Data-driven discovery of dimensionless numbers and governing laws from scarce measurements. *Nat. Commun.* **13** (1), 7562 (2022).

13. S.-M. Udrescu, M. Tegmark, AI Feynman: A physics-inspired method for symbolic regression. *Sci. Adv.* **6** (16), eaay2631 (2020).

14. L. Jofre, Z. R. del Rosario, G. Iaccarino, Data-driven dimensional analysis of heat transfer in irradiated particle-laden turbulent flow. *Int. J. Multiph. Flow* **125**, 103198 (2020).

15. J. Bakarji, J. Callaham, S. L. Brunton, J. N. Kutz, Dimensionally consistent learning with Buckingham Pi. *Nat. Comput. Sci.* **2** (12), 834–844 (2022).

16. Z. del Rosario, M. Lee, G. Iaccarino, Lurking variable detection via dimensional analysis. *SIAM/ASA J. Uncertain. Quantif.* **7** (1), 232–259 (2019).

17. P. G. Constantine, Z. del Rosario, G. Iaccarino, Data-driven dimensional analysis: algorithms for unique and relevant dimensionless groups. *arXiv preprint arXiv:1708.04303* (2017).

18. Z. Xu, X. Zhang, S. Wang, G. He, Artificial neural network based response surface for data-driven dimensional analysis. *J. Comput. Phys.* **459**, 111145 (2022).

19. R. Watanabe, T. Ishii, Y. Hirono, H. Maruoka, Data-driven discovery of self-similarity using neural networks. *Phys. Rev. E.* **111** (2), 024301 (2025).

20. L. Zhang, Z. Xu, S. Wang, G. He, Clustering dimensionless learning for multiple-physical-regime systems. *Comput. Methods Appl. Mech. Eng.* **420**, 116728 (2024).

21. N. Bempedelis, L. Magri, K. Steiros, Extracting self-similarity from data. *arXiv preprint arXiv:2407.10724* (2024).

22. M. Schmidt, H. Lipson, Distilling free-form natural laws from experimental data. *Science* **324** (5923), 81–85 (2009).

23. R. Ma, *et al.*, Building-block-flow model for LES of high-speed flows, in *Center for Turbulence Research Proceedings of the Summer Program* (2024).

24. L. Zhang, G. He, Mutual-information-based dimensional learning: Objective algorithms for identification of relevant dimensionless quantities. *Computer Methods in Applied Mechanics and Engineering* **440**, 117922 (2025).

25. A. Lozano-Durán, G. Arranz, Information-theoretic formulation of dynamical systems: causality, modeling, and control. *Phys. Rev. Res.* **4** (2), 023195 (2022).

26. Y. Yuan, A. Lozano-Durán, Limits to extreme event forecasting in chaotic systems. *Phys. D.* p. 134246 (2024).

27. E. Lutwak, D. Yang, G. Zhang, Cramér-Rao and moment-entropy inequalities for Rényi entropy and generalized Fisher information. *IEEE Trans. Inf. Theory.* **51** (2), 473–478 (2005).

28. T. M. Cover, *Elements of information theory* (John Wiley & Sons) (1999).

29. C. E. Shannon, A mathematical theory of communication. *Bell Syst. Tech. J.* **27** (3), 379–423 (1948).

30. A. Rényi, On measures of entropy and information, in *Proc. 4th Berkeley Symp. Math. Stat. Probab.* (Univ. California Press) (1961), pp. 547–562.

31. N. Hansen, S. D. Müller, P. Koumoutsakos, Reducing the time complexity of the derandomized evolution strategy with covariance matrix adaptation (CMA-ES). *Evol. Comput.* **11** (1), 1–18 (2003).

32. S. Carnot, *Réflexions sur la puissance motrice du feu, et sur les machines propres à développer cette puissance* (Annales des Mines) (1824).

33. G. K. Batchelor, *An introduction to fluid dynamics* (Cambridge Univ. Press) (2000).

34. C. F. Colebrook, Turbulent flow in pipes, with particular reference to the transition region between the smooth and rough pipe laws. *J. Inst. Civ. Eng.* **12** (8), 393–422 (1939).

35. A. J. Smits, I. Marusic, Wall-bounded turbulence. *Phys. Today.* **66** (9), 25–30 (2013).

36. J. Jiménez, Turbulent flows over rough walls. *Annu. Rev. Fluid Mech.* **36** (1), 173–196 (2004).

37. D. Chung, N. Hutchins, M. P. Schultz, K. A. Flack, Predicting the drag of rough surfaces. *Annu. Rev. Fluid Mech.* **53** (1), 439–471 (2021).

38. S. H. Strogatz, *Nonlinear dynamics and chaos: with applications to physics, biology, chemistry, and engineering* (CRC Press) (2018).

39. E. N. Lorenz, Deterministic Nonperiodic Flow. *J. Atmos. Sci.* **20** (2), 130–141 (1963).

40. E. F. Spina, A. J. Smits, S. K. Robinson, The physics of supersonic turbulent boundary layers. *Ann. Rev. Fluid Mech.* **26** (1), 287–319 (1994).

41. A. Trettel, J. Larsson, Mean velocity scaling for compressible wall turbulence with heat transfer. *Phys. Fluids.* **28** (2) (2016).

42. D. Modesti, S. Pirozzoli, Direct numerical simulation of supersonic pipe flow at moderate Reynolds number. *Int. J. Heat Fluid Flow.* **76**, 100–112 (2019).

43. T. Kármán, *et al.*, Mechanische änlichkeit und turbulenz. *Nachr. Ges. Wiss. Göttingen, Math.-Phys. Kl.* **1930**, 58–76 (1930).

44. R. Landauer, Information is physical. *Phys. Today.* **44** (5), 23–29 (1991).

45. R. Landauer, The physical nature of information. *Phys. Lett. A.* **217** (4-5), 188–193 (1996).

46. A. Kraskov, H. Stögbauer, P. Grassberger, Estimating mutual information. *Phys. Rev. E.* **69** (6), 066138 (2004).

47. T. Suzuki, M. Yamada, T. Kanamori, H. Hachiya, M. Sugiyama, Relative density-ratio estimation for robust distribution comparison, in *Proceedings of the 25th International Conference on Machine Learning* (2008), pp. 1243–1250.

48. A. Singh, B. Póczos, L. Wasserman, Nonparametric estimation of conditional differential entropy, in *Advances in Neural Information Processing Systems* (2014), pp. 1370–1378.

49. W. Gao, S. Oh, P. Viswanath, Demystifying fixed k-nearest neighbor information estimators. *IEEE Trans. Inf. Theory.* **64** (9), 6119–6151 (2017).

50. M. I. Belghazi, *et al.*, Mutual Information Neural Estimation, in *Proceedings of the 35th International Conference on Machine Learning* (2018), pp. 531–540.

51. W. H. Press, S. A. Teukolsky, W. T. Vetterling, B. P. Flannery, *Numerical Recipes: The Art of Scientific Computing* (Cambridge University Press) (2007).

52. T. M. Cover, P. E. Hart, Nearest Neighbor Pattern Classification. *IEEE Trans. Inf. Theory.* **13** (1), 21–27 (1967).

53. L. Rayleigh, LIX. On Convection Currents in a Horizontal Layer of Fluid, When the Higher Temperature Is on the Under Side. *Philos. Mag.* **32** (192), 529–546 (1916).

54. H. Blasius, *Grenzschichten in Flüssigkeiten mit kleiner Reibung* (Druck von BG Teubner) (1907).

55. S. A. Dixit, A. Gupta, H. Choudhary, T. Prabhakaran, Generalized scaling and model for friction in wall turbulence. *Phys. Rev. Lett.* **132** (1), 014001 (2024).

56. S. A. Dixit, A. Gupta, H. Choudhary, T. Prabhakaran, Universal scaling of mean skin friction in turbulent boundary layers and fully developed pipe and channel flows. *J. Fluid Mech.* **943**, A43 (2022).

57. M. Thring, Magnetohydrodynamic Power Generation. *Nature* **208** (5014), 966–967 (1965).

58. A. L. Hammond, Magnetohydrodynamic Power: More Efficient Use of Coal. *Science* **178** (4059), 386–387 (1972).

59. A. Glaws, P. G. Constantine, J. N. Shadid, T. M. Wildey, Dimension reduction in magnetohydrodynamics power generation models: Dimensional analysis and active subspaces. *Stat. Anal. Data Min.* **10** (5), 312–325 (2017).

60. D. D. Gu, W. Meiners, K. Wissenbach, R. Poprawe, Laser additive manufacturing of metallic components: materials, processes and mechanisms. *International materials reviews* **57** (3), 133–164 (2012).

61. Y. Yuan, A. Lozano-Durán, Dimensionless learning based on information (2025), `https://doi.org/10.5281/zenodo.17080657`.

Acknowledgments

Author contributions statement

Writing, visualization, validation, methodology, and conceptualization: Y.Y; Writing, project administration, methodology, investigation, funding acquisition, and conceptualization: A.L.-D.

Competing interests statement

There are no conflicts of interest.

Supplementary Materials for
Dimensionless learning based on information

Yuan Yuan* & Adrián Lozano-Durán
*Corresponding author. Email: yuany999@mit.com

Contents

S.1 Challenges and Methods for Dimensionless Learning

A brief overview of dimensionless learning methods and their primary limitations and challenges was provided in the Introduction. In this section, we offer a more in-depth analysis of these challenges, examining both methodological and practical aspects, with particular attention to how they are addressed by IT-π. We also review the key technical strategies adopted by various dimensionless learning approaches, summarizing their key underlying assumptions and modeling frameworks.

S.1.1 Challenges

Table S1 summarizes the key challenges associated with dimensionless learning methods and outlines how each is addressed by IT-π. These challenges can be grouped into the following main categories:

- **Non-uniqueness of dimensionless variables.** Traditional dimensional analysis does not yield unique dimensionless variables. According to the Buckingham-π theorem, the derived dimensionless variables span a linear subspace of exponents, and any basis within this subspace is equally valid. This lack of uniqueness can complicate the identification of the most relevant dimensionless parameters for a given physical system, potentially leading to ambiguity in model interpretation and application. For instance, different sets of dimensionless variables may describe the same system, making it challenging to select the most physically meaningful set without additional context or expertise. Most dimensionless learning methods, including IT-π (see §S.2.1), address this challenge by identifying dimensionless variables that are optimal from a predictive standpoint. However, alternative objectives—such as simplicity of the dimensionless variables or ease of physical interpretability—are also important and have been comparatively less explored in the literature.

- **Assumed model structure.** Most existing dimensionless learning methods rely on a predefined model structure to relate input and output variables. For example, some approaches assume that the relationship between dimensionless groups follows a power-law form, while others adopt polynomial expansions or, in more sophisticated cases, leverage machine learning models such as neural networks. Although these assumptions can simplify model training and interpretation, they inherently constrain the space of admissible functional relationships. In practice, the true underlying dynamics of a physical system may not conform to the assumed model structure. This mismatch can result in suboptimal or biased identification of dimensionless variables, especially in systems governed by highly nonlinear, discontinuous, or multiscale behavior. Consequently, methods that depend on rigid model forms may exhibit limited generalizability across diverse physical domains and may require additional validation or reconfiguration when applied to unfamiliar systems. Model-free approaches, such as IT-π, aim to address this issue by avoiding assumptions about the functional form, instead relying on the information-theoretic irreducible error theorem (see §S.2.1).

- **Applicability to noisy real-world data.** Many dimensionless learning methods are primarily designed for idealized settings in which experiments can be freely conducted and measurement noise is minimal. In contrast, real-world applications—especially in engineering and experimental sciences—often involve data that are noisy, sparse, or incomplete. Such conditions pose significant challenges for dimensionless learning, as noise can obscure the underlying physical relationships and degrade the accuracy of the identified dimensionless variables. IT-π addresses this challenge through its theoretical robustness to noise. This resilience arises from the properties of the information-theoretic irreducible error, whose minimum remains invariant under additive noise (see §S.3.5). We have shown that IT-π can tolerate noise levels of up to 20% without significant degradation in performance, consistently recovering the correct dimensionless relationships across a wide range of test cases.

- **Computational efficiency.** As the complexity of physical systems increases, so too does the computational burden associated with dimensionless learning. The optimization procedures required to identify optimal dimensionless groups can be susceptible to local minima, particularly when employing zero-order methods such as grid search or pattern search. Although increasing the number of initial samples or using global optimization strategies can mitigate this issue, such approaches come at the cost of increased computational expense—posing scalability challenges in high-dimensional parameter spaces or large-scale applications. These computational demands can become a significant bottleneck, especially when repeated evaluations of complex models are involved. Despite these challenges, IT-π demonstrates favorable computational performance. Its cost is generally low, and in worst-case scenarios, it remains comparable to that of other state-of-the-art dimensionless learning methods. Additional details supporting this comparison are provided in the "Methods" section under "Details about comparison with other dimensionless learning methods."

- **Data requirements.** Dimensionless learning methods often require substantial amounts of data to reliably identify predictive dimensionless variables, particularly in high-dimensional settings. As the number of input variables increases, the volume of the associated parameter space grows exponentially, leading to the well-known "curse of dimensionality." In such regimes, data sparsity can undermine the reliability of statistical estimates—especially for metrics such as mutual information or regression error—and may result in inconclusive or misleading outcomes. This challenge is further exacerbated when the underlying relationships between variables are nonlinear or exhibit multi-regime behavior, which requires even denser sampling to capture accurately. IT-π partially mitigates this limitation through its model-free formulation and information-theoretic optimization strategy. As demonstrated in §S.3.1, IT-π remains effective across a range of dimensionalities, provided that the available dataset sufficiently covers the relevant subspaces of interest. Nevertheless, when data are extremely limited or the input space is poorly sampled, the statistical uncertainty in the mutual information estimates can remain large, and the discovered variables should be interpreted with caution. In such cases, IT-π is built-in with uncertainty quantification as described in the next point.

- **Need for uncertainty quantification.** Reliable application of dimensionless learning requires rigorous quantification of uncertainty in the identified dimensionless variables. Without such analysis, it is difficult to assess whether the discovered relationships are statistically significant or merely artifacts of limited sample size, noisy measurements, or overfitting. In particular, when mutual information or regression-based metrics are estimated from finite datasets, the resulting values can exhibit high variance—especially in high-dimensional or poorly sampled regimes—leading to potentially spurious conclusions. While several methods exist for estimating statistical uncertainty, including bootstrapping, subsampling, and analytical approximations, their application requires careful implementation and interpretation. These procedures often increase computational cost and introduce additional methodological complexity, which can deter widespread adoption. IT-π addresses this need directly by incorporating uncertainty quantification into its framework. As described in §S.3.1, the results produced by IT-π are accompanied by error bars on the estimated irreducible error ϵ_{LB}, enabling users to assess the robustness and statistical reliability of the discovered dimensionless variables.

- **Sensitivity to error norm.** Methods often implicitly assume a specific error norm—typically the L_2 norm—when evaluating model performance or identifying optimal dimensionless variables. However, the choice of error norm directly influences which aspects of the data are prioritized. For example, the L_2 norm emphasizes frequent, moderate-magnitude events; higher-order norms (e.g., L_4 or L_∞) place greater weight on extreme events; and lower-order norms (e.g., L_1) emphasize weaker events. This sensitivity can result in substantially different sets of dimensionless variables depending on the norm used, potentially yielding models that are well-suited to certain tasks (e.g., average prediction) but poorly suited to others (e.g., extreme event forecasting). IT-π explicitly addresses this sensitivity through its formulation of the irreducible error bound, which depends on the chosen Rényi entropy order α. This enables the framework to accommodate different L_p norms for quantifying prediction error (see §S.4.1).

- **Dependency on the list of variables.** The effectiveness of any dimensionless learning method critically depends on the completeness of the input list of dimensional variables. If relevant variables are omitted, the resulting dimensionless variables may fail to capture key physical mechanisms, leading to suboptimal or misleading representations. Conversely, including irrelevant or redundant variables can obscure meaningful relationships and increase model complexity unnecessarily. An additional challenge arises with discrete-valued variables, which many prediction-based methods are not well suited to handle due to their reliance on differentiability for gradient-based optimization. IT-π addresses these issues through several mechanisms. It can diagnose missing variables by monitoring the normalized irreducible error, and detect redundancy by systematically analyzing subsets of input combinations (see §S.3.3). Moreover, IT-π ranks input variables by their predictive contribution, enabling users to identify and exclude superfluous inputs that do not significantly decrease the irreducible error. Finally, discrete-valued variables are naturally supported through the discrete formulation of Rényi entropy, making IT-π applicable to mixed-type input spaces.

- **Sensitivity to hyperparameter choices.** Dimensionless learning methods rely on hyperparameters that may influence their performance and the quality of the identified dimensionless variables. These hyperparameters include the degree of polynomial expansions, regularization weights, the number of terms in sparse regression libraries, or architectural choices in neural networks such as depth, width, and activation functions. Improper tuning can lead to overfitting, underfitting, or instability in the discovered dimensionless relationships, particularly when data are limited or noisy. As a result, these methods often require careful calibration or cross-validation, which adds to their computational and methodological complexity. In contrast, IT-π exhibits comparatively low sensitivity to hyperparameter choices. As demonstrated in §S.3.2, its performance remains robust across a wide range of hyperparameter settings, provided a sufficient number of samples are available. This robustness stems from the model-free nature of IT-π, which avoids fitting a specific function to the data and instead relies on information-theoretic criteria to evaluate candidate dimensionless variables.

- **Identification of regimes, self-similarity, and more.** One of the major promises of dimensionless learning is its ability not only to reduce the number of variables but also to uncover deeper physical structures such as distinct regimes of behavior, characteristic scales, and self-similar solutions. However, most existing methods are limited in their ability to systematically detect such features. For instance, identifying regime boundaries—where dominant physical effects change—typically requires prior knowledge or manual inspection of the data. Similarly, discovering self-similar variables or invariant scalings often depends on assumed model structures or predefined transformation groups, which can bias results or limit applicability. IT-π addresses these challenges through its unified framework that is able to tackle identification of regimes and characteristic scales, self-similarity, a ranking of variables, and model efficiency (see Results).

- **Model overfitting.** Overfitting is a significant concern in model-based dimensionless learning methods, particularly when function approximators such as high-degree polynomials, symbolic regressors, or neural networks are used. These methods may achieve near-perfect agreement with the training data by fitting spurious patterns or noise rather than capturing the underlying physical relationships. This is especially problematic in regimes with limited data, where high-capacity models can memorize the training set and generalize poorly to new observations. In such cases, the resulting dimensionless variables may appear predictive during training but fail to retain their relevance under data perturbations or when applied to unseen conditions. IT-π offers a principled approach to diagnose and mitigate overfitting by separating the intrinsic information content of the input-output relationship from the artifacts of a particular model fit. As detailed in §S.3.4, IT-π can also quantify model overfitting using the statistical uncertainty-aware irreducible error, allowing practitioners to assess whether apparent improvements in predictability are statistically significant or likely due to overfitting.

- **Generalization and transferability.** A central challenge in dimensionless learning is ensuring that the identified models or dimensionless variables generalize well to new,

unseen data or to different physical systems. This issue is particularly important when the underlying assumptions, boundary conditions, or parameter distributions shift. In such cases, dimensionless variables discovered from one dataset may fail to capture the dominant physical mechanisms in another, resulting in reduced predictive accuracy or incorrect physical interpretation. This lack of generalization is often not a limitation of the dimensionless learning method itself, but rather a consequence of the training data used. If the data fail to span the relevant physical regimes or omit key phenomena, the learned model will naturally exhibit poor transferability. IT-π provides a partial solution to this issue by offering a model-free formulation that explicitly quantifies the amount of information shared between the selected inputs and the target output. As shown in §S.4.5, IT-π can be used to evaluate the generalization properties of learned dimensionless variables by testing them across independently partitioned datasets. In the example of the ANN model for wall heat flux, we demonstrate that dimensionless variables discovered by IT-π retain their predictive relevance even when applied to data drawn from different subsets of the original parameter space. Nonetheless, ensuring generalizability in entirely new or extrapolative contexts remains a challenging and open problem for all dimensionless learning methods.

S.1.2 Overview of methods

We provide an overview of the methodologies and distinguishing features of various data-driven approaches for dimensionless learning. Several of these methods are summarized in Table 1 of the main text.

- **Scaling Laws** (*11*) combines dimensional analysis with backward elimination in multivariate regression under the assumption of a power-law relationship between input and output variables,

$$\Pi_o = e^{\beta_0} q_1^{\beta_1} \cdots q_n^{\beta_n} + \epsilon,$$

where ϵ is the model error. The optimal coefficient vector $\beta = [\beta_0, \cdots, \beta_n]$ is determined by minimizing the linear regression model error,

$$\min_{\beta} \left\| \log \Pi_o - \beta_0 - \sum_{j=1}^{n} \beta_j \log q_j \right\|_2.$$

- **Active Subspaces** (*17*) integrates dimension reduction techniques with global sensitivity analysis to construct unique dimensionless groups via two algorithms: the response surface-based approach and the finite difference-based approach. The method constructs a response surface that relates the dimensionless output Π_o to the dimensionless input $\mathbf{\Pi} = \mathbf{q}^{\mathbf{W^T}}$, where $\mathbf{W}$ denotes the null space of the dimension matrix $\mathbf{D}$. The log of the input is $\gamma = \log(\mathbf{\Pi}) = \mathbf{W}^T \log(\mathbf{q})$. A model is then used to approximate the output using the log of the input, $\Pi_o = \hat{g}(\gamma) + \epsilon$ where $\hat{g}(\gamma)$ is the predicted response function, and ϵ represents the modeling error. In practice, $\hat{g}$ may be realized through various function approximators, such as kernel regression (*17*) or neural networks (*18*).

Challenge	IT-π Strategy to tackle the challenge	Section
Non-uniqueness	Identification dimensionless variables optimal for predictive performance	§S.2.1
Assumed model structure	Model-free approach based on the information-theoretic irreducible error theorem	§S.2.1
Applicability to noisy data	Theoretical robustness: irreducible error bound invariant under additive noise	§S.3.5
Computational efficiency	Low computational cost; comparable worst-case performance to other methods	Methods
Data requirements	Low sensitivity of the discovered dimensionless variable to sample size	§S.3.1
Uncertainty quantification	Error bars on the estimated irreducible error for statistical significance	§S.3.1
Sensitivity to error norm	Irreducible error bound depending on Rényi entropy order and L_p norm	§S.4.1
List of variables	Diagnose missing/superfluous inputs; handle discrete-valued inputs; rank variables by predictive contribution	§S.3.3
Method hyperparameters	Robust performance across a wide range of hyperparameter settings	§S.3.2
Identification of regimes, self-similarity, and more	Unified framework for discovering regimes, characteristic scales, and self-similar solutions	Results
Model overfitting	Overfitting detected via uncertainty-aware irreducible error	§S.3.4
Generalization	Test learned variables across independently partitioned datasets	§S.4.5

Table S1: Summary of key challenges in dimensionless learning, the IT-π strategies developed to address each challenge, and the manuscript sections where these strategies are presented.

The active subspace is identified through eigen-decomposition,

$$\int \nabla \hat{g} \nabla \hat{g}^T \sigma(\gamma) d\gamma \approx \mathbf{U} \mathbf{\Lambda} \mathbf{U}^T,$$

where $\nabla \hat{g}$ is the gradient of the regression model, $\sigma(\gamma)$ is the weight function, $\mathbf{U}$ is the eigenvector matrix, $\mathbf{\Lambda}$ is a diagonal matrix of eigenvalues. The discovered dimensionless groups are given by $\mathbf{\Pi}^* = [\Pi_1^*, \Pi_2^*, \cdots, \Pi_n^*]$, where

$$\Pi_i^*(\mathbf{q}) = \exp\left(\mathbf{z}_i^T \log(\mathbf{q})\right),$$

where $\mathbf{z}_i = \mathbf{W}\mathbf{u}_i$ and $\mathbf{u}_i$ is the i-th eigenvector from the eigenvector matrix $\mathbf{U}$.

- **AI Feynman** (*13*) discovers symbolic expressions from data by integrating dimensionless principles. The dimensionless input and output are constructed as

$$\Pi_i' \equiv q_1^{W_{i1}} q_2^{W_{i2}} \cdots q_n^{W_{\text{in}}}, \quad \Pi_o' \equiv \frac{q_o}{q_o^*}, \quad q_o^* \equiv q_1^{p_1} q_2^{p_2} \cdots q_n^{p_n},$$

where $\mathbf{Dp} = \mathbf{b}$ with $\mathbf{p} = [p_1, p_2, \cdots]$, and $\mathbf{DW} = \mathbf{0}$, with $\mathbf{D}$ the dimension matrix, $\mathbf{b} = [b_1, b_2, \cdots]$ is the dimension vector of the output. The method then employs a decision tree to systematically explore candidate models and identify a symbolic relationship between Π'_o and $\mathbf{\Pi}'$.

- **Clustering** (*20*) introduces clustering-based methods to identify different physical regimes and discover dominant dimensionless parameters following the active subspace method. Data points γ are clustered into K groups, $\Omega^1, \Omega^2, \ldots, \Omega^K$, using a clustering algorithm based on gradients $\nabla \hat{g}(\gamma)$.

- **PyDimension** (*12*) embeds the principle of dimensional invariance into a two-level polynomial regression scheme to discover dimensionless numbers by solving the optimization problem,

$$\min_{\mathbf{C}, \beta} \|\Pi_o - f(\mathbf{\Pi}(\mathbf{C}), \beta)\|_2,$$

where f is a polynomial regression model, β represents its coefficients, and $\mathbf{C}$ is the basis coefficients for constructing $\mathbf{\Pi}$.

- **BuckiNet** (*15*) uses machine learning and Sparse Identification of Nonlinear Dynamics (SINDy) to collapse data into dimensionless groups by solving a constrained optimization problem,

$$\min_{\mathbf{C}, \psi} \|\Pi_o - \psi(\mathbf{\Pi}(\mathbf{C}))\|_2,$$

where the function ψ serves as an approximation model, which can be implemented using ridge regression, a neural network, or a SINDy-based approach, and $\mathbf{C}$ is the basis coefficients for constructing $\mathbf{\Pi}$.

- **BSM** (*21*) combines optimization and symbolic regression to extract similarity variables by first identifying them and then discovering the analytic form of their transformations. Given a set of similarity variables ξ and $\tilde{q}$, the similarity transformation follows

$$q_o(s, t) \to \tilde{q}_o(\xi),$$

with

$$\xi = \alpha(t)s + \beta(s, t), \quad \tilde{q}_o = \gamma(t)q_o + \delta(s, t),$$

where q_o is the quantity of interest, s and t are the independent variables, ξ is the self similar variable, $\tilde{q}_o$ is the self-similar output, $[\alpha, \beta]$, and $[\gamma, \delta]$ are elementary dilation/translation groups. The similarity variables are determined by solving the optimization problem,

$$\arg\min_{\alpha, \beta, \gamma, \delta} \sum_{i=1}^{n_t} \sum_{j=1}^{n_t} \|\tilde{q}_o(\xi, t_i) - \tilde{q}_o(\xi, t_j)\|_2^2,$$

where i and j denotes the i-th and j-th value of the independent variable t. Symbolic regression is then employed to extract the analytic form of transformation variables $\alpha, \beta, \gamma, \delta$.

- **Information-based methods** have also been proposed in the context of dimensional analysis. To the best of our knowledge, the first attempt to apply information-theoretic principles to dimensionless learning was developed by our group (*23*), where mutual information was used to extract dimensionless variables in hypersonic flows.

$$\mathbf{\Pi}(\mathbf{C}) = \arg \max_{\mathbf{C}} I\left(\Pi_o; \mathbf{\Pi}(\mathbf{C})\right)$$

A subsequent method, referred to as MIDL (*24*), also leveraged mutual information for learning dimensionless variables, with an emphasis on invariance under reparameterizations and robustness to outliers. There are, nonetheless, several key conceptual differences between MIDL and IT-π that are worth highlighting. First, IT-π is rigorously grounded in the irreducible error theorem, while MIDL does not provide a theoretical justification linking mutual information to model error. As shown in §S.2.1, mutual information alone is insufficient to establish this connection; it is the conditional differential entropy of the output given the input that governs the irreducible error. Furthermore, IT-π is formulated using Rényi entropies, allowing the framework to accommodate different error norms. In contrast, MIDL is based solely on Shannon entropy. As demonstrated in §S.4.1, relying exclusively on Shannon mutual information can lead to failure in a variety of scenarios. Finally, IT-π offers additional capabilities beyond identifying dimensionless variables. These include identifying physical regimes, discovering self-similar structures and characteristic scales, and quantifying model efficiency.

S.2 IT-π Formulation

S.2.1 Proof of information-theoretic lower bound to irreducible error

Definitions. Consider the physical law or model

$$\hat{\Pi}_o = f(\mathbf{\Pi}).$$

The irreducible error for a given L_p-norm is defined as

$$\min_f \|\Pi_o - \hat{\Pi}_o\|_p = \min_f \left[\mathbb{E}\left(|\Pi_o - \hat{\Pi}_o|^p\right)\right]^{\frac{1}{p}},$$

where $\mathbb{E}(\ )$ is the expectation operator. The specific conditional Rényi entropy of Π_o given $\Pi = \pi$ is

$$h_\alpha(\Pi_o \mid \mathbf{\Pi} = \pi) = \lim_{\alpha' \to \alpha} \frac{1}{1 - \alpha'} \log\left(\int \rho_{\Pi_o|\mathbf{\Pi}}^{\alpha'}\left(\pi_o \mid \pi\right) d\pi_o\right),$$

such that

$$h_\alpha\left(\Pi_o|\mathbf{\Pi}\right) = \int \rho_{\mathbf{\Pi}}(\pi) h_\alpha(\Pi_o \mid \mathbf{\Pi} = \pi) d\pi.$$

Theorem. The irreducible error is lower bounded by

$$\min_f \|\Pi_o - \hat{\Pi}_o\|_p \geq e^{-I_\alpha(\Pi_o; \mathbf{\Pi})} \cdot c\left(\alpha, p, h_{\alpha,o}\right), \tag{S1}$$

for $\alpha > 1/(1+p)$. The function $c\left(\alpha, p, h_{\alpha,o}\right)$ is given by

$$c\left(\alpha, p, h_{\alpha,o}\right) = e^{h_\alpha(\Pi_o)} \cdot c_1(\alpha, p),$$

$$c_1(\alpha, p) = \begin{cases} (p\alpha + \alpha - 1)^{-\frac{1}{p}+\frac{1}{1-\alpha}} (p\alpha)^{\frac{1}{\alpha-1}} c_2(\alpha, p) & \text{if } \alpha \neq 1, \\ (pe)^{-\frac{1}{p}} c_2(1, p) & \text{if } \alpha = 1, \end{cases}$$

and

$$c_2(\alpha, p) = \begin{cases} \dfrac{p(1-\alpha)^{\frac{1}{p}}}{2\beta\left(\frac{1}{p}, \frac{1}{1-\alpha} - \frac{1}{p}\right)} & \text{if } \alpha < 1, \\ \dfrac{p}{2\Gamma\left(\frac{1}{p}\right)} & \text{if } \alpha = 1, \\ \dfrac{p(\alpha-1)^{\frac{1}{p}}}{2\beta\left(\frac{1}{p}, \frac{\alpha}{\alpha-1}\right)} & \text{if } \alpha > 1, \end{cases}$$

where β is the Beta function and Γ is the Gamma function.

Proof. Applying the law of total expectation, the L_p-norm of the error is decomposed into a weighted sum of the conditional error given each state of the input $\mathbf{\Pi} = \pi$,

$$\left\| \Pi_o - \hat{\Pi}_o \right\|_p = \left[\mathbb{E}\left(\left| \Pi_o - \hat{\Pi}_o \right|^p \right) \right]^{\frac{1}{p}}$$

$$= \left[\int \rho_{\mathbf{\Pi}}(\pi) \mathbb{E}\left(\left| \Pi_o - \hat{\Pi}_o \right|^p \mid \mathbf{\Pi} = \pi \right) d\pi \right]^{\frac{1}{p}},$$

where the L_p-norm of conditional error given $\mathbf{\Pi} = \pi$ is denoted as,

$$\mathbb{E}\left(\left| \Pi_o - \hat{\Pi}_o \right|^p \mid \mathbf{\Pi} = \pi \right) = \int \rho_{\Pi_o - \hat{\Pi}_o \mid \mathbf{\Pi}}\left(\pi_o - \hat{\pi}_o \mid \pi \right) \left| \pi_o - \hat{\pi}_o \right|^p d\pi_o$$

$$= \int \rho_{\mathcal{E}\mid\mathbf{\Pi}}\left(\epsilon \mid \pi \right) |\epsilon|^p d\epsilon$$

$$= \left\| \mathcal{E} \mid \mathbf{\Pi} = \pi \right\|_p^p,$$

where $\mathcal{E} = \Pi_o - \hat{\Pi}_o$ is the error random variable, and $\epsilon = \pi_o - \hat{\pi}_o$ is its realization.

The distribution that maximizes the Rényi entropy of a continuous random variable with a fixed p-th moment is a generalized Gaussian distribution of order α (27) of the form

$$\rho_{\mathcal{E}_G\mid\mathbf{\Pi}}^G(\epsilon \mid \pi) = G\left(\frac{\epsilon}{t}\right) / t,$$

when $\alpha > 1/(1+p)$. The scaling factor t is

$$t = \frac{\left\| \mathcal{E} \mid \mathbf{\Pi} = \pi \right\|_p}{(p\alpha + \alpha - 1)^{-1/p}},$$

and the standard generalized Gaussian distribution of order α is

$$G(x) = \begin{cases} c_2(p, \alpha)\left(1 + (1 - \alpha)|x|^p\right)^{\frac{1}{\alpha-1}} & \text{if } \alpha \neq 1, \\ c_2(p, 1)e^{-|x|^p} & \text{if } \alpha = 1. \end{cases} \tag{S2}$$

The latter implies that the entropy of the conditional error is bounded by the entropy of the conditional error with this follows the generalized Gaussian ($\mathcal{E}_G$) with the same p-th moment for $\alpha > 1/(1+p)$,

$$
\begin{aligned}
h_\alpha(\mathcal{E} \mid \mathbf{\Pi} = \pi) &\leq h_\alpha(\mathcal{E}_G \mid \mathbf{\Pi} = \pi) \\
&= \log \|\mathcal{E} \mid \mathbf{\Pi} = \pi\|_p - \log c_1(\alpha, p).
\end{aligned}
\tag{S3}
$$

This leads to the moment-entropy inequality (27) implies that the L_p-norm of the conditional error $\|\mathcal{E} \mid \mathbf{\Pi} = \pi\|_p$ can be bounded using the entropy of the irreducible error $h_\alpha(\mathcal{E} \mid \mathbf{\Pi} = \pi)$ as

$$
\|\mathcal{E} \mid \mathbf{\Pi} = \pi\|_p \geq e^{h_\alpha(\mathcal{E}|\mathbf{\Pi}=\pi)} \cdot c_1(\alpha, p).
$$

Therefore, the L_p-norm of the error is bounded as

$$
\begin{aligned}
\left\| \Pi_o - \hat{\Pi}_o \right\|_p &= \left[\int \rho_{\mathbf{\Pi}}(\pi) \mathbb{E} \left(\left| \Pi_o - \hat{\Pi}_o \right|^p \mid \mathbf{\Pi} = \pi \right) d\pi \right]^{\frac{1}{p}} \\
&= \left[\int \rho_{\mathbf{\Pi}}(\pi) \|\mathcal{E} \mid \mathbf{\Pi} = \pi\|_p^p d\pi \right]^{\frac{1}{p}} \\
&\geq \left[\int \rho_{\mathbf{\Pi}}(\pi) \left[e^{h_\alpha(\mathcal{E}|\mathbf{\Pi}=\pi)} \cdot c_1(\alpha, p) \right]^p d\pi \right]^{\frac{1}{p}}.
\end{aligned}
$$

Applying Jensen's inequality, $\mathbb{E}[\phi(X)] \geq \phi(\mathbb{E}[X])$, to the convex function $\phi(x) = e^{px}$, we obtain,

$$
\begin{aligned}
\int \rho_{\mathbf{\Pi}}(\pi) e^{ph_\alpha(\mathcal{E}|\mathbf{\Pi}=\pi)} d\pi &\geq e^{p \int \rho_{\mathbf{\Pi}}(\pi) h_\alpha(\mathcal{E}|\mathbf{\Pi}=\pi) d\pi} \\
&= e^{p \int \rho_{\mathbf{\Pi}}(\pi) h_\alpha(\Pi_o - f(\pi)|\mathbf{\Pi}=\pi) d\pi} \\
&\overset{(1)}{=} e^{p \int \rho_{\mathbf{\Pi}}(\pi) h_\alpha(\Pi_o|\mathbf{\Pi}=\pi) d\pi} \\
&= e^{ph_\alpha(\Pi_o|\mathbf{\Pi})},
\end{aligned}
$$

where (1) follows from the fact that adding a constant $f(\pi)$ does not change the conditional Renyi entropy. Substituting this bound into the previous inequality,

$$
\begin{aligned}
\forall f, \quad \left\| \Pi_o - \hat{\Pi}_o \right\|_p &\geq \left[c_1^p(\alpha, p) e^{ph_\alpha(\Pi_o|\mathbf{\Pi})} \right]^{\frac{1}{p}} \\
&= c_1(\alpha, p) e^{h_\alpha(\Pi_o|\mathbf{\Pi})}.
\end{aligned}
$$

and therefore,

$$
\min_f \left\| \Pi_o - \hat{\Pi}_o \right\|_p \geq e^{-I_\alpha(\Pi_o;\mathbf{\Pi})} \cdot c\left(\alpha, p, h_{\alpha,o}\right).
$$

We refer to

$$
\epsilon_{LB} \equiv \max_\alpha \left[e^{-I_\alpha(\Pi_o;\mathbf{\Pi})} \cdot c\left(\alpha, p, h_{\alpha,o}\right) \right],
$$

as the information-theoretic irreducible error.

$\square$

The main assumption in the derivation of the information-theoretic irreducible error, ϵ_{LB}, is the existence of the conditional differential entropy, $h(\cdot \mid \cdot)$, which is a fairly general

condition. Under this assumption, ϵ_{LB} represents a fundamental mathematical constraint that any predictive model must satisfy. This constraint remains valid even in the presence of strong nonlinearities and large prediction errors. Another important observation is that ϵ_{LB} does not depend solely on the mutual information between input and output. It also depends on the error norm p and the information content of the output, quantified by $h_{\alpha,o}$, through the scaling function $c(\alpha, p, h_{\alpha,o})$. This implies that even when the mutual information between input and output is non-zero, ϵ_{LB} may still be large if the output information $h_{\alpha,o}$ is high, resulting in a large value of $c(\alpha, p, h_{\alpha,o})$. In such scenarios, models are fundamentally limited in their ability to exploit the available mutual information between input and output, and large prediction errors become unavoidable.

S.2.2 Pseudocode of IT-π

Algorithm 1 IT-π: Dimensionless learning based on information

---

Require: Dimensional input $\mathbf{q}$, output q_o, null space of the dimension matrix $\mathbf{W}$.

Ensure: Optimal dimensionless input $\boldsymbol{\Pi}^*$, dimensionless output Π_o^*.

1: **Define** exponent coefficients $\mathbf{C}$ and $\mathbf{c}_o$:

$$\boldsymbol{\Pi}(\mathbf{C}) = \mathbf{q}^{\mathbf{WC}}, \quad \Pi_o(\mathbf{c}_o) = q_o^{\mathbf{Wc}_o}.$$

2: **Define** the L_p-norm exponent when measuring the error : p.

3: **Define** the population size in CMA-ES (the number of candidate solutions sampled at each iteration): M.

4: **Objective:** Identify the optimal dimensionless input and output to minimize the irreducible model error

$$\boldsymbol{\Pi}^*, \Pi_o^* = \arg\min_{\boldsymbol{\Pi},\Pi_o} \max_{\alpha} [\epsilon_{LB}] = \arg\min_{\mathbf{C},\mathbf{c}_o} J,$$

where the fitness is

$$J = \max_{\alpha} \left[e^{-I_\alpha \left(\Pi_o(\mathbf{c}_o); \boldsymbol{\Pi}(\mathbf{C}) \right)} c(\alpha, p, h_{\alpha,o}) \right].$$

5: Initialize CMA-ES population over $(\mathbf{C}, \mathbf{c_o})$ by generating a Gaussian distribution with an initial mean vector and covariance matrix.

6: **while** not converged **do**

7: $\quad \{\mathbf{C}_i, \mathbf{c}_{o,i}\}_{i=1}^M \leftarrow$ sample new population

8: $\quad$ **for** $i = 1$ to M **do**

9: $\quad\quad$ Compute dimensionless inputs $\boldsymbol{\Pi} = \mathbf{q}^{\mathbf{WC}_i}$

10: $\quad\quad$ Compute the dimensionless output $\Pi_o = q_o^{\mathbf{Wc}_{o,i}}$

11: $\quad\quad$ Estimate the irreducible error $\epsilon_{LB} = e^{-I_\alpha \left(\Pi_o(\mathbf{c}_o); \boldsymbol{\Pi}(\mathbf{C}) \right)} c(\alpha, p, h_{\alpha,o})$

12: $\quad\quad$ Evaluate the fitness $J_i = \max_\alpha [\epsilon_{LB}]$ using golden-section search over $\alpha \in \left(\frac{1}{1+p}, 10 \right]$

13: $\quad$ **end for**

14: $\quad$ Update CMA-ES distribution using fitnesses $\{J_i\}$

15: **end while**

16: **return** Optimal $\boldsymbol{\Pi}^*, \Pi_o^*$

S.2.3 Infinite equivalent solutions of IT-π under bijective transformations

The Rényi mutual information $I_\alpha(\Pi_o; \boldsymbol{\Pi})$ is invariant under bijective transformations applied to $\boldsymbol{\Pi}$. Specifically, if T is the bijective transformations applied to $\boldsymbol{\Pi}$,

$$\tilde{\boldsymbol{\Pi}} = T(\boldsymbol{\Pi}),$$

then the Rényi mutual information remains invariant under bijective transformations,

$$I_\alpha\left(\Pi_o; \tilde{\boldsymbol{\Pi}}\right) = I_\alpha\left(\Pi_o; \boldsymbol{\Pi}\right).$$

This invariance implies the existence of infinitely many equivalent optimal solutions for IT-π, as any bijective transformation of the optimal inputs preserves an equivalent mutual information. This is consistent with the intuition that when building a model, applying a bijective transformation to the input does not alter the amount of information available about the output. Consequently, models constructed with bijectively transformed inputs are equivalent in terms of their predictive capacity.

For example, for the Rayleigh problem, the mutual information remains the same for

$$I_\alpha(\Pi^*; \Pi^o) = I_\alpha\left(\frac{1}{\Pi^*}; \Pi^o\right),$$

under the bijective transformation $T(x) = 1/x$. Therefore,

$$T(\Pi^*) = t^{0.5}\mu^{0.5}/(y\rho^{0.5})$$

is an equivalent optimal solution as

$$\Pi^* = y\rho^{0.5}/\left(t^{0.5}\mu^{0.5}\right).$$

Proof. Under the bijective transformation T, the marginal probability distribution function $\rho_{\tilde{\boldsymbol{\Pi}}}$ transforms according to the change-of-variables formula,

$$\rho_{\tilde{\boldsymbol{\Pi}}}\left(\tilde{\pi}\right) = \rho_{\boldsymbol{\Pi}}\left(\pi\right) \cdot \left|J_T\left(\pi\right)\right|^{-1},$$

where

$$J_T\left(\pi\right) = \left|\det\left(\frac{\partial T}{\partial \pi}\right)\right|$$

is the Jacobian determinant of the transformation T.

Similarly, the joint probability distribution function transforms as

$$\rho_{\Pi_o, \bar{\boldsymbol{\Pi}}}\left(\pi_o, \tilde{\pi}\right) = \rho_{\Pi_o, \boldsymbol{\Pi}}\left(\pi_o, \pi\right) \cdot |1|^{-1} \cdot \left|J_T(\pi)\right|^{-1}.$$

Therefore, the conditional probability distribution function transforms as

$$\rho_{\Pi_o|\tilde{\boldsymbol{\Pi}}}\left(\pi_o \mid \tilde{\pi}\right) = \frac{\rho_{\Pi_o, \bar{\boldsymbol{\Pi}}}\left(\pi_o, \tilde{\pi}\right)}{\rho_{\tilde{\boldsymbol{\Pi}}}\left(\pi\right)} = \rho_{\Pi_o|\boldsymbol{\Pi}}\left(\pi_o \mid \pi\right),$$

which remains unchanged under the transformation since the Jacobian terms cancel out.

The conditional Renyi entropy under the transformation is

$$
\begin{aligned}
h_\alpha\left(\Pi_o \mid \tilde{\mathbf{\Pi}}\right) &= \lim_{\alpha' \to \alpha} \frac{1}{1-\alpha'} \int \rho_{\tilde{\mathbf{\Pi}}}(\tilde{\pi}) \log\left(\int \rho_{\Pi_o|\tilde{\mathbf{\Pi}}}^{\alpha'}\left(\pi_o \mid \tilde{\pi}\right) \cdot d\pi_o\right) d\tilde{\pi} \\
&= \lim_{\alpha' \to \alpha} \frac{1}{1-\alpha'} \int \rho_{\mathbf{\Pi}}\left(\pi\right) \cdot \left|J_T\left(\pi\right)\right|^{-1} \log\left(\int \rho_{\Pi_o|\mathbf{\Pi}}^{\alpha'}\left(\pi_o \mid \pi\right) \cdot d\pi_o\right) \left|J_T\left(\pi\right)\right| d\pi \\
&= \lim_{\alpha' \to \alpha} \frac{1}{1-\alpha'} \int \rho_{\mathbf{\Pi}}(\pi) \log\left(\int \rho_{\Pi_o|\mathbf{\Pi}}^{\alpha'}\left(\pi_o \mid \pi\right) \cdot d\pi_o\right) d\pi \\
&= h_\alpha\left(\Pi_o \mid \mathbf{\Pi}\right).
\end{aligned}
$$

Therefore, the Renyi mutual information remains unchanged,

$$
\begin{aligned}
I_\alpha\left(\Pi_o; \tilde{\mathbf{\Pi}}\right) &= h_\alpha\left(\Pi_o\right) - h_\alpha\left(\Pi_o \mid \tilde{\mathbf{\Pi}}\right) \\
&= h_\alpha\left(\Pi_o\right) - h_\alpha\left(\Pi_o \mid \mathbf{\Pi}\right) \\
&= I_\alpha\left(\Pi_o; \mathbf{\Pi}\right)
\end{aligned}
$$

$\square$

S.2.4 Discovery of optimal characteristic scales

Consider the dimensional inputs $\mathbf{q} = [\mathbf{q}_v, \mathbf{q}_p]$, where $\mathbf{q}_v = \left[q_{v_1}, q_{v_2}, \ldots, q_{v_{n_v}}\right]$ consists of n_v variables that change during each simulation or experiment, and $\mathbf{q}_p = \left[q_{p_1}, q_{p_2}, \ldots, q_{p_{n_p}}\right]$ consists of n_p parameters that remain fixed within a given simulation or experiment but may change across different cases. After applying IT-π, the dimensionless variable Π_i^* is constructed by non-dimensionalizing each q_{v_k} using the characteristic scales

$$
\mathbf{S} = [S_1, S_2, \ldots, S_{n_u}],
$$

and the dimensionless parameter

$$
\mathbf{\Pi}_p = [\Pi_{p_1}, \Pi_{p_2}, \cdots, \Pi_{p_{n_u}}],
$$

both of which depend on the components of $\mathbf{q}_p$. The characteristic scales correspond to one of the fundamental units (length, time, mass, electric current, temperature, amount of substance, or luminous intensity) and can be expressed as

$$
S_i = q_{p_1}^{a_{s,i1}} \, q_{p_2}^{a_{s,i2}} \cdots q_{p_{n_p}}^{a_{s,i\,n_p}} \equiv \mathbf{q}_p^{\mathbf{a}_{s,i}},
$$

with the exponent vector

$$
\mathbf{a}_{s,i} = \left[a_{s,i1}, a_{s,i2}, \ldots, a_{s,i\,n_p}\right].
$$

The exponent vectors are arranged in the characteristic-scales coefficient matrix $\mathbf{A}_s$ (with size $n_u \times n_p$) and are constrained to one of the fundamental units. This is enforced by the equation

$$
\mathbf{D}_{\mathbf{q}_p} \mathbf{A}_s^T = \mathbf{I}, \tag{S4}
$$

where $\mathbf{D}_{\mathbf{q}_p}$ is the dimension matrix for the parameters and $\mathbf{I}$ is the identity matrix.

For example, consider the Malkus water wheel characterized by the vector of parameters

$$\mathbf{q}_p = [r,\ \phi,\ I,\ \nu,\ K,\ g],$$

the dimension matrix for parameters is

$$\mathbf{D}_{\mathbf{q}_p} = \begin{array}{c|cccccc} & r & \phi & I & \nu & K & g \\ \hline [\text{time}] & 0 & -1 & 0 & -1 & -1 & -2 \\ [\text{mass}] & 0 & 1 & 1 & 1 & 0 & 0 \end{array},$$

and a possible characteristic-scales coefficient matrix is

$$\mathbf{A}_s = \begin{array}{c|cccccc} & r & \phi & I & \nu & K & g \\ \hline S_t & 0 & 0 & 0 & 0 & -1 & 0 \\ S_m & -1 & 0 & 1 & 0 & 2 & -1 \end{array}$$

to guarantee

$$\mathbf{D}_{\mathbf{q}_p} \mathbf{A}_s^T = \begin{bmatrix} 1 & 0 \\ 0 & 1 \end{bmatrix},$$

i.e., S_t has units of time and S_m has the units of mass.

Similarly, each component of the dimensionless parameter $\mathbf{\Pi}_p$ is expressed as

$$\Pi_{p_i} = q_{p1}^{a_{p,i1}}\, q_{p2}^{a_{p,i2}} \cdots q_{pn_p}^{a_{p,i\,n_p}} \equiv \mathbf{q}_p^{\mathbf{a}_{p,i}},$$

where

$$\mathbf{a}_{p,i} = \left[a_{p,i1}, a_{p,i2}, \ldots, a_{p,i\,n_p} \right],$$

is chosen to ensure that Π_{p_i} is dimensionless. After appling IT-π, each dimensionless variable Π_i^* can be reformulated as

$$\Pi_i^* = \left(\frac{q_{v_1}}{\mathbf{S}^{\mathbf{d}_{i,1}}} \right)^{\beta_{i,1}} \left(\frac{q_{v_2}}{\mathbf{S}^{\mathbf{d}_{i,2}}} \right)^{\beta_{i,2}} \cdots \left(\frac{q_{v_j}}{\mathbf{S}^{\mathbf{d}_{i,j}}} \right)^{\beta_{i,j}} \cdot \Pi_{p_i}, \tag{S5}$$

where

$$\mathbf{S}^{\mathbf{d}_1} \equiv S_1^{d_{11}}\, S_2^{d_{21}} \cdots S_{n_u}^{d_{n_u\,1}},$$

and similarly for $\mathbf{S}^{\mathbf{d}_j}$ with $j = 2, \ldots, n_v$. Here, $\mathbf{d}_{i,j} = [d_{i,1j}, d_{i,2j}, \ldots, d_{i,n_u\,j}]$ denotes the dimensional vector associated with the variable q_{v_j}, and $\beta_{i,j}$ is the exponent of q_{v_j} in Π_i^*.

To determine the characteristic scales $\mathbf{S}$ and the dimensionless parameter $\mathbf{\Pi}_p$, we need to express the optimal solution $\mathbf{\Pi}^*$ as a combination of the characteristic scales constructed using $\mathbf{q}_p$. The reminder of the units represent the (residual) dimensionless parameter. Mathematically, this is formulated as the solution to the linear equation obtained by taking the log on both sides of Eq. (S5), while simultaneously satisfying the constraints in Eq (S4),

$$\mathbf{A}_p = -\mathbf{D}_{\mathbf{q}_v}\, \mathbf{A}_s + \mathbf{A}_{\Pi_p}, \quad s.t. \quad \mathbf{D}_{\mathbf{q}_p} \mathbf{A}_s^T = \mathbf{I}, \tag{S6}$$

where the matrix $\mathbf{A}_p$ (of size $l^* \times n_p$) represents the contribution of $\mathbf{q}_p$ to each dimensionless variable Π_i^* and its rows are given by

$$\mathbf{a}_{p,i} = \left[a_{p,i1}, a_{p,i2}, \ldots, a_{p,i\,n_p} \right].$$

S16

The matrix $\mathbf{D}_{\mathbf{q}_v}$ represents the the fundamental units of the variables $\mathbf{q}_v$ in Π_i^*, such that the i-th row of $\mathbf{D}_{\mathbf{q}_v}$ is a $1 \times n_u$ vector given by the $\sum_{k=1}^{j} \mathbf{d}_{i,k}\, \beta_{i,k}$ from Eq. (S5) for the i-th dimensionless variable Π_i^*. The matrix $\mathbf{A}_s$ is the characteristic-scales coefficient matrix to be determined (with size $n_u \times n_p$), and each row is denoted by $\mathbf{a}_{s,i}$. The residual matrix $\mathbf{A}_{\Pi_p}$ corresponds to the coefficients of the dimensionless parameters $\mathbf{\Pi}_p$, also to be determined.

Considering again the example of the Malkus water wheel, the vector of variables is characterized by

$$\mathbf{q}_v = [\omega,\, m_1,\, m_2].$$

Using IT-π, we identify the following optimal dimensionless variables:

$$\Pi_1^* = \frac{r\, g\, m_1}{I\, K^2}, \quad \Pi_2^* = \frac{v\, \omega}{I\, K^2}, \quad \Pi_o^* = \frac{\dot{\omega}}{K^2}.$$

The dimension matrix [mass, time] for these variables is given by

$$\mathbf{D}_{q_v} = \begin{array}{c|cc} & S_t & S_m \\ \hline \Pi_1^* & 0 & 1 \\ \Pi_2^* & -1 & 0 \\ \Pi_o^* & -2 & 0 \end{array}$$

and the coefficient matrix (in the order $[r,\, \phi,\, I,\, \nu,\, K,\, g]$) for the optimal variables is

$$\mathbf{A}_p = \begin{array}{c|cccccc} & r & \phi & I & \nu & K & g \\ \hline \Pi_1^* & 1 & 0 & -1 & 0 & -2 & 1 \\ \Pi_2^* & 0 & 0 & -1 & 1 & -2 & 0 \\ \Pi_o^* & 0 & 0 & 0 & 0 & -2 & 0 \end{array}$$

Equation (S6) is solved using the algorithm outlined below, which iteratively minimizes $\mathbf{A}_{\Pi_p}$ to identify the characteristic scales. The solution to the characteristic-scale coefficient matrix is

$$\mathbf{A}_s = \begin{array}{c|cccccc} & r & \phi & I & \nu & K & g \\ \hline S_t & 0 & 0 & 0 & 0 & -1 & 0 \\ S_m & -1 & 0 & 1 & 0 & 2 & -1 \end{array}$$

which leads to the characteristic time (S_t) and mass scales (S_m)

$$S_t = \frac{1}{K} \quad \text{and} \quad S_m = \frac{I\, K^2}{r\, g}.$$

The corresponding residual matrix is

$$\mathbf{A}_{\Pi_p} = \begin{array}{c|cccccc} & r & \phi & I & \nu & K & g \\ \hline \Pi_{p1} & 0 & 0 & 0 & 0 & 0 & 0 \\ \Pi_{p2} & 0 & 0 & -1 & 1 & -1 & 0 \\ \Pi_{p3} & 0 & 0 & 0 & 0 & 0 & 0 \end{array},$$

indicating that the additional dimensionless parameter is given by

$$\mathbf{\Pi}_p = [\Pi_{p1}, \Pi_{p2}, \Pi_{p3}] = \left[1, \frac{\nu}{I\, k}, 1\right].$$

The dimensionless variables in terms of the characteristic time scale and mass scale, and dimensionless parameter are

$$\Pi_1^* = \frac{m_1}{S_m}, \quad \Pi_2^* = \omega \, S_t \, \Pi_{p2}, \quad \Pi_o^* = \dot{\omega} \, S_t^2.$$

Algorithm 2 Iterative Identification for Characteristic Scales

---

Require: $\mathbf{D_{q_v}}$ and $\mathbf{A}_p$.
Ensure: $\mathbf{A}_{\Pi_p}$ and $\mathbf{A}_s$
 1: **Initialize:** $\mathbf{D}_{\mathbf{q}v}^{\text{orig}} \leftarrow \mathbf{D_{q}}v$, $\mathbf{A}_p^{\text{orig}} \leftarrow \mathbf{A}_p$, $n \leftarrow 0$
 2: **for** $n = 1$ to N_{iter} **do**
 3:     Solve for $\mathbf{A}_s^{(n)} = \arg\min_{\mathbf{A}_s} \|\mathbf{D_{q}}_v \mathbf{A}_s + \mathbf{A}_p\|_2 + \|\mathbf{D_{q_p}} \mathbf{A}_s^T - \mathbf{I}\|_2$
 4:     Compute residuals: $\mathbf{A}_{\Pi_p} = \mathbf{D_{q}}_v \mathbf{A}_s^{(n)} + \mathbf{A}_p$
 5:     **if** $|\mathbf{A}_{\Pi_{p\,i}}| \leq \epsilon$ for all i **then**
 6:         **break**
 7:     **else**
 8:         Select a row i with $|\mathbf{A}_{\Pi_{p\,i}}| > \epsilon$ and remove it
 9:         Update: $\mathbf{D_{q}}_v \leftarrow \mathbf{D_{q}}_v \setminus \mathbf{D}_{\mathbf{q}v,i}$, $\mathbf{A}_p \leftarrow \mathbf{A}_p \setminus \mathbf{A}_{p,i}$
10:     **end if**
11: **end for**
12: **Final Calculation:** $\mathbf{A}_{\Pi_p}^{\text{final}} = \mathbf{D}_{\mathbf{q}v}^{\text{orig}} \mathbf{A}_s^{(n)} + \mathbf{A}_p^{\text{orig}}$
13: **Output:** $\mathbf{A}_{\Pi_p}^{\text{final}}$ and $\mathbf{A}_s^{(n)}$

S.3   Robustness Analysis

In this section, we present a robustness analysis of IT-π alongside other dimensionless learning methods. We begin by assessing how the amount of training data influences the fidelity of the learned dimensionless groups, then examine the impact of key hyperparameter settings and the choice of input variables on both convergence and predictive accuracy. To detect overfitting, we introduce diagnostics that reveal when a model begins to memorize rather than generalize. We also show the role of the Rényi entropy order α in shaping the balance between information of preservation and error norm. Finally, to evaluate resilience under realistic conditions, we subject IT-π to a noisy-data study that incorporates all validation cases from the main text.

S.3.1   Sensitivity to the amount of training data

We evaluate the statistical uncertainties in the irreducible error, model efficiency, and dimensionless variables from IT-π. Estimating these uncertainties is essential to determine whether the conclusions drawn are statistically significant or potentially inconclusive due to limited data.

The statistical uncertainty in the normalized irreducible error, $\Delta\tilde{\epsilon}_{LB}$, arising from the finite sample size, is defined as the difference between the error bound estimated using the full dataset (N_{samples}) and that estimated using half the data ($N_{\text{samples}}/2$). This difference serves as a proxy for the expected variation in $\tilde{\epsilon}_{LB}$ if the number of samples were doubled. This approach is used throughout the manuscript to compute the error bars for $\tilde{\epsilon}_{LB}$. Since the normalized irreducible error is upper bounded by 1, $\Delta\tilde{\epsilon}_{LB}$ can be directly interpreted as a relative uncertainty. A similar procedure is applied to estimate the statistical uncertainty in model efficiency, given by $\Delta\eta = \Delta\epsilon_{LB}^*/\epsilon_f$. The final source of uncertainty concerns the persistence of the identified dimensionless variables with increasing sample size. As shown below, even when uncertainties in $\tilde{\epsilon}_{LB}$ and η are non-negligible, the dimensionless variables identified from IT-π remain remarkably robust.

We evaluate the estimated irreducible model error, its associated statistical uncertainty, and the sensitivity of the identified dimensionless variable as a function of sample size for the Rayleigh problem. The results are presented in Figure S1.

- **Irreducible error.** As shown in Figure S1(a), the estimated irreducible error $\tilde{\epsilon}_{LB}$ is initially overestimated and exhibits artificially high values for small sample sizes. However, it progressively converges to the correct value (zero) as the number of samples increases.

- **Uncertainty in irreducible error.** Figure S1(b) displays the uncertainty $\Delta\tilde{\epsilon}_{LB}$ associated with the estimated irreducible error. As expected, this uncertainty decreases monotonically with increasing sample size. This behavior provides a useful diagnostic within IT-π: it can be used to (1) assess the statistical reliability of the estimated error in Figure S1(a) and (2) extrapolate the number of samples required to achieve a desired confidence level when working with limited data.
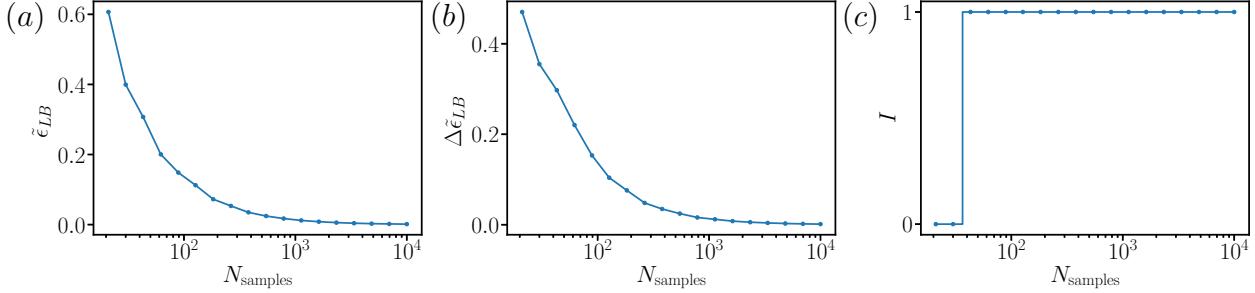
Figure S1: (a) Estimated normalized irreducible error $\tilde{\epsilon}_{LB}$, (b) uncertainty in the normalized irreducible error $\Delta\tilde{\epsilon}_{LB}$, and (c) binary indicator of whether the identified dimensionless variable matches the analytical solution (1 = correct, 0 = incorrect), all shown as functions of the number of samples N_{samples}.

- **Sensitivity of the identified dimensionless variable.** Figure S1(c) presents an indicator function that takes the value 1 when the identified dimensionless variables are correct and 0 otherwise. The results demonstrate that the discovered dimensionless variable remains remarkably stable across a broad range of sample sizes. Deviations occur only when the number of samples is very small (a handful), indicating that the method is generally robust to moderate data scarcity.

- **Sensitivity to extremely limited data.** Finally, we assess the impact of extremely limited data on the reliability of dimensionless variables identified by Active Subspaces, PyDimension, BuckiNet, BSM, and IT-π to the Rayleigh problem using datasets with 8 and 27 samples. As shown in Table S2, when 27 samples are available, only IT-π successfully recovers the analytical dimensionless variable, whereas the other methods yield spurious results. In contrast, with only 8 samples, the discovered exponents vary significantly across methods, all deviating from the analytical solution. These results indicate that IT-π requires a comparable or smaller amount of data than other methods to identify reliable dimensionless variables.

N_{samples}	Active Subspaces	PyDim-ension	Bucki-Net	BSM	IT-π (Current)
27	$y^{1.0}t^{-0.4}U^{0.2}(\mu/\rho)^{-0.6}$	$y^{1.0}t^{-1.0}U^{-1.0}$	$y^{1.0}t^{-0.84}U^{-0.67}(\mu/\rho)^{-0.16}$	$y^{1.0}U^{-1.0}(\mu/\rho)^{1.0}$	$y^{1.0}t^{-0.5}(\mu/\rho)^{-0.5}$
8	$y^{1.0}t^{-0.38}U^{0.23}(\mu/\rho)^{-0.62}$	$y^{1.0}t^{-1.0}U^{-1.0}$	$y^{1.0}t^{-1.0}U^{-1.0}$	$y^{1.0}t^{0.42}U^{-0.15}(\mu/\rho)^{0.57}$	$y^{1.0}t^{-0.86}U^{-0.72}(\mu/\rho)^{-0.14}$

Table S2: Dimensionless variable Π^* identified by different methods on the Rayleigh problem with 27 and 8 samples. The analytical optimal dimensionless input is $y^{1.0}t^{-0.5}(\mu/\rho)^{-0.5}$.

S.3.2 Sensitivity to hyperparameter choices

We investigate the impact of estimation strategies and hyperparameter configurations on various dimensionless-learning methods. Results for the Rayleigh problem with 1,000 samples are summarized in Table S3.

For IT-π, we evaluate two mutual-information estimators: the binning method and the KSG estimator (*46*). The binning method partitions the joint distribution into a fixed number of bins; a common rule of thumb is to choose the number of bins proportional to the square root of the sample size, yielding approximately 30–35 bins for 1,000 samples. Here, we vary the bin count from 10 to 100 to assess its effect. The KSG estimator, by contrast, estimates local densities via k–nearest-neighbor distances; we test k in the range 5–10, a standard choice that balances bias and variance. As shown in Table S3, all configurations recover the analytically derived dimensionless variable, demonstrating that IT-π is robust to estimator selection and hyperparameter settings when sufficient data are available.

Table S3 also summarizes the sensitivity of each method to its hyperparameters. The results show that, except for Active Subspaces, different hyperparameter settings can yield markedly different dimensionless variables. By comparison, IT-π exhibits similar or lower sensitivity to hyperparameter choice for the same number for samples.

Method	Method/Hyperparameters	Hyperparameter Settings	Discovered Π^*
IT-π	Binning estimation: Range of number of bins	10–100	$y^{1.0}\, t^{-0.5}\, (\mu/\rho)^{-0.5}$
	KSG Estimator: Range of number of neighbors	5–10	$y^{1.0}\, t^{-0.5}\, (\mu/\rho)^{-0.5}$
Active Subspaces	Kernel width γ	$\gamma = 1$	$y^{1.0}\, t^{-0.5}\, (\mu/\rho)^{-0.5}$
		$\gamma = 10$	$y^{1.0}\, t^{-0.5}\, (\mu/\rho)^{-0.5}$
PyDimension	Polynomial regression order m	$m = 5$	$y^{1.0}\, t^{-0.5}\, (\mu/\rho)^{-0.5}$
		$m = 10$	$y^{0.7}\, t^{-0.3}\, (\mu/\rho)^{-0.4}\, U^{0.1}$
BuckiNet	Kernel width γ, Ridge reg. α, ℓ_1 reg. l_1	$\gamma = 1, l_1 = 10^{-3}, \alpha = 10^{-4}$	$y^{1.0}\, t^{-0.5}\, (\mu/\rho)^{-0.5}$
		$\gamma = 10, l_1 = 10^{-3}, \alpha = 10^{-4}$	$y^{1.0}\, t^{-0.63}\, (\mu/\rho)^{-0.37}\, U^{-0.25}$
BSM	Dimension regularization weight w	$w = 10^{-3}$	$y^{1.0}\, t^{-0.5}\, (\mu/\rho)^{-0.5}$
		$w = 10^{-6}$	$y^{1.0}\, t^{-0.51}\, (\mu/\rho)^{-0.23}\, U^{-0.54}$

Table S3: Discovered dimensionless variables Π^* for various dimensionless-learning methods under different hyperparameter settings on the Rayleigh problem.

S.3.3 Sensitivity to input variable selection

This section examines how the choice of input variables influences the results of the discovered dimensionless variables. In particular, we consider three important scenarios: missing variables, redundant variables, and discrete-valued variables.

- **Missing variables** arise when relevant dimensional variables are omitted from the analysis—either because they are inaccessible, unmeasurable, or discarded a priori. In such situations, IT-π still returns the best possible dimensionless variables within the set of available inputs. We illustrate this with the Rayleigh problem, where the

analytically optimal dimensionless input variable is

$$\Pi^* = \frac{y}{\sqrt{(\mu/\rho)\,t}}$$

given the complete set of dimensional inputs $\mathbf{q} = [U, y, t, \mu, \rho]$. Suppose, however, that the variable y is unavailable, and the input list is restricted to $\mathbf{q} = [U, t, \mu, \rho]$. In this case, IT-$\pi$ identifies the dimensionless variable as

$$\frac{U^{1.0}t^{0.5}}{(\mu/\rho)^{0.5}}.$$

Naturally, this result does not coincide with the analytically correct expression, as recovering the latter is impossible without y. However, the discovered variable is still optimal within the limited set of inputs. A key feature of IT-π is its ability to detect the presence of missing variables through a non-zero irreducible error. In this example, the irreducible error increases from $\epsilon = 0\%$ (when y is included) to $\epsilon = 100\%$ (when y is omitted), signaling the information loss due to the missing variable.

- **Redundant variables** arise when input variables contain highly similar or identical information. Consider the Rayleigh problem with the set of dimensional inputs $\mathbf{q} = [U, y, t, \mu, \rho, \nu]$, where the kinematic viscosity is defined as $\nu = \mu/\rho$. In this case, ν carries the same information as the ratio μ/ρ, since $I_\alpha(\nu; \mu/\rho) = \infty$. Including both ν and μ/ρ in the input list introduces redundancy. Such redundancy leads to infinitely many equivalent optimal solutions. For example, the dimensionless input

$$\Pi^* = \frac{y}{\sqrt{(\mu/\rho)t}} = \frac{y}{\sqrt{\nu t}} = \frac{y}{\sqrt{(\mu/\rho)^\beta \nu^{1-\beta} t}}$$

remains unchanged for any value of $\beta \in [0, 1]$, since all these expressions contain the same information about the output. Formally, they yield identical mutual information with the dimensionless output:

$$I_\alpha\left(\frac{y}{\sqrt{(\mu/\rho)t}}; \Pi_o\right) = I_\alpha\left(\frac{y}{\sqrt{(\mu/\rho)^\beta \nu^{1-\beta} t}}; \Pi_o\right).$$

IT-π is able to addresses redundancy by exhaustively searching over all combinations of input variables—e.g., $[q_i]$, $[q_i, q_j]$, $[q_i, q_j, q_k]$, etc.—and selecting the smallest subset that minimizes the irreducible error ϵ_{LB}. In this example, the minimal non-redundant set would be $[U, y, t, \nu]$. This redundancy-aware selection strategy could, in principle, be extended to other dimensionless learning frameworks.

- **Discrete-valued variables** refer to input variables that take on only a finite set of values (e.g., $x = 1, 2, 3, 4, \ldots$). The presence of such variables does not fundamentally change the operation of IT-π, as both Rényi entropy and mutual information are well defined for discrete, continuous, or mixed-type variables. Therefore, the objective of the optimization-maximizing the mutual information between the input and the

output, or equivalently minimizing the irreducible error, remains valid. This enables the identification of the most predictable dimensionless variables, even when some of the input variables are discrete. In contrast, methods based on predictive models, such as those employing neural networks, may face challenges in handling discrete inputs. These approaches typically assume continuous and differentiable variables to compute gradients required for optimization during model training, which can limit their applicability or performance in settings involving discrete-valued features.

S.3.4 Diagnostics for detecting overfitting

We discuss the contrasting roles of irreducible error and model overfitting. When a sufficiently large number of samples is available (as discussed in §S.3.1), IT-π provides a reliable estimate of the irreducible error, ϵ_{LB}^*, which represents the fundamental limit below which no model—regardless of complexity—can improve its predictive performance. In this regime, model performance is best assessed by the efficiency metric η. However, for finite sample sizes, it is well known that an overly complex model may achieve perfect prediction on the training data by memorizing it (i.e. overfitting). This phenomenon does not contradict the concept of irreducible error, as a model that overfits the training data typically fails to generalize and performs poorly on new samples drawn from the same underlying probability distribution. For example, fitting ten data points with a model containing a thousand parameters may yield excellent agreement with the training data, yet fail in new samples following the same distribution. In contrast, as the number of samples approaches infinity, the performance of any model is ultimately bounded by the irreducible error regardless of its complexity.

To evaluate model performance under finite data conditions, we compare the model error ϵ_f against the uncertainty-aware irreducible error, expressed as $\epsilon_{LB}^* \pm \Delta\epsilon_{LB}^*$. The methodology for computing $\Delta\epsilon_{LB}^*$ is described in §S.3.1. Based on the relationship between ϵ_f, ϵ_{LB}^*, and $\Delta\epsilon_{LB}^*$, we classify model performance into three distinct regimes:

- **Suboptimal model within uncertainty:**

$$\epsilon_{LB}^* + \Delta\epsilon_{LB}^* < \epsilon_f.$$

  In this regime, the model error exceeds the irreducible error by more than the estimated uncertainty, indicating room for improvement.

- **Optimal model within uncertainty:**

$$\epsilon_{LB}^* - \Delta\epsilon_{LB}^* \leq \epsilon_f \leq \epsilon_{LB}^* + \Delta\epsilon_{LB}^*.$$

  The model error is statistically indistinguishable from the irreducible error, suggesting that the model is performing optimally given the available data.

- **Overfitting model within uncertainty:**

$$\epsilon_f < \epsilon_{LB}^* - \Delta\epsilon_{LB}^*.$$

  In this case, the model achieves an error lower than the estimated irreducible bound, which typically indicates overfitting—i.e., the model is capturing noise in the training data rather than generalizable structure.

To illustrate the procedure described above, we construct a synthetic example in which samples of the input variable Π are drawn uniformly from the interval $[0, 1]$. The output is defined as a smooth, nonlinear function of Π with added Gaussian noise:

$$\Pi_o = \Pi(1 - \Pi)(1 - 2\Pi)(1 - 3\Pi)(1 - 4\Pi)(1 - 5\Pi) + 0.3\,\mathcal{N}(0, 1).$$

Given access only to the input Π, the optimal predictive model is

$$\hat{\Pi}_o^* = \Pi(1 - \Pi)(1 - 2\Pi)(1 - 3\Pi)(1 - 4\Pi)(1 - 5\Pi),$$

and the irreducible error corresponds to the added Gaussian noise term, $0.3\,\mathcal{N}(0, 1)$. The analytical L_2 norm of this irreducible error is

$$\epsilon_{LB}^{*\mathrm{analytical}} = \sqrt{\mathbb{E}\left[\left(\Pi_o - \hat{\Pi}_o^*\right)^2\right]} = 0.3.$$
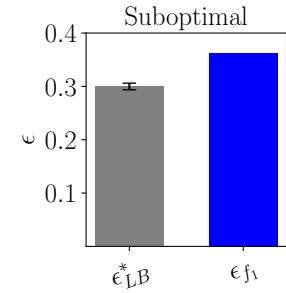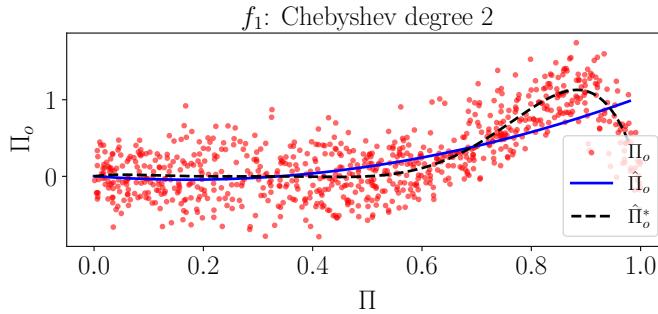
This value represents the minimum achievable error for any model, regardless of its complexity, in the limit of infinite data. In practice, using a finite sample of $N = 800$ data points, we estimate the irreducible error bound ϵ_{LB}^* and its associated statistical uncertainty $\Delta\epsilon_{LB}^*$ as

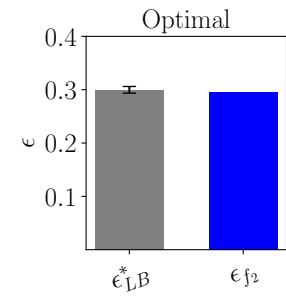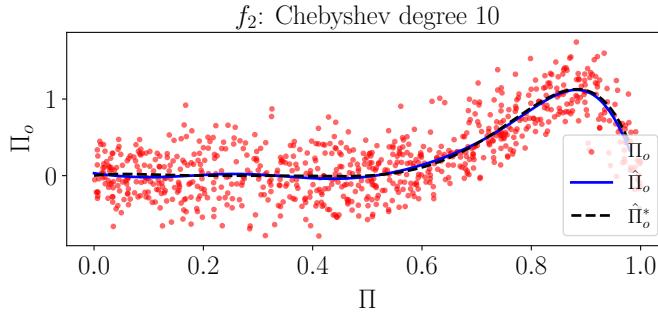$$\epsilon_{LB}^* = 0.2998, \quad \Delta\epsilon_{LB}^* = 0.0063.$$

We trained three different models on the finite-sample dataset to predict the output $\hat{\Pi}_o$: a low-degree Chebyshev polynomial (degree 2) f_1, a higher-degree Chebyshev polynomial (degree 10) f_2, and a spline f_3 with a smoothing parameter 30. The performance of the models are summarized in Figure S2.

- Panel (a) shows the performance of degree 2 Chebyshev polynomial f_1. The model $\hat{\Pi}_o$ has too few parameters to approximate accurately the analytical optimal model $\hat{\Pi}_o^*$. The model error is $\epsilon_{f_1} = 0.3627$, which exceeds the upper bound of the irreducible error interval $\epsilon_{LB}^* + \Delta\epsilon_{LB}^*$. According to the criterion, this model is classified as suboptimal, which is consistent with the visible underfitting in the plot.

- Panel (b) shows the performance of the degree 10 Chebyshev polynomial f_2. This model $\hat{\Pi}_o$ closely matches the analytical optimal model $\hat{\Pi}_o^*$ without introducing excessive oscillations. The error $\epsilon_{f_2} = 0.2945$ falls within the uncertainty interval $[\epsilon_{LB}^* - \Delta\epsilon_{LB}^*, \epsilon_{LB}^* + \Delta\epsilon_{LB}^*]$. According to the criterion, this model is optimal within uncertainty, consistent with the visually good fit.

- Panel (c) displays the performance of the smoothing spline f_3. Visually, this model $\hat{\Pi}_o$ over-fits the noisy fluctuations. The error $\epsilon_{f_3} = 0.1937$ is below the lower bound of the irreducible error interval $\epsilon_{LB}^* - \Delta\epsilon_{LB}^*$. According to our criterion, the model is classified as overfitting, which agrees with the observed tendency to fit noise rather than only the true predictable function.
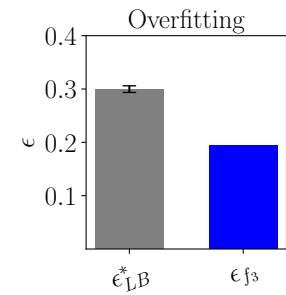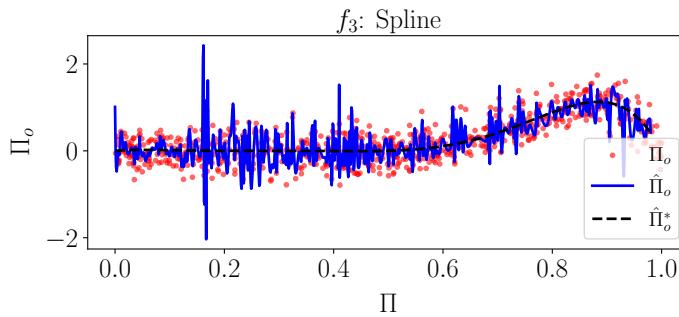
Figure S2: Example of how statistical uncertainty in the estimated irreducible error can be used to diagnose model overfitting. Three models, (a), (b), and (c), are fitted to the same dataset and evaluated against the estimated irreducible error. In each case, the left panel shows the analytical optimal model (dashed), the fitted model prediction (blue), and the noisy output data (red). The corresponding bar plots on the right compare the model error ϵ_f with the irreducible error ϵ_{LB}^* and its uncertainty $\Delta\epsilon_{LB}^*$. Based on this comparison, the models are classified as: (a) suboptimal, (b) optimal within uncertainty, and (c) overfitting.

S.3.5 Robustness of IT-π to noise

Effect of Noise across Benchmark Cases
We systematically evaluate the impact of noise on IT-π across all benchmark cases. Gaussian noise of increasing intensity is added to the dimensional variables, and IT-π is then reapplied to recover the optimal dimensionless variables. The results, summarized in Table S4, demonstrate that IT-π consistently recovers the correct dimensionless relationships even under noise levels as high as 20%. Below, we provide additional details of the procedure for two representative cases: the Rayleigh problem and the Colebrook equation.

Noise Level	1%	5%	10%	20%
Rayleigh problem	✓	✓	✓	✓
Colebrook equation	✓	✓	✓	✓
Malkus waterwheel	✓	✓	✓	✗
Rayleight-Bénard convection	✓	✓	✓	✓
Blasius boundary layer	✓	✓	✓	✓

Table S4: Effect of noise on the discovered dimensionless variable by IT-π for all validation cases. Four noise levels are tested: $1\%, 5\%, 10\%, 20\%$. ✓ indicates that the method successfully recovered the analytical dimensionless variable.

Rayleigh problem. We evaluate the robustness of IT-π on the Rayleigh problem by introducing noise into the velocity profile as follows:

$$u_{\text{noisy}} = u + \epsilon,$$

where

$$u = U \operatorname{erfc}\left(\frac{\xi}{2}\right)$$

is the noiseless solution, and

$$\epsilon \sim \mathcal{N}\left(0, (\sigma \cdot U)^2\right)$$

represents Gaussian noise with zero mean and a standard deviation proportional to U. Here, σ is a scaling factor that determines the noise level as a fraction of U. We test four noise levels: 1%, 5%, 10% and 20%, corresponding to $\sigma = 0.01$, 0.05, 0.1, and 0.2, respectively. Figure S3 visualizes the relationship between Π_o^* and Π^* as discovered by IT-π at different noise levels. For all noise levels, the resulting dimensionless variable agrees with that obtained from the noiseless data:

$$\Pi^* = y^{1.0} \, t^{-0.5} \, \mu^{-0.5} \, \rho^{0.5}.$$

Colebrook equation We assess the robustness of IT-π under noisy data using the Colebrook equation. To simulate measurement noise, we perturb the friction coefficient as

$$C_{f,\text{ noisy}} = C_f + \epsilon,$$

where C_f is the noiseless solution computed from the Colebrook equation and
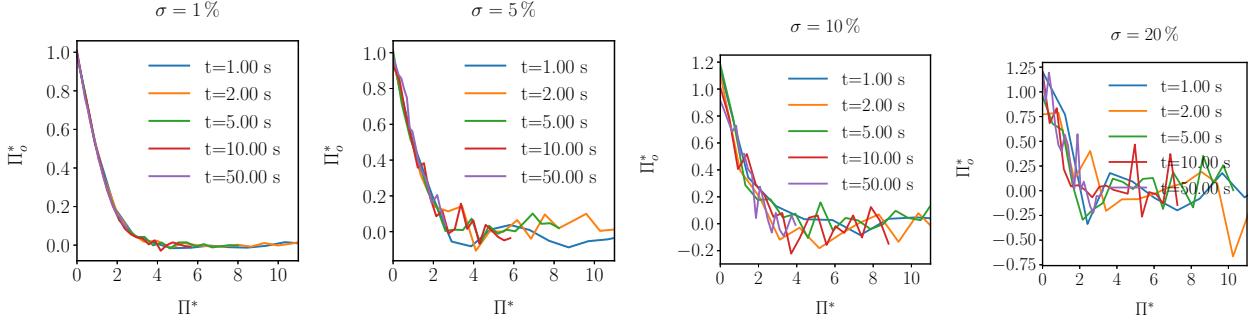
$$\epsilon \sim \mathcal{N}\left(0, (\sigma \cdot C_f)^2\right)$$

Figure S3: Robustness of IT-π to noise for Rayleigh problem. Visualization of Π_o^* as a function of Π^* for different noise levels.

is the zero-mean Gaussian noise with standard deviation proportional to C_f. We evaluate four noise levels of 1%, 5%, 10% and 20% ($\sigma = 0.01, 0.05, 0.1,$ and 0.2, respectively). Figure S4 visualizes the relationship between Π_o^* and Π^* as discovered by IT-π at different noise levels. Across all noise levels, the identified dimensionless variables remain consistent with those from the noiseless data,

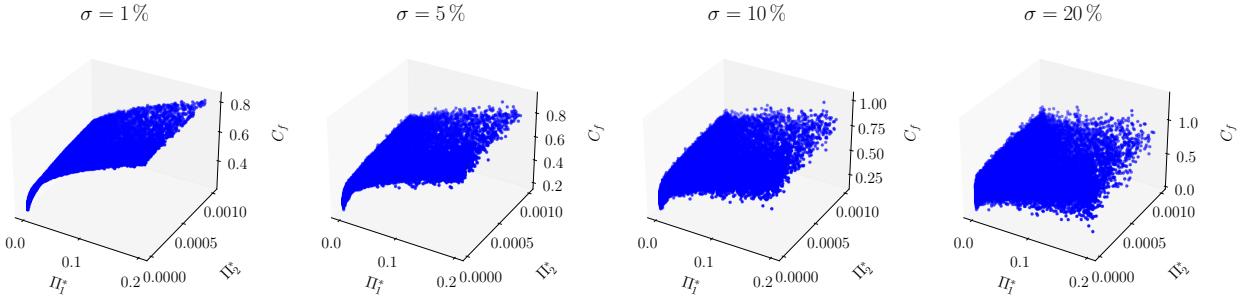$$\Pi_1^* = \frac{k}{D}, \quad \Pi_2^* = \frac{\mu}{U\rho D}.$$

Figure S4: Robustness of IT-π to noise for Colebrook equation. Visualization of Π_o^* as a function of Π^* for different noise levels.

Theoretical Analysis of IT-π under Noise

The robustness of IT-π to noise can be explained by the invariance of the optimal mutual information under additive noise. Consider the assumption of additive noise sources $\mathbf{W}_I$ and W_O, which are independent of each other and also independent of $\mathbf{\Pi}$ and Π_o. Let us also assume that there are no statistical uncertainties in the estimation of the mutual information. By the data processing inequality (*28*), we have

$$I_\alpha\big(\mathbf{\Pi} + \mathbf{W}_I; \Pi_o + W_o\big) \leq I_\alpha\big(\mathbf{\Pi}; \Pi_o\big),$$

which implies that the mutual information generally decreases due to the added noise.

However, while this degradation increases the irreducible error, the optimal dimensionless variables remain unchanged if $\mathbf{\Pi}^*$, Π_o^* are jointly Gaussian distributed, $\mathbf{W_I}$ and W_O are independent Gaussian variables,

$$\mathbf{\Pi}^*, \ \Pi_o^* = \arg\min_{\mathbf{\Pi}, \Pi_o} \max_\alpha[\epsilon_{LB}] = \arg\min_{\mathbf{\Pi}+\mathbf{W}_I, \Pi_o+W_O} \max_\alpha[\epsilon_{LB}].$$

This invariance under noise ensures that IT-π consistently identifies the most predictive dimensionless inputs, despite the reduction in mutual information caused by noise. This is a key property that makes IT-π robust in real-world applications where noisy measurements are inevitable.

Proof. Consider the minimizer for the irreducible error $\mathbf{\Pi}^*$, $\Pi_o^* = \arg\min_{\mathbf{\Pi}, \Pi_o}[\epsilon_{LB}]$ which is equivalently the minimizer for the conditional entropy $\mathbf{\Pi}^*$, $\Pi_o^* = \arg\min_{\mathbf{\Pi}, \Pi_o} h_\alpha(\Pi_o \mid \mathbf{\Pi})$, which indicates that

$$\forall \Pi_o, \mathbf{\Pi} \quad h_\alpha(\Pi_o \mid \mathbf{\Pi}) \geq h_\alpha(\Pi_o^* \mid \mathbf{\Pi}^*).$$

We want to prove that adding independent Gaussian noise to both the input and output preserves the minimizer of the conditional entropy,

$$h_\alpha(\Pi_o \mid \mathbf{\Pi}) \geq h_\alpha(\Pi_o^* \mid \mathbf{\Pi}^*) \Rightarrow h_\alpha(\Pi_o + W_O \mid \mathbf{\Pi} + \mathbf{W}_I) \geq h_\alpha(\Pi_o^* + W_O \mid \mathbf{\Pi}^* + \mathbf{W}_I).$$

To prove that, consider the Rényi conditional differential entropy jointly Gaussian random variables is given by

$$h_\alpha(\Pi_o \mid \mathbf{\Pi}) = \frac{1}{2} \log\left(2\pi \operatorname{Var}(\Pi_o \mid \mathbf{\Pi})\right) - \frac{1}{2(1-\alpha)} \log\alpha.$$

Since the logarithm is an increasing function, it follows that

$$h_\alpha(\Pi_o \mid \mathbf{\Pi}) \geq h_\alpha(\Pi_o^* \mid \mathbf{\Pi}^*) \quad \Longleftrightarrow \quad \operatorname{Var}(\Pi_o \mid \mathbf{\Pi}) \geq \operatorname{Var}(\Pi_o^* \mid \mathbf{\Pi}^*).$$

Because the noise $\mathbf{W}_I$ and W_O is independent and Gaussian, it follows that

$$\operatorname{Var}(\Pi_o + W_O \mid \mathbf{\Pi} + \mathbf{W}_I) = \operatorname{Var}(\Pi_o \mid \mathbf{\Pi} + \mathbf{W}_I) + \operatorname{Var}(W_O)$$
$$\operatorname{Var}(\Pi_o^* + W_O \mid \mathbf{\Pi}^* + \mathbf{W}_I) = \operatorname{Var}(\Pi_o^* \mid \mathbf{\Pi}^* + \mathbf{W}_I) + \operatorname{Var}(W_O)$$

Therefore, the ordering of the variances is preserved:

$$\operatorname{Var}(\Pi_o + W_O \mid \mathbf{\Pi} + \mathbf{W}_I) \geq \operatorname{Var}(\Pi_o^* + W_O \mid \mathbf{\Pi}^* + \mathbf{W}_I),$$

which implies

$$h_\alpha(\Pi_o + W_O \mid \mathbf{\Pi} + \mathbf{W}_I) \geq h_\alpha(\Pi_o^* + W_O \mid \mathbf{\Pi}^* + \mathbf{W}_I).$$

Therefore,

$$\forall \Pi_o, \mathbf{\Pi} \quad h_\alpha(\Pi_o \mid \mathbf{\Pi}) \geq h_\alpha(\Pi_o^* \mid \mathbf{\Pi}^*) \Rightarrow h_\alpha(\Pi_o + W_o \mid \mathbf{\Pi} + \mathbf{W}_I) \geq h_\alpha(\Pi_o^* + W_o \mid \mathbf{\Pi}^* + \mathbf{W}_I),$$

which indicates

$$\mathbf{\Pi}^*, \Pi_o^* = \arg\min_{\mathbf{\Pi}, \Pi_o} \max_\alpha [\epsilon_{LB}] = \arg\min_{\mathbf{\Pi} + W_I, \Pi_o + W_O} \max_\alpha [\epsilon_{LB}].$$

$\square$

S.3.6 Effect of the order α in the Rényi entropy

Rényi entropy introduces the order α that generalizes the classic Shannon entropy, which corresponds to the special case $\alpha = 1$. The value of α controls the relative emphasis placed on different regions of the error distribution $\mathcal{E}$. Lower values of α assign greater weight to the tails—highlighting rare events—while higher values emphasize the mode of the distribution. This flexibility makes Rényi entropy particularly suitable when the conditional density $\rho(\Pi_o \mid \Pi)$ is heavy-tailed, asymmetric, or multi-modal. This is leveraged by IT-π to estimate the irreducible error for different L_p-norms by finding the best value of α as part of the optimization problem. When the error distribution is approximately Gaussian or concentrated, the influence of α is minimal, and standard Shannon entropy is typically sufficient.

In the cases discussed in the main text, where the irreducible error is close to zero and the error norm of interest is set to $p = 2$, varying the Rényi entropy order has small or no impact on the minimum irreducible error ϵ_{LB}^* and the resulting dimensionless variables Π^*. Hence, the standard Shannon entropy ($\alpha = 1$) is sufficient in such cases. To illustrate this, we consider the Rayleigh problem and plot ϵ_{LB} as a function of the coefficient β for different values of α=0.5, 1.0, and 1.5. The candidate dimensionless variable is expressed as

$$\Pi = \sqrt{\frac{y}{Ut}} \left(\frac{Uy}{\mu/\rho} \right)^{\beta},$$

where β is the optimization parameter. As shown in Figure S5, across all tested values of α, the optimal coefficient remains $\beta^* = 0.5$, indicating that the discovered variable is insensitive to the choice of α in this case.
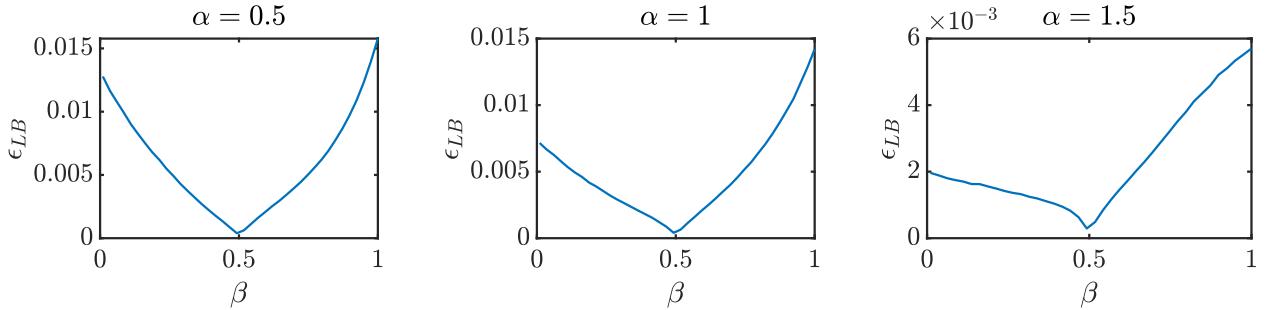

Figure S5: Comparison of ϵ_{LB} as a function of β for different values of α in the Rayleigh problem.

In other situations, the choice of α plays a fundamental role in identifying the optimal dimensionless variables. This is demonstrated in §S.4.1, where we show that the optimal variables depend on whether the goal is to predict extreme events or more frequent occurrences, as determined by the choice of error norm. The reader is referred to that section for further details.

S.4 Additional Validation

S.4.1 Optimal dimensionless inputs adapted to different error norms

We present a validation case that examines how the optimal dimensionless input Π^*, discovered by IT-π, varies depending on the selected L_p-norm for the error. One scenario where this behavior is particularly relevant is in the prediction of extreme events, which is crucial for mitigating risks associated with rare but high-impact occurrences. As a representative example, we define the dimensionless output $\Pi_o^*(t)$ as

$$\Pi_o^*(t) = \begin{cases} \Pi_2(t) & \text{if } |\Pi_o(t - \delta t)| > 2, \\ \Pi_1(t) & \text{if } |\Pi_o(t - \delta t)| \leq 2, \end{cases}$$

where δt is the time step, and Π_1 and Π_2 denote two dimensionless variables drawn from different distributions. Specifically, $\Pi_1 \sim U(-2.1, 2.1)$ is uniformly distributed, while $\Pi_2 \sim \mathcal{N}(0, 5)$ follows a normal distribution, as shown in Figure S6(a). In this example, the inputs are already dimensionless, allowing us to focus on the ability of IT-π to identify inputs optimized for a given L_p error norms. For large L_p-norms, the error is predominantly driven by extreme values determined by the information in $\Pi^* = \Pi_2$. Conversely, for small L_p-norms, the error is mainly influenced by $\Pi^* = \Pi_1$, which governs the weak variations in Π_o^*.

We apply IT-π to identify optimal inputs for two norms, $p = 1$ and $p = 10$. The candidate dimensionless variables can be expressed as $\Pi = \Pi_1 \Pi_2^\beta$, where β is a free parameter. Figures S6(b) and (c) illustrate how the irreducible error depends on β for the two error norms.

To identify α^* that generates the tightest possible bound, we perform a golden-section search over $\alpha \in \left(\frac{1}{1+p}, 10 \right]$. As shown in Figure S6(d) and (e), the value of α^* that generates the tightest bound ϵ_{LB} varies with the norm used. For $p = 1$ (panel (b)), the optimal dimensionless variable is $\Pi^* = \Pi_1$, corresponding to $\beta^* = 0$. The tightest bound is achieved using $\alpha^* = 1.0$. In contrast, for $p = 10$ (panel (c)), IT-π identifies $\Pi^* = \Pi_2$, consistent with $\beta^* \to \infty$. The tightest bound is achieved when α^* is close to 0.3. This validation case demonstrates that IT-π can effectively tailor the optimal dimensionless input Π^* to the chosen L_p-norm.
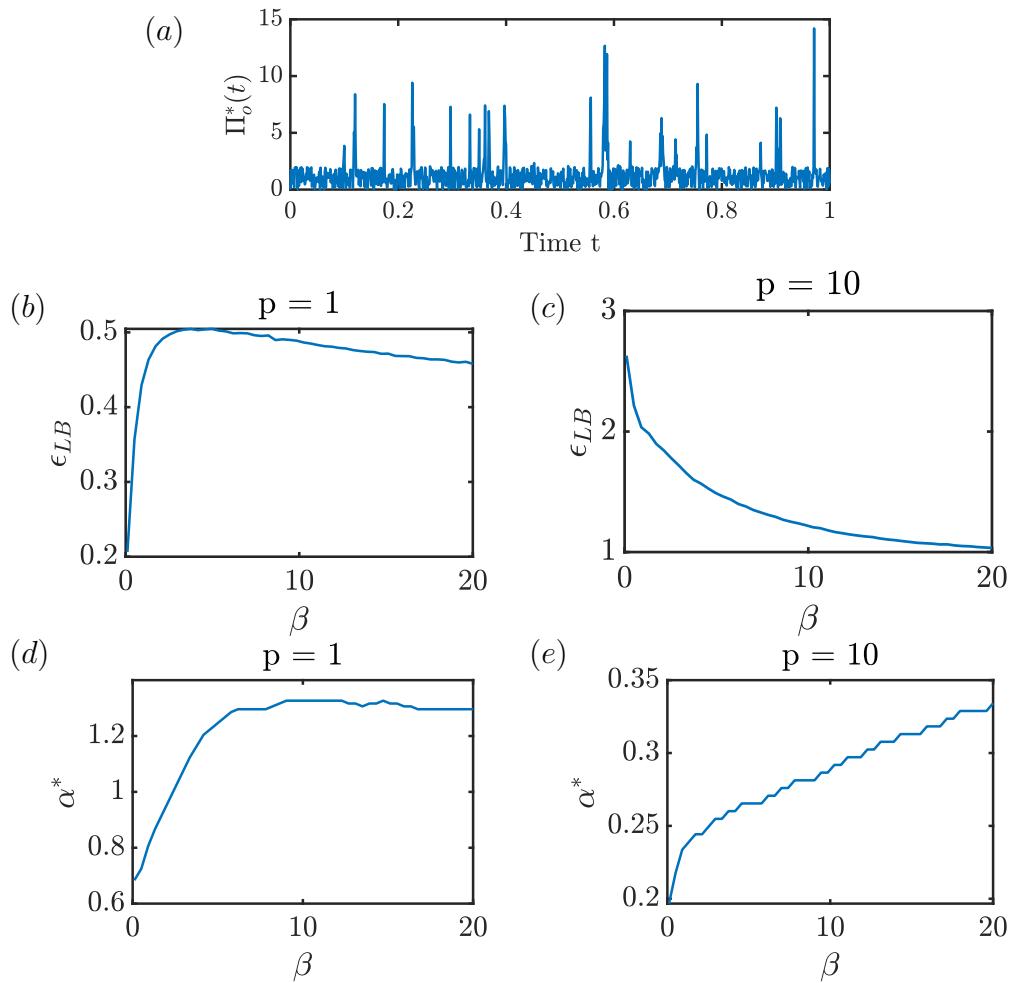
Figure S6: (a) Time evolution of $\Pi_o^*(t)$. (b,c) Irreducible error $\epsilon_{LB}(\Pi)$ for $\Pi = \Pi_1 \Pi_2^\beta$ as a function of β for (b) $p = 1$ and (c) $p = 10$. (d,e) α^* corresponds to the value that yields the tightest bound as a function of β for (d) $p = 1$ and (e) $p = 10$.

S.4.2 Details of the dimensionless input discovered by other methods

The dimensionless input discovered by other methods using the same output Π_o^* across all validation and application cases in the main text, is summarized in Table S5.

Method	Active Subspaces	PyDimension	BuckiNet	BSM
Rayleigh problem	$yt^{-0.5}(\mu/\rho)^{-0.5}$	$yt^{-0.5}(\mu/\rho)^{-0.5}$	$yt^{-0.5}(\mu/\rho)^{-0.5}$	$yt^{-0.5}(\mu/\rho)^{-0.5}$
Colebrook equation	$[(U\rho D/\mu)^{-0.3}(k/D)^{0.4},$ $(U\rho D/\mu)^{-0.4}(k/D)^{-0.6}]$	$\mu^{-0.8}U^{0.8}\rho^{0.8}D^{0.3}k^{0.5}$	$[U\rho k/\mu,$ $(U\rho D/\mu)(D/k)]$	N/A
Malkus waterwheel	$[\frac{r^{1.6}q_1^{1.6}I^{1.2}g^{1.9}\omega^{0.3}m_1^{1.0}}{v^{2.9}K^{2.7}m_2^{0.8}},$ $\frac{r^{0.1}v^{0.1}K^{0.1}g^{0.1}m_1^{0.8}}{q_1^{0.3}I^{0.2}\omega^{0.2}m_2^{0.3}}]$	$\frac{I^{0.8}g\omega^{0.2}m_1^{0.8}m_2^{0.4}}{r^{1.6}q_1^{1.5}v^{0.5}K^{0.2}}$	$[\frac{rI^{1.8}K^{2.5}\omega^{1.7}m_2^{1.25}}{q_1^{0.5}v^2g^{0.8}m_1^{0.7}},$ $\frac{rq_1K^{0.5}}{v^{0.3}g^{0.7}m_1^{0.8}}]$	N/A
Rayleight-Bénard convection	$\rho^{0.6}h^{2.1}\Delta Tg^{0.7}\alpha/(\mu^{0.6}\kappa^{0.8})$	$\rho h^3\Delta Tg\alpha/(\mu\kappa)$	$h^{-3.6}\Delta T\alpha\mu^{9.3}g^{-1.2}\kappa^{-6.9}\rho^{-9.3}$	N/A
Blasius boundary layer	$U^{0.5}y^{1.0}\rho^{0.5}/(\mu^{0.5}x^{0.5})$	$U^{0.5}y^{1.0}\rho^{0.5}/(\mu^{0.5}x^{0.5})$	$U^{0.5}y^{1.0}\rho^{0.5}/(\mu^{0.5}x^{0.5})$	$U^{0.5}y^{1.0}\rho^{0.5}/(\mu^{0.5}x^{0.5})$
Velocity scaling	$(\rho/\rho_w)^{-0.25}(\mu_w/\mu)$	$(\rho/\rho_w)^1(\mu/\mu_w)^{0.9}\left(y\rho\sqrt{\tau_w/\rho_w}/\mu\right)^{-0.3}$	$y\rho_w\sqrt{\tau_w/\rho_w}\mu^{-0.333}\mu_w^{-0.667}$	N/A
Wall flux	$\Pi_\tau=[\frac{(T/T_w)^{0.1}(y/k_{rms})^{0.7}ES^{0.1}}{M^{0.1}(y/Ra)^{0.7}},$ $\frac{(T/T_w)^{0.6}Re^{0.1}(y/Ra)^{0.2}ES^{0.3}}{M^{0.2}(y/Ra)^{0.2}}]$ $\Pi_q=[\frac{(T/T_w)^{0.7}(y/k_{rms})^{0.1}}{(y/Ra)^{0.1}},$ $\frac{(y/k_{rms})^{0.7}}{(T/T_w)^{0.1}(y/Ra)^{0.7}}]$	$\Pi_\tau=\frac{Pr^{0.1}(y/Ra)^{0.7}}{(T/T_w)^{0.2}Re^{0.8}(y/k_{rms})^{0.1}ES^{0.4}}$ $\Pi_q=\frac{Pr^{0.7}(y/Ra)^{0.8}}{Re^{0.6}(y/k_{rms})^{0.6}}$	$\Pi_\tau=[\frac{(T/T_w)^{0.5}\cdot Re^{0.5}\cdot(y/k_{rms})^{0.3}\cdot(y/Ra)^{0.3}\cdot ES^{0.8}}{M^{0.1}\cdot Pr^{0.3}},$ $\frac{(T/T_w)^{0.6}\cdot Re^{0.1}\cdot M^{0.9}\cdot Pr^{0.4}\cdot(y/Ra)^{0.5}}{(y/k_{rms})^{0.8}\cdot ES^{0.8}}]$ $\Pi_q=[\frac{(T/T_w)^{1.0}\cdot Re^{0.5}}{M^{0.1}\cdot(y/k_{rms})^{0.5}\cdot ES^{0.2}},$ $\frac{(T/T_w)^{2.3}\cdot Re^{0.9}\cdot(y/Ra)^{0.1}}{M^{1.0}\cdot Pr^{0.1}\cdot ES^{2.5}}]$	N/A
Skin friction	$U_\infty^{0.25}(\nu/\rho)^{-0.14}M^{-0.05}\delta^{0.12}\delta^*\theta^{-0.92}$	$U_\infty^{0.8}(\nu/\rho)^{-0.2}M^{-0.3}\delta^{0.3}\delta^*\theta^{-0.8}$	$U_\infty^{1.6}(\nu/\rho)^1M^{-1.3}\delta^{-1.9}\delta^*\theta^{1.2}$	N/A
MHD power generator	$l^3\rho\frac{dp}{dx}/\mu^2$	$l^3\rho\frac{dp}{dx}/\mu^2$	$l^3B_0^{5.5}\eta^{-2.8}\frac{dp}{dx}^{-0.8}\mu^{-1}\rho^{-0.8}$	N/A
Laser-metal interaction	$\eta P^{-0.03}\rho^{0.03}C_p^{-0.41}(T_1-T_0)^{-0.41}r_0^{0.81}\alpha^{0.08}$	$\frac{\eta P}{(T_1-T_0)\rho C_p\sqrt{\alpha V_s}r_0^3}$	$\eta P^{-0.1}\rho C_p^{0.1}(T_1-T_0)^{0.5}r_0^{-1}\alpha^{-0.1}$	N/A

Table S5: Comparison of Active Subspaces, PyDimension, BuckiNet, and BSM across validation and application cases. The table presents the discovered inputs $\mathbf{\Pi}$ identified by each method. N/A refers to 'not applicable'.
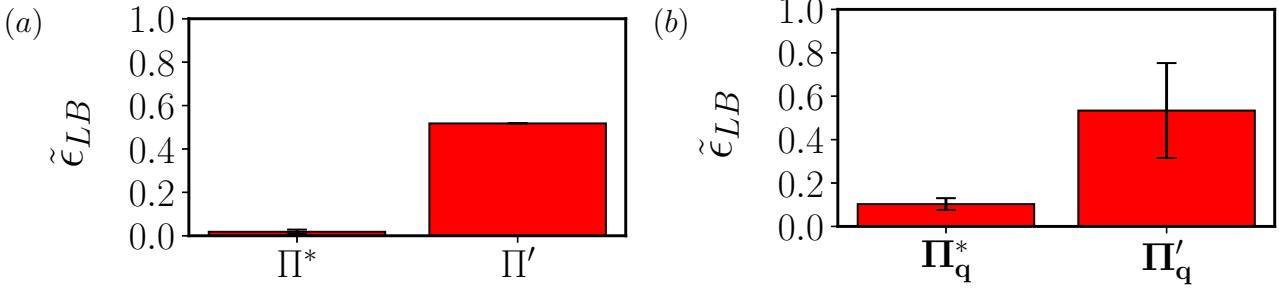
Figure S7: Comparison of optimal and suboptimal dimensionless variables in terms of the normalized irreducible error, $\tilde{\epsilon}_{LB}(\Pi)$, for (a) the Rayleigh problem using a single input Π^* (optimal) and Π' (suboptimal) and (b) dimensionless learning for wall fluxes using the two optimal inputs in $\mathbf{\Pi}^*$ and the four suboptimal inputs in $\mathbf{\Pi}'$.

S.4.3 Comparison of optimal and suboptimal dimensionless variables

We show the advantage of using IT-π compared to a suboptimal solution from Buckingham-π theorem. We illustrate this in two different problems: the Rayleigh problem and dimensionless learning for wall fluxes.

The Rayleigh Problem. Let us assume we want to explain the dimensionless output u/U using only one dimensionless variable. A simple suboptimal dimensionless input extracted from the Buckingham-π theorem is $\Pi' = y/(Ut)$. Figure S7(a) shows that Π' yields a normalized irreducible error of approximately 50%, whereas the optimal dimensionless variable from IT-π achieves an irreducible error close to 0%.

Dimensionless learning for wall fluxes. The suboptimal dimensionless inputs, denoted as $\mathbf{\Pi_q}'$, are constructed from the Buckingham-π theorem as follows:

$$\Pi'_{q,1} = \frac{y\,u\,\rho}{\mu}, \quad \Pi'_{q,2} = \frac{u}{\sqrt{c_p\,T}}, \quad \Pi'_{q,3} = \frac{c_p\,\mu}{\kappa}, \quad \Pi'_{q,4} = \frac{y}{k_{\mathrm{rms}}}.$$

These variables are chosen because they coincide with four well-known dimensionless groups in the fluid dynamics community: the local Reynolds number, Mach number, Prandtl number, and the relative roughness height. Hence, they can be expected to be a reasonable choice by experts in the field. Figure S7(b) indicates that, despite containing four variables, the suboptimal inputs $\mathbf{\Pi_q}'$ yield an irreducible error of 0.6 compared to 0.1 when using the optimal inputs $\mathbf{\Pi_q}^*$, even though the latter comprises only two dimensionless variables. When training neural networks with the ANN$_3$ architecture, using four suboptimal inputs results in a reduced efficiency of 82% despite using four inputs instead of two.

S.4.4 Comparison of gradient-based and IT-π rankings

We compare the sensitivity of the discovered dimensionless variables and their associated importance rankings between gradient-based methods and IT-π. Three challenging scenarios

are considered: (i) when the list of dimensional input variables is incomplete, (ii) when the magnitudes of the input variables differ significantly, and (iii) when the available data are limited relative to the input dimensionality. We show that, in such cases, gradient-based methods may fail to accurately identify and rank the variables that are truly important for predicting the output. In contrast, IT-π performs robustly, correctly identifying the most predictive input variables and their relative importance.

As presented in the Results section of the main text, the ranking in IT-π is constructed by ordering the normalized irreducible error associated with each individual dimensionless variable. For example, if

$$\epsilon_{LB}(\Pi_2) \geq \epsilon_{LB}(\Pi_1) \geq \cdots \geq \epsilon_{LB}(\Pi_4),$$

then Π_4 is identified as the most predictive variable and Π_2 as the least predictive. This ranking reflects the relative informativeness of each variable in predicting the output.

In the gradient-based ranking frameworks, the importance of dimensionless variables is quantified using a derivative-based global sensitivity metric. This is achieved by expressing the physical relationship in a dimensionless form and applying a logarithmic transformation to the dimensionless inputs. Then, the importance of the i-th input variable is defined as

$$\nu_i = \int \left(\frac{\partial}{\partial \gamma_i} g(\gamma) \right)^2 \rho(\gamma) \, d\gamma = \mathbb{E}\left[\left(\frac{\partial}{\partial \gamma_i} g(\gamma) \right)^2 \right], \qquad i = 1, \ldots, m, \qquad \text{(S7)}$$

where $g(\gamma)$ is the response surface (i.e. model), $\rho(\gamma)$ is a probability density over the input space, and $\gamma_i = \log(\Pi_i)$ denotes the i-th log-transformed dimensionless variable. The metric ν_i measures the average change in the output g as Π_i is perturbed within the support of ρ. If $\nu_i > \nu_j$, then perturbing Π_i is expected to influence g more than perturbing Π_j, on average. This provides a natural definition of variable importance and allows for a ranking based on the sensitivity of the output to each input direction. For the response surface g, we employ a kernel regression model with a scaled radial basis function kernel, where the kernel width is treated as a learnable hyperparameter and adaptively optimized during training. Next, we discuss several challenging scenarios, each accompanied by an illustrative example.

- **Incomplete list of dimensional input variables**

  We analyze the case in which one or more relevant dimensional variables are missing from the input set. This is a common situation that may arise when certain variables are not measurable, are unknown, or are discarded a priori under the assumption that they are irrelevant. To illustrate this scenario, we construct an example in which one relevant dimensional variable is omitted from the input list. The output is defined as

  $$\Pi_o = \Pi_1^{1/3} \Pi_2^{2/3} \Pi_3,$$

  where

  $$\Pi_1 = \frac{u_1 y}{\mu/\rho}, \quad \Pi_2 = \frac{u_2 y}{\mu/\rho}, \quad \Pi_3 = \frac{u_3 y}{\mu/\rho},$$

  and u_1, u_2, u_3 are velocities, y is a characteristic length, μ is the dynamic viscosity, and ρ is the density. The available input variables are given by $\mathbf{q} = [u_1, u_2, y, \mu, \rho]$,

which excludes u_3—a variable necessary for accurately predicting Π_o. The analytically optimal dimensionless input based on the available set $\mathbf{q}$ is:

$$\Pi^{*,\text{Analytical}} = \Pi_1^{1/3}\Pi_2^{2/3} = \frac{u_1^{1/3}u_2^{2/3}y}{\mu/\rho}.$$

We generate 1,000 samples of the dimensional inputs and the corresponding output, and apply both gradient-based ranking and IT-π to identify the dominant dimensionless variable.

Gradient-based ranking results in the dominant input direction

$$\Pi^{*,\text{Gradient-based}} = \frac{u_1^{0.7}u_2^{0.26}y}{\mu/\rho},$$

which does not recover the true analytical solution. The deficiency arises from the fact that gradient-based methods rely on the gradient of a model g, which approximates the true physical relationship. However, when a key dimensional input is missing, the model g becomes a projection of the true relationship onto a lower-dimensional subspace that excludes an essential direction. This omission prevents the computed dimensionless variables from fully spanning the relevant physical parameter space. As a result, the gradient information becomes misleading: variables that are actually important may appear unimportant, and vice versa. This distortion compromises the reliability of gradient-based rankings, making them an inaccurate reflection of the true influence of the underlying dimensionless variables.

IT-π ranking correctly identifies the optimal input,

$$\Pi^* = \frac{u_1^{0.33}u_2^{0.67}y}{\mu/\rho} \approx \frac{u_1^{1/2}u_2^{2/3}y}{\mu/\rho},$$

despite the missing variable. The reason for this success arises from the fact that, unlike gradient-based methods—which rely on a complete set of dimensional inputs to compute sensitivities—IT-π does not rely on gradients or predefined model structures. Instead, the discovery of predictive dimensionless variables is formulated as an optimization problem, where the objective is to minimize the irreducible error. This model-free, information-theoretic formulation results in greater robustness of the method. As a result, when a relevant input variable is missing, IT-π is still able to identify the best possible predictive dimensionless combination from the available inputs—without generating distorted rankings or depending on incomplete gradient information. This makes IT-π particularly well-suited for real-world scenarios in which some relevant physical variables may be unmeasurable or unknown a priori.

- **Magnitude of input variables differs significantly**

  The second challenging situation arises when the range of values taken by a variable differs significantly from that of others, even though this disparity is not reflected in the

governing equation itself. To illustrate this case, we construct an analytical example in which the output Π_o is related to the inputs $\mathbf{\Pi} = [\Pi_1, \Pi_2]$ as follows:

$$\Pi_o = \sin\left(\log\left(\Pi_1\right)\right) + \log(\Pi_2) = \sin(\gamma_1) + \gamma_2,$$

where

$$\Pi_1 = e^{\gamma_1}, \quad \Pi_2 = e^{\gamma_2},$$

and

$$\gamma_1 = \log(\Pi_1) \sim \text{Uniform}[0, 1], \quad \gamma_2 = \log(\Pi_2) \sim \text{Uniform}[0, 0.02].$$

Note that the values taken by Π_2 are much smaller in magnitude than those of Π_1. In this example, Π_1 is significantly more informative, as it explains nearly all of the variance in the output. In contrast, Π_2 contributes only a small perturbation and effectively behaves as noise.

Gradient-based ranking. The gradient-based sensitivities are given by

$$\nu_1 = \mathbb{E}\left[\left(\frac{\partial \Pi_o}{\partial \gamma_1}\right)^2\right] = \mathbb{E}\left[\cos^2(\gamma_1)\right] = \frac{1}{2} + \frac{\sin(2)}{4} \approx 0.727,$$

$$\nu_2 = \mathbb{E}\left[\left(\frac{\partial \Pi_o}{\partial \gamma_2}\right)^2\right] = \mathbb{E}\left[1^2\right] = 1.$$

As shown in the left panel of Figure S8, the gradient-based criterion incorrectly ranks Π_2 as more important than Π_1. This outcome arises because the gradient-based metric does not account for the significantly narrower range of values of Π_2, which contributes negligibly to the overall variability of Π_o. Despite its high gradient magnitude, Π_2 behaves effectively as noise, while Π_1 governs most of the output variance.

IT-π ranking. The ranking fromIT-π is based on the irreducible error of each individual variable

$$\tilde{\epsilon}_{LB}(\Pi_1) = 0.03, \quad \tilde{\epsilon}_{LB}(\Pi_2) = 0.99.$$

As shown in the right panel of Figure S8, IT-π correctly identifies Π_1 as the dominant contributor. This example highlights that gradient-based rankings must be applied with caution when input variables differ significantly in scale. This limitation can be easily mitigated by standardizing the dimensional input variables to lie within similar ranges before model fitting and gradient computation. Nonetheless, IT-π does not require such preprocessing as its formulation is inherently invariant to input scaling.

- **Available data are limited relative to the input dimensionality**

  The third challenging scenario arises when only a limited number of samples are available for analysis. To illustrate this case, we revisit the Rayleigh problem under data-scarce conditions, specifically considering a setting with only 27 samples. As shown in Table S2, IT-π successfully recovers the known optimal dimensionless variable, whereas the gradient-based method (Active Subspaces) fails to identify the correct ranking and

instead produces a spurious leading variable. This failure stems from the fact that, in high-dimensional settings with limited data, the surrogate response surface fitted by Active Subspaces is poorly constrained and does not faithfully represent the underlying physical relationship. Although IT-π is also susceptible to errors when data are extremely sparse, it tends to perform more reliably by avoiding the use of gradient estimates from surrogate models, resulting in greater robustness under limited data conditions.
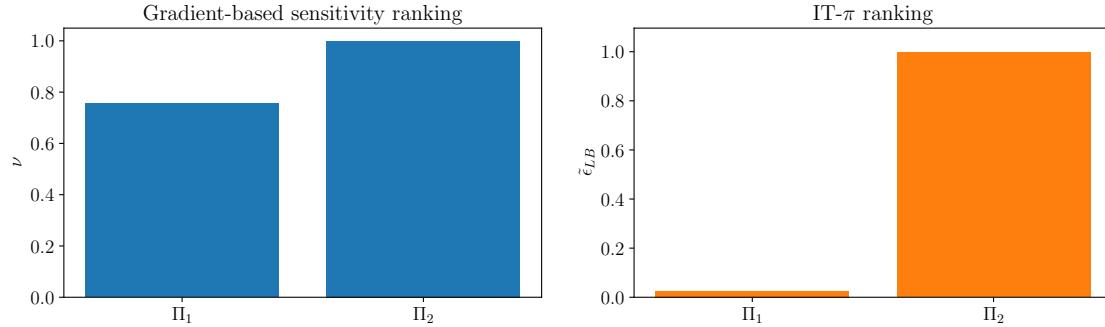

Figure S8: Comparison between gradient-based and IT-π rankings of input variables in the presence of large variations in input magnitudes. In the gradient-based ranking, higher values of ν indicate greater importance, whereas in the IT-π ranking, lower values of ϵ_{LB} correspond to higher predictive relevance.

S.4.5 Data partitioning and generalization in heat flux ANN

As discussed in §S.1.1, a central challenge in data-driven dimensionless learning is the transferability and generalizability of the discovered dimensionless variables. We argued that this limitation often stems not from the learning method itself, but from the selection of the training data. Here, we validate the generalizability of the dimensionless variables identified for the heat flux model using the ANN described in the Applications section of the manuscript.

The model was constructed by partitioning the dataset into training (70%), validation (15%), and testing (15%) subsets. The dimensionless variables identified by IT-π were derived using only the training data and validated on the held-out validation set; the test set remained completely unused during the discovery phase. Final performance was assessed using the testing set, which contains previously unseen cases not involved in model training.

Table S6 summarizes the wall roughness topology (denoted by "Roughness ID"), Mach number (M_c), Reynolds number (Re_c), and set assignment. The "Roughness ID" labels each of the ten irregular, multiscale rough surfaces, which are generated using Gaussian probability density function. Additional details about the dataset are provided in Ref. (*23*). Figure S9 shows the epoch-by-epoch errors for training, validation, and test sets. The similarity of these curves indicates the generalization within the sampled Π-space. At convergence, the training, validation, and test mean squared errors correspond to approximately 0.63%, 0.64%, and 0.63% of the variance of the target variable, respectively. These results confirm the ability

of the model to generalize and accurately predict unseen cases with performance comparable to that on the training data.
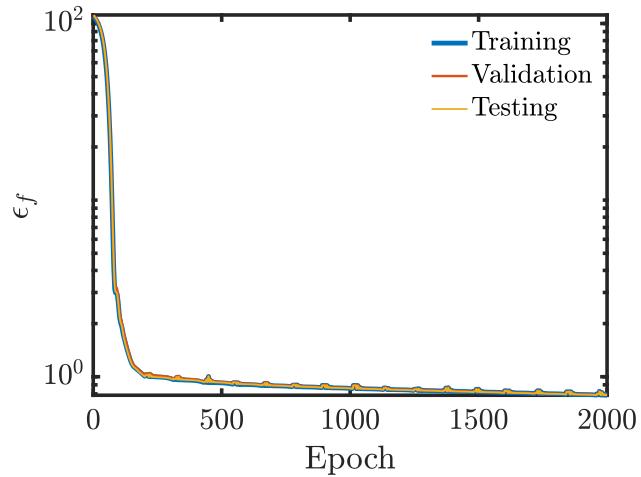

Figure S9: Model error of ANN$_3$ across training, validation, and test datasets as a function of training epochs.

Table S6: Dataset splits of ANN model for wall heat flux.

Roughness ID	M_c	Re_c	Set
1	1	4000	validation
1	1	8000	training
1	1	16000	training
1	2	8000	training
1	2	16000	training
1	4	8000	test
1	4	16000	test
2	1	4000	training
2	1	8000	validation
2	1	16000	training
2	2	4000	training
2	2	8000	test
2	2	16000	validation
2	4	8000	training
2	4	16000	training
3	1	4000	training
3	1	8000	training
3	1	16000	training
3	2	8000	training
3	2	16000	training
3	4	8000	training
3	4	16000	training
4	1	4000	validation
4	1	8000	training
4	1	16000	training
4	2	8000	test
4	2	16000	training

Roughness ID	M_c	Re_c	Set
4	4	8000	training
4	4	16000	training
5	1	8000	training
5	1	16000	training
5	2	8000	training
5	2	16000	training
5	4	8000	training
5	4	16000	training
6	2	8000	training
6	2	16000	training
6	4	8000	training
6	4	16000	training
7	2	8000	test
7	2	16000	training
7	4	8000	training
7	4	16000	training
8	2	8000	training
8	2	16000	training
8	4	8000	validation
8	4	16000	test
9	2	8000	training
9	2	16000	training
9	4	8000	training
9	4	16000	validation
10	2	8000	training
10	2	16000	validation
10	4	8000	training
10	4	16000	test